BRAZOS CHLORIDE FEASIBILITY STUDY PHASE I

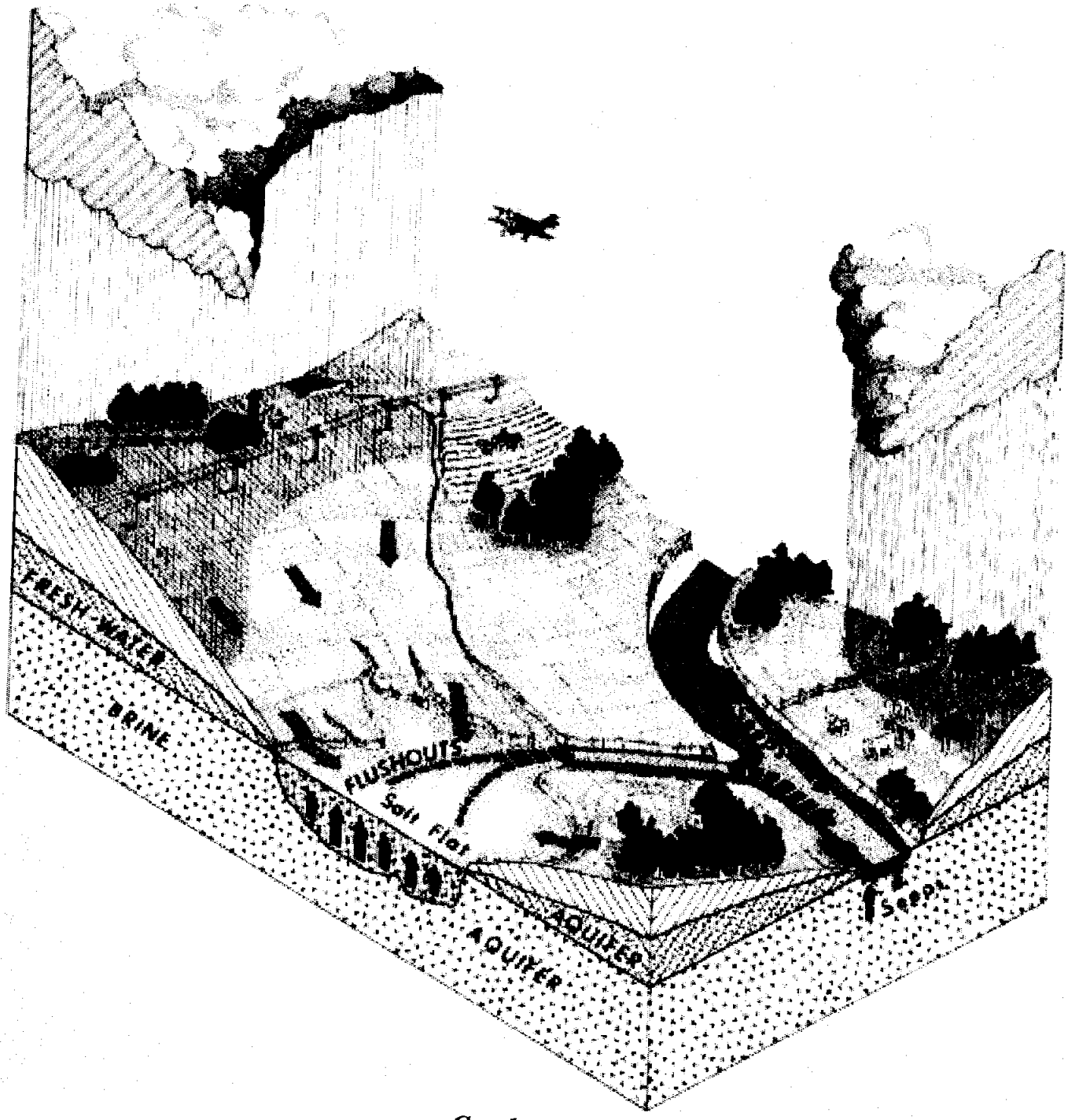

Conducted by
THE US ARMY CORPS OF ENGINEERS
For
THE TEXAS WATER DEVELOPMENT BOARD
APRIL 1994

BRAZOS CHLORIDE STUDY

SALT CROTON CREEK, TEXAS

PHASE I

APRIL 1994

Prepared By

U.S. ARMY CORPS OF ENGINEERS
FORT WORTH DISTRICT
P.O. BOX 17300
FORT WORTH, TEXAS 72102-0300

BRAZOS CHLORIDE STUDY
FOR
SALT CROTON CREEK, TEXAS

TABLE OF CONTENTS

TABLES

FIGURES

APPENDICES

BRAZOS CHLORIDE STUDY
SALT CROTON CREEK
PHASE I

INTRODUCTION

This report presents the results of investigations conducted along the Brazos River Basin to determine the feasibility of brine removal in the Salt Croton Creek area. The Brazos River Basin is extends from eastern New Mexico across the state of Texas to the Gulf of Mexico.

Study Authority

This report is submitted under the authority of Section 22 of the Water Resources Development Act of 1974 (as amended). These laws authorize the Chief of Engineers to cooperate with States in the preparation of plans for the development, utilization, and conservation of water and related resources of drainage basins located within the boundaries of the State. Assistance is provided on the basis of State requests rather than through Congressional study authorization. The regulation states that based on personnel and funding capabilities, commanders shall cooperate with States by providing planning assistance in an effective and timely manner and in accordance with the guidelines. The Texas Water Development Board (TWDB) requested an evaluation by the Corps of Engineers. This Section 22 study was initiated following a 1992 letter agreement between the (TWDB) and the U.S. Army Corps of Engineers.

Study Purpose and Scope

The purpose of this study is to evaluate the technical and economic feasibility of controlling the discharge of brine into the Salt Croton Creek in the Dove Creek Salt Flat area. The study will also examine the water quality and the availability of water supply in the Brazos River Basin. To evaluate the two-fold control process the study will be conducted in two phases. Phase I evaluates the technical feasibility of using multi-recovery wells to reduce the brine discharge. The second phase, Phase II, will focus on the technical feasibility of deep-well injection disposal of the recovered brine. Phase II will fully evaluate the economic feasibility and environmental impacts of both control processes.

Phase I, contained herein, includes the development of a three-dimensional finite element model which was used to optimize the parameters of the recovery wells, design the recovery field and develop a preliminary cost estimate.

Study Participants and Coordination

This Section 22 study was directed by the Fort Worth District, Corps of Engineers in partnership with the TWDB. The study was cost shared on a 70/30 percent basis between the Government and the TWDB. A study management team was established for this study. The team was comprised of Corps representatives from relevant disciplines, the TWDB's Chief of the Water Supplies Section, and Dr. Wesley P. James, an associate professor of the Environmental and Water Resources Engineering Department of Civil Engineering at Texas A and M University. Throughout the study, coordination was maintained with the U.S. Fish and Wildlife Service, Texas Parks and Wildlife Departments, and the State Historical Preservation Officer.

Prior Studies and Reports

The following studies and reports were referenced in relation to this study:

Natural Salt Pollution Control Study, Brazos River Basin, Texas, Volumes 1-4, and Draft Environmental Impact Statement, U.S. Army Engineer district, Fort Worth, 29 June 1973.

Final Environmental Impact Statement, Natural Salt Pollution Control Study, Brazos River Basin, Texas, U.S. Army Corps of Engineers, Fort Worth District, January 1976.

Natural Salt Pollution Control Study, Brazos River Basin, Texas, 95th Congress, 1st Session, House Document No. 95-101, 16 March 1977.

Brazos Natural Salt Pollution Control, Brazos River Basin, Texas, Design Memorandum No. 1, General Phase I - Plan Formulation, Main Report and Draft Supplement to Final Environmental Impact Statement, April 1983.

STUDY AREA DESCRIPTION

This section describes the study area and its existing water quality problems from a broad perspective. The material discussed includes information ranging from the general terrain and climate of the study area to the related water resource problems and needs.

Brazos River Basin Description

The Brazos River rises in the eastern part of New Mexico, approximately 30 miles west of the Texas-New Mexico boundary line, and flows in a general southeasterly direction for a distance of 1,210 miles, to its mouth in the Gulf of Mexico. It is one of the longest, and has the greatest watershed area of any river in the State of Texas. The drainage area is shown in figure 1.

The watershed area is about 45,000 square miles, of which 2,673 square miles are in the State of New Mexico and about 10,000 square miles is noncontributing. The watershed has a total length of approximately 640 miles, and is relatively long and narrow in shape, increasing gradually from a width of about 60 miles in the headwater area to a maximum width of approximately 120 miles in the vicinity of Waco, and then gradually decreasing to a width of only about 10 miles near the mouth.

The upper part of the Brazos River watershed lies in the High Plains, a flat, semiarid region with numerous closed basins. With the exception of a very narrow belt immediately adjacent to the tributaries, the watershed in the High Plains region consists of numerous disconnected sinks and a few streams ending in basins without an outlet. It is estimated that there are 9,500 square miles in this region that do not contribute to the Brazos River drainage. The contributing drainage area is about 35,720 square miles.

Descending from the broad smooth plateau of the High Plains, the Brazos River traverses a wide area of the strongly rolling and deeply dissected North Central Plains to the Balcones fault zone near Waco. Below Waco, the river enters the Coastal Plains, an area varying in topography extending to the Gulf.

The main stem of the Brazos River is formed by the junction of Salt Fork and Double Mountain Fork, whose parallel basins form the upper watershed. Below the confluence of these streams, the principal tributaries are Clear Fork, Bosque River, Little River, and Yequa Creek, which enter from the right bank and the Navasota River, which enters from the left bank. In addition, there are numerous smaller tributaries that enter the main stream throughout its course.

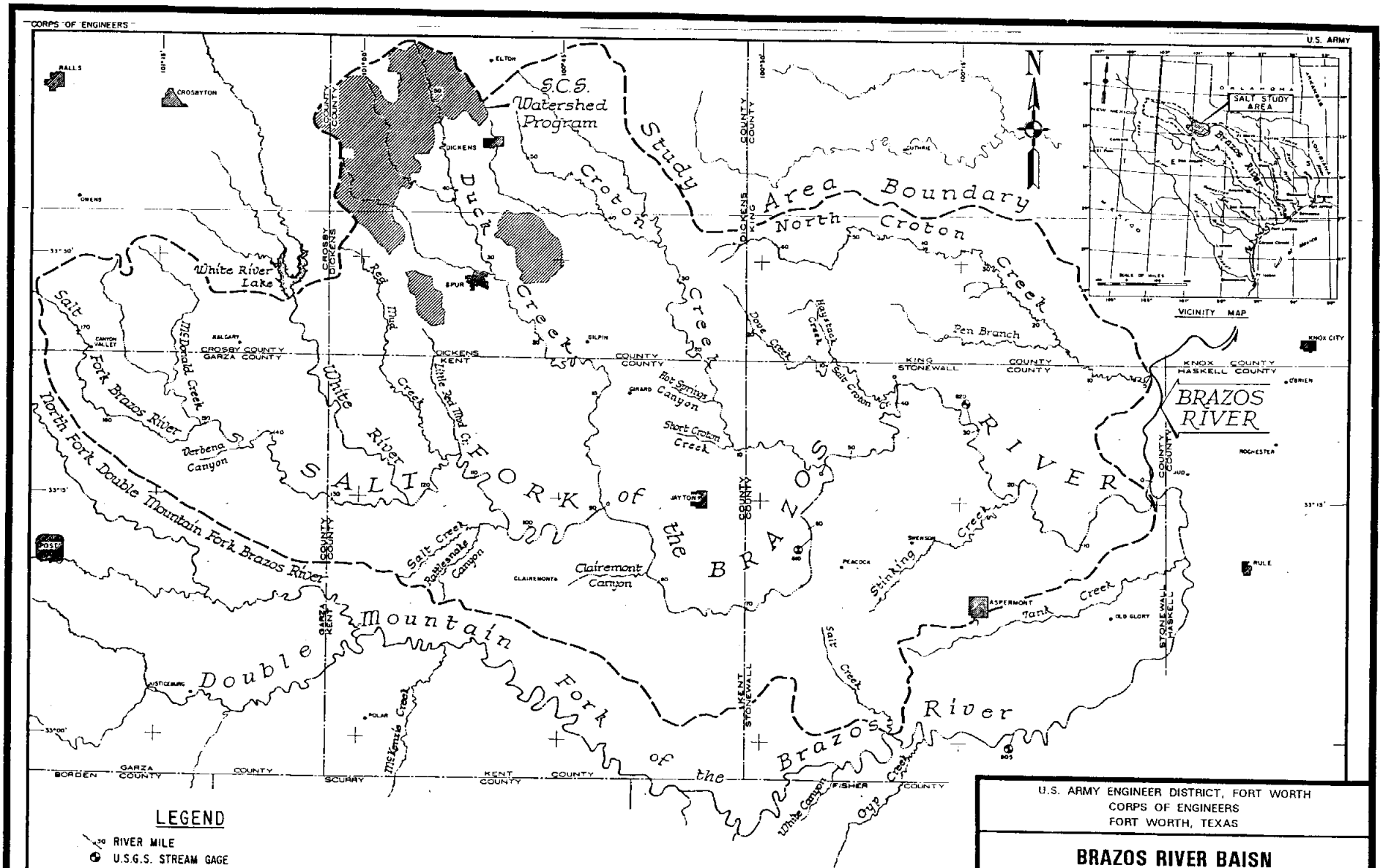

LEGEND

- RIVER MILE
- U.S.G.S. STREAM GAGE
- SOIL CONSERVATION SERVICE WATERSHED PROGRAM
- U.S. HIGHWAY AND ROUTE NUMBER
- STATE HIGHWAY AND ROUTE NUMBER
- FARM TO MARKET HIGHWAY AND ROUTE NUMBER

THIS MAP IS NOT TO SCALE

U.S. ARMY ENGINEER DISTRICT, FORT WORTH
CORPS OF ENGINEERS
FORT WORTH, TEXAS

BRAZOS RIVER BAISN
CHLORIDE
DRAINAGE AREA MAP

FIGURE 1

Dove Creek Salt Flat Description

One of the largest salt flats, Dove Creek, is located at the confluence of Haystack and Dove Creeks. These creeks merge to form Salt Croton Creek, a left bank tributary to the Salt Fork of the Brazos. A location map of the Dove Creek Salt Flat is presented in figure 2. This salt flat may contribute about 50 percent of the brine discharged into the Upper Brazos Basin and was therefore selected as the primary area for application for the ground water model.

Environmental setting

Habitat types existing in the study are: deciduous scrubland (mesquite dominated), evergreen scrubland (juniper dominated), grassland (buffalograss dominated), and riparian (saltcedar dominated). Land uses in the study area consist of 80 percent pastureland and rangeland, 15 percent cropland, and 5 percent miscellaneous.

The terrestrial habitat is of low quality. Wildlife species, such as white-tailed deer, Rio Grande turkey, bobcat, raccoon and various nongame species, are concentrated in the habitats along area watercourses. Population sizes are low in this ecoregion. Bobwhite and scaled quail, mourning doves, cottontails and jackrabbits, badgers, pocket gophers, and other reptilian and avian species, are found in the upland sites.

No significant sport fishery exists in the Salt Fork of the Brazos or its tributaries. Existing permanent fish populations are not typical of Texas streams in that they include several salt tolerant (euryhaline) species of the Cyprinidae (minnow), Poecilliidae (topminnow), and Cyprinodontidae (killifish) families. Additionally, Centrarchidae (sunfish) and Ictaluridae (catfish) are present under favorable flow and habitat conditions.

Two major environmental factors account for the limited populations of game fish. These are high Total Dissolved Solids (TDS) content and low stream flows with an associated lack of adequate cover. Also supporting the lack of game fish is the incidence of high water temperatures due at least in part to shallow depths. The saline nature of these areas inhibits biological productivity, but supported populations provide a food base for certain shore birds, wading birds, and small mammals which find their place in the adjacent arid terrestrial ecosystem.

Due to the extremely high levels of TDS existing in Salt Croton Creek (mean TDS, 47,409 ppm), no aquatic life exists in Salt Croton Creek except during periods of high flows. Although no fish exist in Salt Croton Creek, there are zooplankton, macroplankton, bluegreen algae and bacteria that tolerate the high salinity.

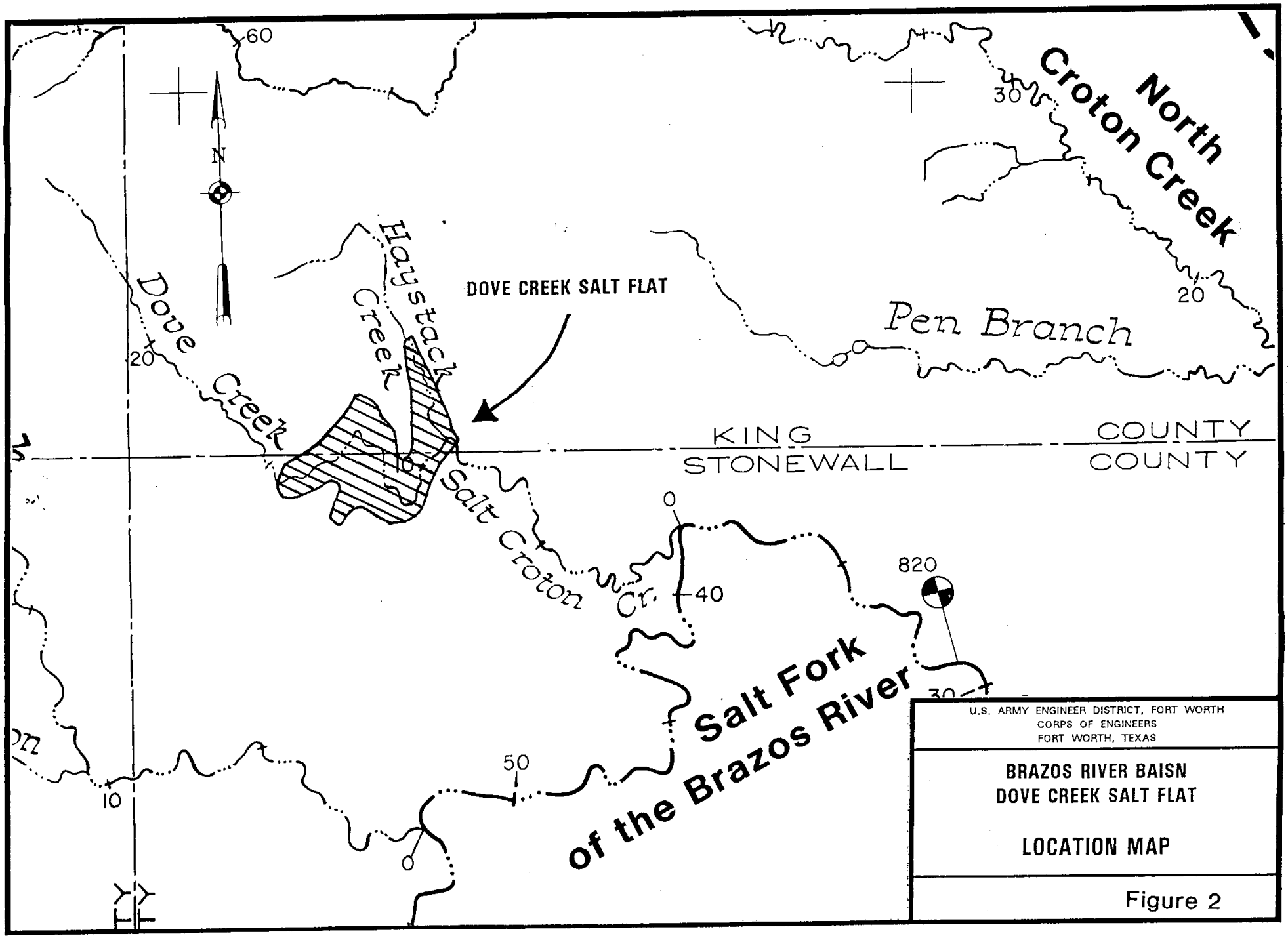
North Croton Creek
DOVE CREEK SALT FLAT
Haystack Creek
Dove Creek
Pen Branch
KING COUNTY
STONEWALL COUNTY
Salt Croton Cr.
Salt Fork of the Brazos River
60
30
20
20
0
40
820
30
50
10
0
N
U.S. ARMY ENGINEER DISTRICT, FORT WORTH
CORPS OF ENGINEERS
FORT WORTH, TEXAS
BRAZOS RIVER BAISN
DOVE CREEK SALT FLAT
LOCATION MAP
Figure 2

The mainstem of the Brazos, from its origin at the confluence of the Double Mountain and Salt Forks of the Brazos above Possum Kingdom Reservoir, does support a sport fishery. This reach contains freshwater fish (piscivorous) of the Ictaluridae (catfish), Catostomidae (sucker), Sciaenidae (drum), Cyprinidae (minnow), Clupeidae (herring), Lepisosteidae (gar), Centrarchidae (sunfish), Cyprinodontidae (killifish) and Poecillidae (topminnow) families.

United States Fish and Wildlife Service (USFWS) and Texas Parks and Wildlife Department (TPWD) were contacted concerning the proposed action and there are no threatened or endangered species in the area or critical habitats. The study area is located within the migratory routes of the black capped vireo (*Vireo atricapillus*), bald eagle (*Haliaeetus leucocephalus*), american peregrine falcon (*Falco peregrinus anatum*), whooping crane (*Grus americana*), interior least tern (*Sterna antillarum athalossos*), which are listed as endangered, and the arctic peregrine falcon (*Falco peregrinus tundrius*), piping plover (*Charadrius medodus*), which are listed as threatened by USFWS. The TPWD also lists the following species as threatened for the study area: Texas kangaroo rat (*Dipodomys elator*), white-faced ibis (*Plegadis chihi*), Texas horned lizard (*Phrynosoma cornutum*), and the Brazos water snake (*Nerodia harteri harteri*).

It was determined that the proposed project would not adversely affect any species listed or proposed for listing as endangered or threatened or any critical habitat; therefore in accordance with the Endangered Species Act a formal Section 7 consultation is not necessary.

The cultural resources work for this study was conducted to follow cultural resources law under the National Historic Preservation Act of 1966, as amended (PL-96-515), the Archeological and Historical Preservation Act of 1974, as amended (PL-93-291), the National Environmental Policy Act of 1969 (PL-90-190), and Executive Order #11593 - "Protection and Enhancement of the Cultural Environment".

The Texas Archeological Research Laboratory (State of Texas central archeological records repository) was contacted in April of 1993 for the locations and records of any known cultural resources sites and possible National Register of Historic Places properties within the project area. A number of cultural resources sites are currently known within the general project area. The Texas State Historic Preservation Officer was notified of the potential construction project in April 1993.

Only part of the proposed Salt Croton Creek Project area has been surveyed in the past, with 16 known sites recorded by past cultural resources surveys. Prior to any construction activities, it will be necessary to conduct a cultural resources survey. The objective of the survey is to identify and preliminarily assess the significance and importance of potential cultural resource sites in the area of project impact. If significant cultural resource sites are discovered, an evaluation to determine their significance is necessary.

PROBLEM IDENTIFICATION

The Brazos River basin suffers from natural salt pollution. Sodium chloride significantly affect the amount of usable water available from the Brazos. The water in the three main-stem reservoirs in the headwaters of the Brazos basin is unsuitable for municipal use and irrigation of many crops without the use of costly desalination processes. The water quality of the Brazos River varies from the headwaters of the basin to the Gulf of Mexico. Previous reports by the Corps of Engineers indicate that the water quality throughout the basin is generally considered unsuitable for municipal water supplies in the entire length of the river. According to a 1993 report written by Ralph A. Wurbs, Awes S. Karama, Ishtiaque Saleh, and C. Keith Ganze entitled, "Natural Salt Pollution and Water Supply Reliability in the Brazos River Basin", the water quality in the Brazos River is degraded due to natural contamination by salts consisting largely of sodium chloride with moderate amounts of calcium sulfate and other dissolved solids. They identified the groundwater emissions from the Salt Fork of the Brazos River watershed, Double Mountain Fork Brazos River, and the North Croton Creek watersheds as the primary source of the salinity. These problems signify the need for greater understanding of the salt pollution impacts and provides a challenge to develop reliable cost effective control measures.

PROJECT ANALYSIS

Groundwater analysis

A full three-dimensional finite element model to simulate groundwater flow under steady-state conditions was developed to design and evaluate the recovery system. The model was verified and applied to the Dove Creek Salt Flat area. The model was used to determine the affects of implementaion of the proposed recovery well system on the water quality of the Brazos River. The model indicates that a brines recovery system located in the discharge zone of the aquifer will eliminate the natural salt springs and seeps in the Dove Creek area which contributes half of the chloride concentration in the upper portion of Brazos River. Therefore, the recovery system has the potential to reduce the chloride concentration in the Brazos River by almost 50 percent. A complete of the model and the analysis in presented ion Appendix A.

Recovery design system

A recovery design system was developed by Dr. Wesley James, Associate Professor of Environmental and Water Resources Engineering at Texas A&M University. The report entitled, "Evaluation and Partial Control of Natural Salt Spring and Seeps in the Dove Creek Area, Upper Brazos River Basin, Part I Recovery System Design" is included as Appendix A.

The preliminary design consists of ten wells spaced approximately 1,500 feet apart, on a north-south line through the Dove Creek salt flat area. A map depicting the well sites is shown in Figure 3. The well depth ranges from 65 feet to 195 feet with an average depth of 115 feet. It is anticipated that by lowering the hydrostatic head in the salt water aquifer, the discharge will be eliminated from the springs and seeps. The design also includes measures for reversing the hydraulic gradient at the surface so that the direction of percolation is downward to eliminate the build-up of salt at the surface of the salt flat.

The brine will be recovered through the wells and pumped into the buried six-inch and eight-inch PVC collector pipes. The pump capacity and motor size for each well varies depending on the aquifer characteristics. The collector pipeline will then transfer the brine into the collector station for injection into the formation. Additional studies will be completed on the brine during Phase II of the study process. Questions concerning the content of gases within the brine will be addressed during the second phase. The system design will be refined during the second phase of the Brazos Chloride study.

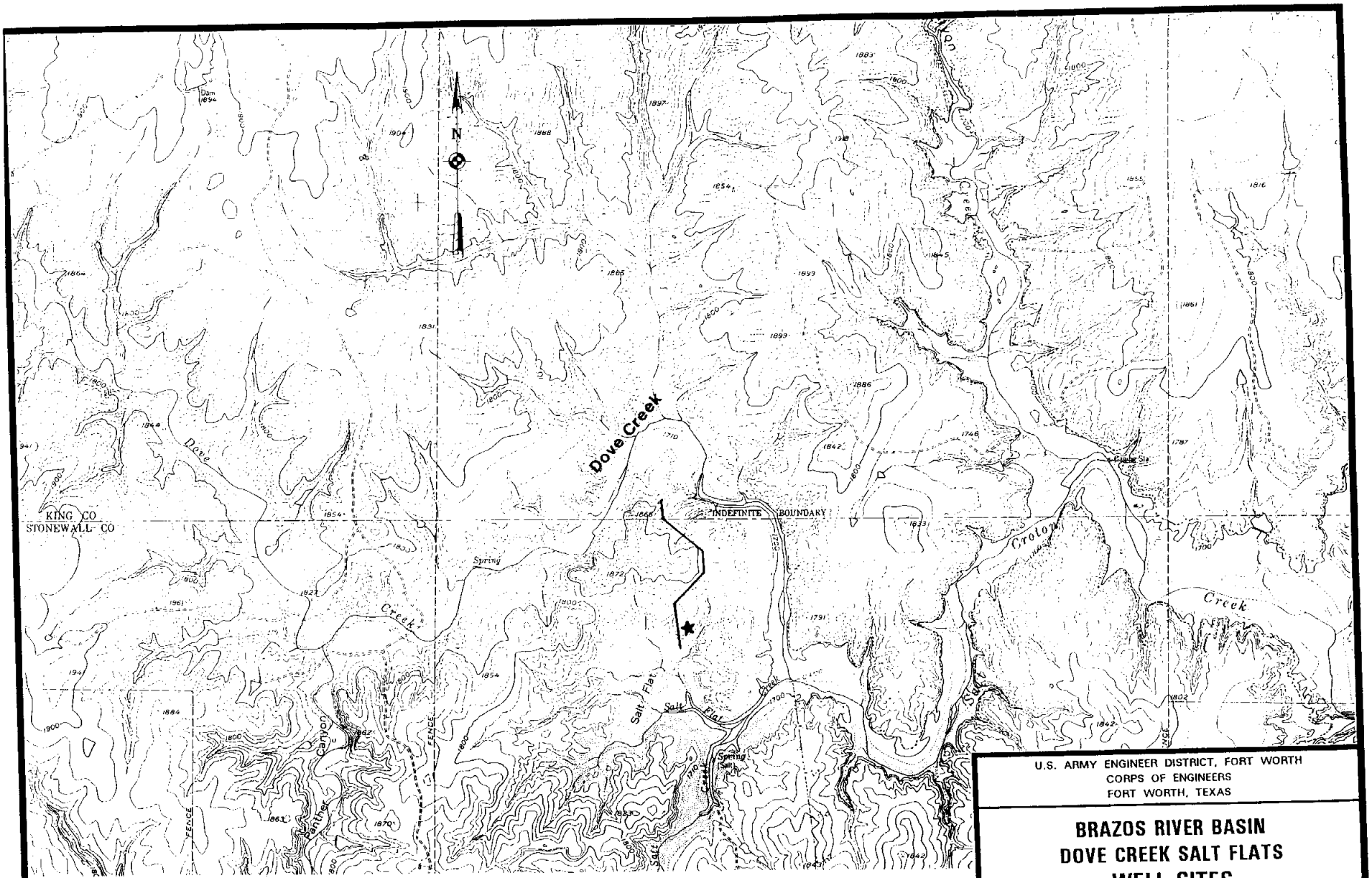

- General Location of Recovey Wells

★-Brine Collection Station

SCALE 1:24 000

1 MILE

1000 0 1000 2000 3000 4000 5000 6000 7000 FEET

1 KILOMETER

CONTOUR INTERVAL 20 FEET

U.S. ARMY ENGINEER DISTRICT, FORT WORTH
CORPS OF ENGINEERS
FORT WORTH, TEXAS

BRAZOS RIVER BASIN
DOVE CREEK SALT FLATS
WELL SITES

FIGURE 3

PROJECT COSTS

Preliminary Cost Estimate

Based on the information provided in the design report, a preliminary cost estimate for the recovery design system was developed. The estimated total project costs were approximately $1.8 million. A summary of the cost estimate is shown in table 1. The detailed account of the project costs is presented in Appendix B. The cost estimate was based on the following data and assumptions:

a) Ten recovery wells spaced 1,500 feet apart with an average depth of 115 feet.

b) One injection well with a depth of 5,280 feet.

c) Lump sum installation of new transmission lines, line poles, and transformers.

d) Real estate costs for permanent easement for operation maintainence.

e) A 30 percent contingency allowance for unknown final design factors.

TABLE 1

ESTIMATED COST OF RECOVERY SYSTEM

DESCRIPTION	*ESTIMATED COST*	*CONTINGENCY*	*TOTAL COST*
Recovery Wells	129.4	38.8	168.2
Injection well	806.1	241.8	1,047.9
Collector Station	27.9	8.4	36.3
PVC Pipeline	160.7	48.2	208.9
Data Acquisition System	79.8	23.9	103.7
Electrical System	168.3	50.5	218.8
Real Estate	25.0	7.5	32.5
Total	**$1,397.2**	**$419.1**	**$1,816.3**

SUMMARY AND CONCLUSIONS

The first phase of this feasibility analysis has produced a finite element model that assisted in the preliminary design and evaluation of a brine recovery system. The model showed that the poor water quality of the Brazos River Basin can be attributed to the naturally occurring salt pollution along the Upper Brazos Basin. The model shows that 50 percent of the chloride is derived from brine aquifers in the Dove Creek area. Based on the results of this model, installation of ten wells throughout the Dove Creek Salt Flat area will lower the hydrostatic head in the salt water aquifer and significantly reduce the natural springs and seeps. Consequentially, the water quality of the Brazos River should improve over time with the reduction of chloride pollution.

Follow on studies in the second phase will more fully evaluate the costs of a brine disposal system using deep-well injection, as well as document the economic and environmental impacts from the proposed system.

APPENDIX A

THREE DIMENSIONAL MODEL AND RECOVERY SYSTEM DESIGN

EVALUATION AND PARTIAL CONTROL OF NATURAL SALT SPRING AND SEEPS IN THE DOVE CREEK AREA, UPPER BRAZOS RIVER BASIN, PART I RECOVERY SYSTEM DESIGN

for

U.S.Army Corps of Engineers
Texas Water Development Board Brazos Chloride Study

by

Wesley P. James
Panfilo A. Masciangliolí
Kesava B. Chakka

through the

Texas Engineering Experiment Station
Texas A&M University
College Station, TX 77843

February 1994

ABSTRACT

The average salt load in the Brazos River at Possum Kingdom Reservoir is 1000 tons per day. Subsurface brine in the Dove Creek area has a chloride concentration of 100,000 mg/l. The brine springs and seeps in the Dove Creek area discharge 500 tons per day of chloride with a flow rate of only 2.0 cfs. Controlling the brine springs and seeps in the Dove creek area has the potential of reducing the chloride cncentration in the Brazos River by nearly 50 percent.

A preliminary design of the brine recovery system was presented in this phase of study. A full three-dimensional finite element model to simulate ground water flow under steady-state conditions was developed to design and evaluate the recovery system. The main characteristic of the model is that it can consider very anisotropic and heterogeneous media. The resulting system of equations is solved using iterative Gauss-Seidel method, together with a pointer matrix used to save memory and computation time, avoiding the storage of most of the zeros of the resulting sparse matrix.

The model was applied in the evaluation of a brine

recovery wells system in the Dove Creek area in the Upper Brazos River, Texas, where a natural salt pollution exists. From this study it was concluded that:

1. The water quality in the Brazos River is seriously degraded by natural salt pollution in the Upper Brazos River.

2. Controlling the natural salt springs and seeps in the Dove Creek area will reduce the chloride concentration in the Brazos River by nearly 50 percent.

3. There are two brine aquifers in the Dove Creek area that contribute to the natural salt pollution of the Brazos River.

4. A variable density model is not required to evaluate the recovery system.

5. The brine that is discharged as natural springs and seeps in the Dove Creek area is from two sources, (1)local recharge and (2) deep-basin.

6. Permeability measurements of the brine aquifer taken several miles away from the discharge zone are not representative values for the design of the recovery system.

7. A shallow-well, low-volume, brine recovery system located in the discharge zone of the brine aquifer will eliminate the natural salt springs and seeps in the Dove Creek area.

8. The amount of brine recovery to be pumped from the recovery system to control the natural brine springs and seeps in Dove Creek area is expected to change very little from year to year.

TABLE OF CONTENTS

LIST OF FIGURES

Page

LIST OF TABLES

INTRODUCTION

The water quality in the Brazos River is seriously degraded and is generally poor because of the natural salt pollution. The source of the salt pollution is primarily brine springs and seeps in the Salt Fork Brazos River watershed. Water quality in the Brazos River improves downstream of Whitney Reservoir due to dilution by good quality water from tributaries in the lower basin. Water in the three main stream reservoirs (Possum Kingdom, Granbury and Whitney) is unsuitable for municipal water supply without costly treatment. Natural salt pollution significantly impacts water resources development of the basin and the state. If the Brazos River is to be a part of the Trans-Texas water transfer to South Texas, the water quality of the river will have to be improved.

The area that includes brine seeps and springs is in the Rolling Plains in north-central Texas and is bounded by the caprock escarpment of the southern High Plains on the west, the Salt Fork of the Red River on the north and the Double

Mountain Fork of the Brazos River on the south. Ground surface elevation ranges from approximately 1,600 ft msl at the eastern boundary to about 2,800 ft msl at the western boundary. Numerous intermittent streams cross the area flowing generally eastward. The climate of the Rolling Plains is semiarid with an average annual rainfall of 22 inches and an average lake evaporation of 62 inches per year.

Salt seeps and springs and salt flats occur along major streams. The largest salt flats are Hot Springs and Short Croton along Croton Creek in northeastern Kent County, Dove Creek and Haystack Canyon in southwestern King and northwestern Stonewall Counties, Jonah Creek and Salt Creek in northwestern Childress County, and Elm Fork in northern Harmon County (Richter and Kreitler, 1986).

Management of a groundwater system means making decisions without violating specified constraints about quantity of water to be withdraw per year, location of pumping wells and their rates, control conditions at aquifer boundaries, and decisions related to groundwater quality. Management requires the ability to forecast the aquifer's response to planned

operations. The necessary information about the response of the system is provided by a model that describes the behavior of the groundwater system in response to some action. Because of the heterogeneity of the considered domain, the irregular shape of its boundaries, and the complex form of various source functions, only numerical models can provide the required forecast. The most important part of the modeling procedure is a complete understanding of the processes that take place on the considered system, identify those parts of the system's behavior that are relevant to the problem, and those parts that may be neglected. On these bases, a conceptual model is created, a numerical model is constructed, and a computer program is prepared.

The knowledge of the groundwater flow behavior is essential for management decision related with water quality. If the fluid's density is unaffected by changes in concentration, then the groundwater flow behavior can be used as input information for pollution models. Nevertheless, when the fluid's density is a function of pressure and concentration of the concerned pollutant, then the groundwater

flow equation and the pollution equations have to be solved simultaneously.

Depending upon the complexity of both, the geology and the groundwater flow, and the required application of the results, one-, two-, or three-dimensional flow models can be used. A three-dimensional approach is necessary when the geology is complex, and the groundwater flow in all directions is considered important.

Many two-dimensional flow models have been created during the last decades. Although a three-dimensional model is in general a better approach for simulating the three-dimensional character of a real aquifer, the development was limited due to the requirement of computer with large core storage and high speed. Nevertheless, due to the rapid development of computers with high memory capacity and fast processing, the development of three-dimensional flow models have been increasing during the last twenty years. In general, the first of those models were developed using the finite difference technique, while lately, the finite element method has been preferred due to its versatility in considering complex

the fluid was developed. In the second stage, modifications of the constant density model were made in order to consider the groundwater flow of two fluids with different densities when a sharp interface between the two fluids exists. Among the activities related with the development of the model, are the elaboration of appropriate algorithms to generate automatically the three-dimensional mesh, and to solve the huge system of equations that is normally generated on three-dimensional approaches. A new method to evaluate the mean permeability of each of the elements that intersect more than one geologic unit with different permeabilities, is also included.

The model was verified by comparing the results of test simulations with available analytical solutions, and with other available numerical models for simpler cases.

Finally, the model was applied to the Dove Creek area, in the upper Brazos River, Texas, where a proposed plan of brine recovery wells system is being designed in order to reduce the natural salt pollution that affects the quality of the Brazos River.

REVIEW OF GROUNDWATER MODELING LITERATURE

Numerical modeling of groundwater is a relatively new field. Since the mid-1960's, significant progress has been made in the development and application of numerical models for groundwater-related resources management. The classic approach in describing the dynamics of groundwater systems was to solve the flow equations together with the appropriate boundary and initial conditions. The analytical difficulties of solving the equations limit this approach to relatively simple cases. A need for general applicable approaches to solve the equations of flow for the complex problems encountered in real field situations gave rise in recent years to digital models. The computer methods provide solutions for the equations of flow for complex field problems, and thereby provide means for simulating the operation and response of very complicated systems. The advent in recent years of high speed, large capacity digital computers has increased the capability to solve equations of flow for many complex problems by digital methods, and digital computers now play a

major role in groundwater analysis.

The first three-dimensional (3-D) models were developed in France in the late sixties and in Japan in the early seventies. These models are mentioned in Van der Heijde et al (1985), but are not referenced because either the codes or the documentation were unavailable.

One of the earliest contributors to three-dimensional modeling was Freeze (1971), who used a finite difference model to investigate the nature of base flow generation in a small-scale hypothetical basin. One of the first documented and available three-dimensional models was developed by Huang and Wu (1974). They developed a transient finite element model to determine the drawdown around a partially penetrating well of finite radius, for an anisotropic and heterogeneous confined aquifer. Cheung and Skjolingstad (1974) studied the transient behavior of free surface groundwater seepage using both, two-dimensional and three-dimensional finite element models. France (1974) developed a three-dimensional finite element model for analyzing either steady state or transient groundwater flow problems. Huang and Wu (1975) presented a

three-dimensional finite element model programmed for a high-speed computer for simulating groundwater flow in confined aquifers. Trescott (1975) developed a three-dimensional finite difference model for predictions of heads, flow rates, and drawdowns in anisotropic and heterogeneous porous medium. Modified versions of this model include evapotranspiration and interaction between rivers and upper aquifer. Narasimhan and Witherspoon (1976) developed a general model for both two-dimensional and three-dimensional flow based on the integrated finite difference method for saturated and unsaturated flow. Gupta and Tanji (1976) used a three-dimensional isoparametric finite element model in the analysis of flow in Sutter Basin in California. This model appears to be better suited for steady state cases, as the authors present no evidence of an atmospheric boundary capability in the form of a movable boundary. Frind and Verge (1978) designed a three-dimensional Galerkin finite element model, based on the general saturated-unsaturated continuity equations. They also examined practical aspects of three-dimensional modeling of groundwater flow. Taylor and Huyakorn (1978) also developed a three-dimensional

groundwater flow model with convective dispersion. Posson et al (1980) developed a transient three-dimensional finite difference model to determine heads, drawdown, and water balance for anisotropic and heterogeneous porous medium. This model has been extensively modified. Liggett (1983) developed a three-dimensional steady-state flow model using the boundary integral equation method. Gupta, Cole, and Pinder (1984) developed a three-dimensional finite element model (FE3DGW) to simulate groundwater flow for multiaquifer systems. Badu and Pinder (1984) used a finite element-finite difference alternating direction algorithm to develop a three-dimensional groundwater transport model. McDonald and Harbaugh (1984) developed a modular three-dimensional finite difference groundwater flow model. The major options of this model include procedures to simulate the effects of wells, recharge, rivers, drains, evapotranspiration, and general-head boundaries. This model is widely used. Nawalany (1986) developed a model based on the so called Transport Velocity Representation (TVR) of groundwater flow. This model can be classified as a three-dimensional finite element-finite

difference numerical model of steady state groundwater flow. Gambolati, Pini, and Tucciarelli (1986) used the conjugate gradient method to develop a three-dimensional finite element model of subsurface flow with automatic mesh generation. Huyakorn, Jones, and Peter (1986) developed a finite element algorithm for simulating three-dimensional groundwater flow and solute transport in multilayer systems of several aquifers and aquitards. This formulation take advantage of the nature of flow in such multilayer systems. Reeves et al (1986) presented one of the last versions of the Sandia Waste-Isolation Flow and Transport Model (SWIFT). This model was developed for use in simulating the transport of radionuclides dissolved in groundwater. It is a finite difference, transient, three-dimensional code, which also solves the coupled equations for fluid flow, head transfer, and brine transport in saturated porous media. It evolved from the U.S. Geological Survey code SWIP (Survey Waste Injection Program) (INTERCOMP, 1976). Aral (1990) developed a very well documented finite element groundwater flow model for multilayer aquifers under steady state conditions.

THEORETICAL DEVELOPMENT OF A GROUNDWATER MODEL

The Mass Balance Equation

If we consider that the mass of water completely fills the void space of a porous media, then the mass balance equation can be written in the form (Bear and Verruijt, 1987)

$$-\nabla \cdot \rho \vec{q} = \frac{\partial (n\rho)}{\partial t} \qquad (1)$$

where ρ = the density of the fluid (M/L^3),

$\vec{q}$ = the specific discharge (L/T), and

n = the porosity.

Equation (1) states that the excess of efflux over influx of mass, per unit volume and per time, which is the divergence of the flux vector of mass ($\vec{j}=\rho\vec{q}$), is equal to the increase in water mass per unit volume of porous medium per unit time.

For an incompressible fluid, and a nondeformable porous medium (or for steady flow), $\partial(n\rho)/\partial t=0$, and equation (1)

becomes

$$\nabla \cdot \rho \vec{q} = 0 \qquad (2)$$

If the fluid is also homogeneous (fluid of constant density), then equation (2) reduces to

$$\nabla \cdot \vec{q} = 0 \qquad (3)$$

The Motion Equation

In 1856, Henry Darcy (Darcy, 1856) investigated the flow of water in vertical homogeneous sand filter in connection with the fountains of the city of Dijon (France). From his experiments, Darcy concluded that the rate of flow (volume of water per unit time), Q, is proportional to the cross-sectional area A, proportional to the difference in water level elevations in the inflow and exit reservoirs of the filter (h_1-h_2), and inversely proportional to the filter's length, L. The combination of these conclusions give the famous Darcy's law

$$Q = KA\frac{(h_1 - h_2)}{L} \tag{4}$$

where K is a coefficient of proportionality.

When the flow is three-dimensional, and the medium is homogeneous and anisotropic, the generalization of equation (4) is (Bear and Verruijt, 1987)

$$\vec{q} = [K]\cdot\vec{j} = -[K]\cdot\nabla\phi = -\frac{[k]}{\mu}\cdot(\nabla P + \gamma\nabla z) \tag{5}$$

where $\vec{q}$ = the specific discharge vector = $n\vec{v}$ (L/T),

n = the porosity of the medium,

$\vec{v}$ = the velocity vector of the fluid (L/T),

ϕ = the piezometric head = $z+P/\gamma$ (L),

z = the elevation of the point (L),

P = the pressure (M/LT^2),

γ = the specific weight of the fluid = ρg (M/L^2T^2),

ρ = the mass density of the fluid (M/L^3),

g = the acceleration of gravity (L/T^2),

[K] = the second rank tensor of hydraulic conductivity of an anisotropic medium = $[k]\gamma/\mu$ (L/T),

$[k]$ = the second rank tensor of permeability of an anisotropic medium (L^2), and

μ = the dynamic viscosity of the fluid (M/LT).

In equation (5), $-(\nabla p+\gamma\nabla z)$ represents the driving force, per unit volume of fluid, due to pressure gradient and to gravity. This force is balanced by the drag or resistance to the flow, at the solid-fluid interface, expressed by $\vec{q}\mu[k]^{-1}$.

Development of the Governing Equations

When two miscible fluids like fresh water and salt water are in motion within a porous medium, the interfacial tension between the two fluids is zero, and the two fluids dissolve each other due to the hydrodynamic dispersion, creating what is called a transition zone (Bear, 1972). A distinct fluid-fluid interface does not exist. Yet, in many cases of practical interest, the transition zone is narrow relative to the size of the flow domain, such that for practical purposes a fictitious abrupt interface may be assumed to separate the two fluids. Although this is an approximate approach, whenever

justified, it appreciably simplifies the treatment of the two-fluid flow problem.

Let D denote some porous medium domain occupied by the two fluids, 1 and 2 (see Figure 1). Let B_1 and B_2 denote the portion of the external boundary of D in contact with the fluids 1 and 2, respectively. If the fluids are incompressible, a piezometric head h can be defined within each subregion.

$$h_1 = h_1(x,y,z) = z + \frac{P}{\gamma_1} \qquad in \ D_1 \qquad (6)$$

$$h_2 = h_2(x,y,z) = z + \frac{P}{\gamma_2} \qquad in \ D_2 \qquad (7)$$

where P is the pressure, z is the vertical coordinate, and γ_1 and γ_2 are the specific weight of fluids 1 and 2, respectively.

Because the densities of fluids 1 and 2 are different but constant, the continuity equation for homogeneous fluids, equation (3), can be used together with the motion equation, equation (5). Introducing equation (5) into equation (3), we

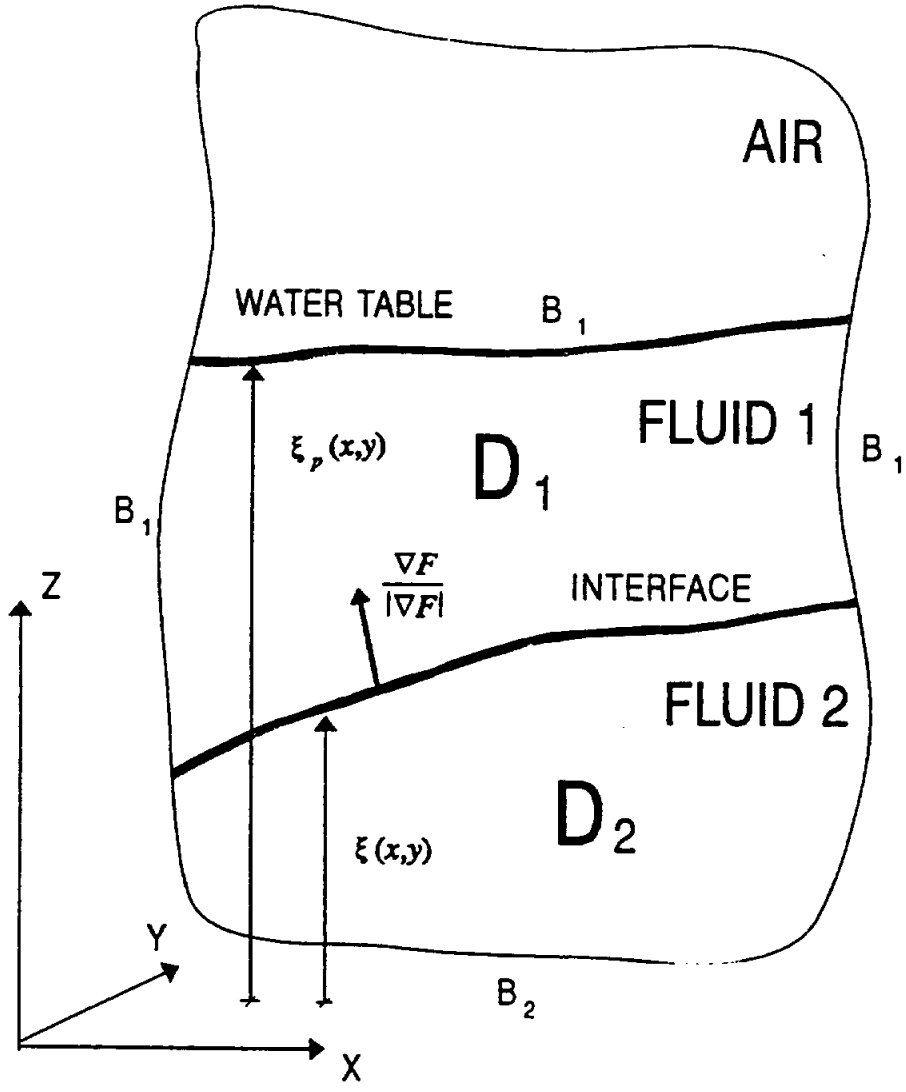

Figure 1. Definition of variables used to describe the flow of two fluids separated by a sharp interface.

get the two equations that govern the motion of the fluid 1 within domain 1, and the flow of fluid 2 within domain 2. Therefore, the model describing the flow in both regions can be stated in the following way. Determine h_1 in D_1 and h_2 in D_2 such that

$$\nabla \cdot \left(\frac{\gamma_1}{\mu_1} [k_1] \cdot \nabla h_1 \right) = 0 \qquad in \quad D_1 \tag{8}$$

$$\nabla \cdot \left(\frac{\gamma_2}{\mu_2} [k_2] \cdot \nabla h_2 \right) = 0 \qquad in \quad D_2 \tag{9}$$

where k_1 and k_2 are the permeabilities of media D_1 and D_2, respectively, and μ_1 and μ_2 are the viscosities of fluids 1 and 2, respectively.

Boundary Conditions

Boundary conditions for h_1 on B_1 and h_2 on B_2 are the usual ones encountered in the flow of a single fluid. That is, constant head or Dirichlet boundary condition, and specified

flux or Neumann boundary condition. However, the boundary condition on the interface requires special attention, because as in the case of a phreatic surface, the location of the interface is unknown until the problem is solved.

For steady state, the interface surface can be represented by an equation whose general form is $F(x,y,z)=0$. Denoting the elevation of points on the interface by $\xi=\xi(x,y)$, then F can be written as

$$F = z - \xi(x,y) = 0 \qquad (10)$$

The pressure at a point $P(x,y,\xi)$ on the interface is the same when approached from both sides. Hence, from equations (6) and (7) we get

$$\xi(x,y) = h_2 \frac{\gamma_2}{\gamma_2 - \gamma_1} - h_1 \frac{\gamma_1}{\gamma_2 - \gamma_1} \qquad (11)$$

Once the distribution of h_1 and h_2 are known, then the location of the interface can be determined using equation (11).

The other condition on the interface is that the specific discharge must be the same on both sides. Since each fluid is confined to its own subregion, and the interface is stationary, the interface acts as an impervious boundary to each of the two subregions. In each region, only components of the specific discharge that are tangent to the interface are possible. Because F is the function that define the interface, then $\nabla F/|\nabla F|$ is a unit vector perpendicular to the interface at a specified point. Therefore, the condition of impervious boundary for the interface can be stated as

$$\vec{q}_1 \cdot \hat{n}_1 = \frac{\gamma_1}{\mu_1}[k_1]\cdot\nabla h_1 \cdot \frac{\nabla F}{|\nabla F|} = 0$$

$$\vec{q}_2 \cdot \hat{n}_2 = \frac{\gamma_2}{\mu_2}[k_2]\cdot\nabla h_2 \cdot \frac{\nabla F}{|\nabla F|} = 0 \qquad \textbf{(12)}$$

Using the definitions of F and ξ we get

$$\frac{\gamma_1}{\mu_1}[k_1]\cdot\nabla h_1\cdot\nabla\left(z - h_2\frac{\gamma_2}{\gamma_2-\gamma_1} + h_1\frac{\gamma_1}{\gamma_2-\gamma_1}\right) = 0 \qquad on \quad z=\xi$$

$$\frac{\gamma_2}{\mu_2}[k_2]\cdot\nabla h_2\cdot\nabla\left(z - h_2\frac{\gamma_2}{\gamma_2-\gamma_1} + h_1\frac{\gamma_1}{\gamma_2-\gamma_1}\right) = 0 \qquad on \quad z=\xi \tag{13}$$

We can see the nonlinear behavior of these conditions on the interface. This fact makes it almost impossible to solve this problem analytically.

The boundary conditions on the phreatic surface can be easily derived from the previous analysis of the interface. If it is assumed on the interface analysis that the overlying fluid is air (subscript=0), and the underlying fluid is fresh water, then $\gamma_0=0$, and from the equation (11) we get

$$\xi_p(x,y) = h_1 \tag{14}$$

ξ_p denoting the location of the phreatic surface. Similarly, from equation (12), we get

$$\vec{q}_1 \cdot \hat{n} = \frac{\gamma_1}{\mu_1}[k_1]\cdot\nabla h_1 \cdot \hat{n} = \frac{\gamma_1}{\mu_1}[k_1]\cdot\nabla h_1 \cdot \nabla(z - h_1) = 0 \quad on \quad z = \xi_p \qquad (15)$$

where $\hat{n}$ is the unit vector normal to the phreatic surface. Equations (8) and (9), subject to the boundary conditions (11), (13), (14), and (15), are the equations used to solve for the unknown h_1 and h_2.

The boundary condition given by equation 11 is difficult to implement in the model, because the piezometric head just above and below the interface should be known. Instead, we can consider a static salt water, this simplifies the implementation of the boundary condition on the interface.

Defining S_x and S_y as the coordinates along the interface in the direction x, and y, respectively, and taking the derivatives of equation 11 with respect to S_x and S_y (see Figure 2), we obtain

$$\frac{\partial \xi}{\partial S_x} = \frac{\gamma_s}{\gamma_s - \gamma_f}\frac{\partial h_s}{\partial S_x} - \frac{\gamma_f}{\gamma_s - \gamma_f}\frac{\partial h_f}{\partial S_x} = \sin\alpha \qquad (16)$$

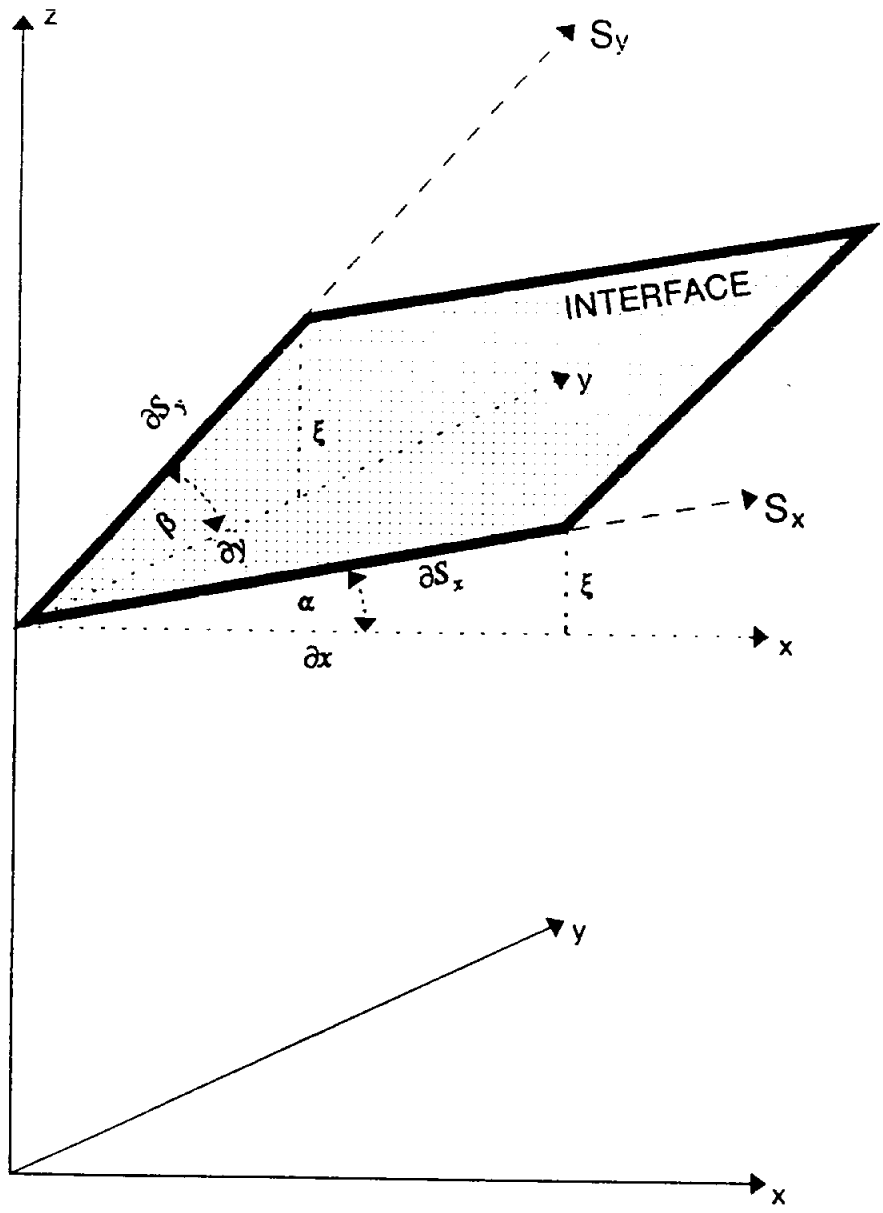

Figure 2. Definition of variables used to describe the boundary condition at the interface.

$$\frac{\partial \xi}{\partial S_y} = \frac{\gamma_s}{\gamma_s - \gamma_f} \frac{\partial h_s}{\partial S_y} - \frac{\gamma_f}{\gamma_s - \gamma_f} \frac{\partial h_f}{\partial S_y} = \sin \beta \qquad (17)$$

where α is the angle of the interface above a horizontal datum in the x direction, and β is the angle of the interface above a horizontal datum in the y direction. $(\partial h_s/\partial S_x)$ and $(\partial h_f/\partial S_x)$ are proportional to the velocity of the two fluids in the direction S_x, and $(\partial h_s/\partial S_y)$ and $(\partial h_f/\partial S_y)$ are proportional to the velocity of the two fluids in the direction S_y. Applying the chain rule to equations (16) and (17), we get

$$\frac{\partial \xi}{\partial S_x} = \frac{\gamma_s}{\gamma_s - \gamma_f} \frac{\partial h_s}{\partial x} \frac{\partial x}{\partial S_x} - \frac{\gamma_f}{\gamma_s - \gamma_f} \frac{\partial h_f}{\partial x} \frac{\partial x}{\partial S_x} = \sin \alpha \qquad (18)$$

$$\frac{\partial \xi}{\partial S_y} = \frac{\gamma_s}{\gamma_s - \gamma_f} \frac{\partial h_s}{\partial y} \frac{\partial y}{\partial S_y} - \frac{\gamma_f}{\gamma_s - \gamma_f} \frac{\partial h_f}{\partial y} \frac{\partial y}{\partial S_y} = \sin \beta \qquad (19)$$

Because we are using linear interpolation functions for the finite element approach, we can approximate $(\partial x/\partial S_x) \approx \cos\alpha$, and $(\partial y/\partial S_y) \approx \cos\beta$. Then, equations (18) and (19) transform to

$$\tan \alpha = \frac{\gamma_s}{\gamma_s - \gamma_f} \frac{\partial h_s}{\partial x} - \frac{\gamma_f}{\gamma_s - \gamma_f} \frac{\partial h_f}{\partial x} \quad (20)$$

$$\tan \beta = \frac{\gamma_s}{\gamma_s - \gamma_f} \frac{\partial h_s}{\partial y} - \frac{\gamma_f}{\gamma_s - \gamma_f} \frac{\partial h_f}{\partial y} \quad (21)$$

For stable upconing under steady state conditions, and assuming a static salt water, the piezometric head for the salt water, h_s, is constant, and therefore, $(\partial h_s/\partial x) = (\partial h_s/\partial y) = 0$. With this simplification, equations (20) and (21) reduce to

$$\tan \alpha = \frac{\partial \xi}{\partial x} = -\frac{\gamma_f}{\gamma_s - \gamma_f} \frac{\partial h_f}{\partial x} \quad (22)$$

$$\tan \beta = \frac{\partial \xi}{\partial y} = -\frac{\gamma_f}{\gamma_s - \gamma_f} \frac{\partial h_f}{\partial y} \quad (23)$$

These conditions can now be easily introduced into the finite element formulation.

If the location of the interface is known at x=0 and y=0, then the interface can be built from the piezometric head

values previously calculated at the nodes that represent the interface. Consider that the interface is represented by the nodes shown in Figure 3. In term of the indexes i and j, equations (22) and (23) can be written as

$$\xi(i+1,j) = \xi(i,j) + \frac{\gamma_f}{\gamma_s - \gamma_f} (h_f(i+1,j) - h_f(i,j)) \qquad (24)$$

$$\xi(i,j+1) = \xi(i,j) + \frac{\gamma_f}{\gamma_s - \gamma_f} (h_f(i,j+1) - h_f(i,j)) \qquad (25)$$

Equations (24) and (25) are the equations used in the model to evaluate the interface location.

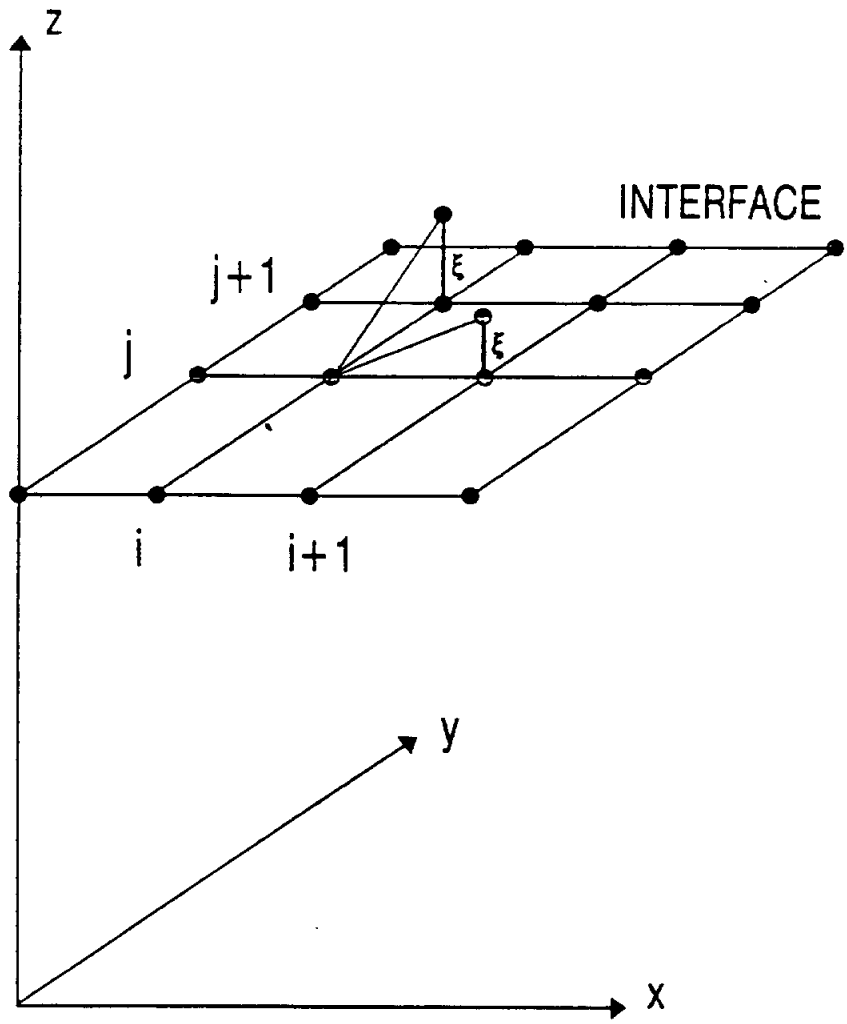

Figure 3. Representation of the interface by nodes.

Finite Element Equations

Because equations (8) and (9) have the same form, but written for different variables and parameters, we can develop the finite element equations only for a general type of equation.

In this step, we have to derive an integral formulation for the governing groundwater flow equations. This integral formulation leads to a system of algebraic equations which can be solved for values of piezometric head at each node in the mesh. To derive the integral formulation, the method of weighted residuals is used. This is a general approach widely used in the finite element modeling.

The Method of Weighted Residuals

In the method of weighted residuals, an approximate solution to the boundary value problem is defined. When this approximate solution is substituted into the governing differential equation, a residual error occurs at each point

in the problem domain. The weighted average of the residuals for each node in the finite element mesh is forced to be equal to zero.

Consider a differential equation of the form

$$L(h(x,y,z)) = 0 \qquad (26)$$

where L is the differential operator, and h is the field variable. An approximate solution $\hat{h}$ can be defined in the form

$$\hat{h}(x,y,z) = \sum_{i=1}^{m} N_i(x,y,z)\, h_i \qquad (27)$$

where N_i = the interpolation functions,

h_i = the unknown values of the field variable at the nodes, and

m = the number of nodes in the mesh.

When the approximate solution is substituted into equation (26), the differential equation is no longer satisfied exactly, and a residual error R is generated.

$$L(\hat{h}(x,y,z)) = R(x,y,z) \neq 0 \qquad (28)$$

The residual varies from point to point within the problem domain, therefore, the residual cannot be forced to be zero at certain specified points because it may then become unacceptable large elsewhere in the problem domain (Istok, 1989). For this reason, in the method of weighted residuals, the weighted average of the residuals at the nodes is forced to be equal to zero.

$$\int\int_D\int W(x,y,z)\ R(x,y,z)\ dD = 0 \qquad (29)$$

where W is a weighing function, and D represents the problem domain. Substituting equation (28) into equation (29) we have for the three-dimensional case

$$\iiint_D W(x,y,z)\, L(\hat{h}(x,y,z))\, dD = 0 \qquad \textbf{(30)}$$

The approximate solution $\hat{h}$ was defined in equation (27) in terms of some interpolation functions N_i and the unknown values of the field variable at the nodes. This applied over the whole domain under consideration in which m refers to the total number of discrete values or nodes. This concept can be modified subdividing the domain into elements, as shown in Figure 4, the variable value within that subregion can now be defined in terms of discrete values on the boundary or within that region.

In the finite element method, $\hat{h}$ is defined in a piece-wise form over the problem domain. The value of $\hat{h}$ within any element e, $\hat{h}^e$, is given by

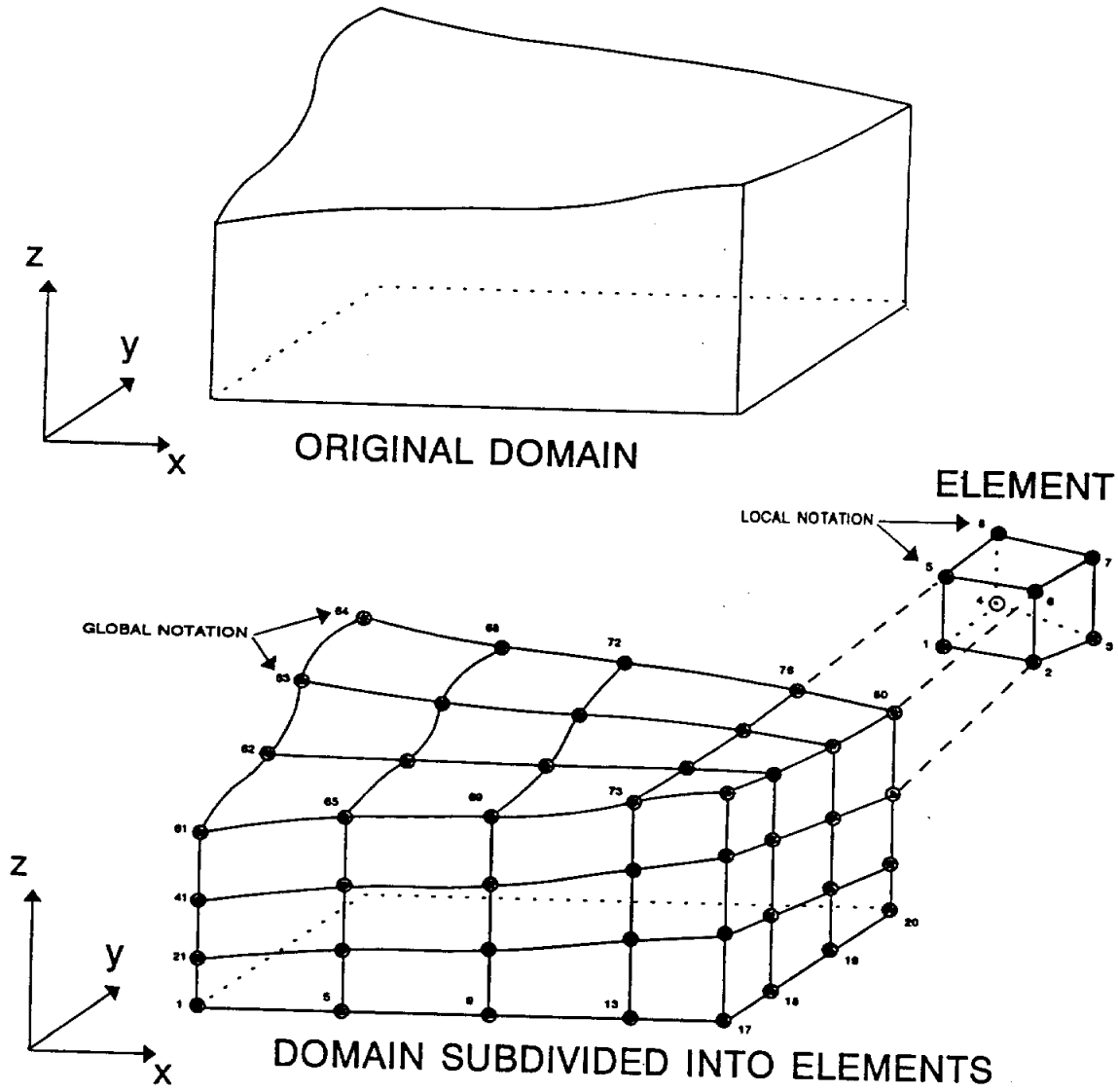

Figure 4. Subdivision of a domain into elements.

$$\hat{h}^e(x,y,z) = \sum_{i=1}^{n} N_i^e \, h_i \qquad (31)$$

where N_i^e = the element interpolation functions, defining one for each node,

h_i = the unknown values of the field variable at each node of the element, and

n = the number of nodes within the element.

The residual now becomes,

$$R(x,y,z) = L(\hat{h}^e(x,y,z)) \qquad (32)$$

such that equation (29) can be rewritten as

$$\iiint_D W(x,y,z) \, L(\hat{h}^e(x,y,z)) = 0 \qquad (33)$$

Substituting the representative form of equations (8) or (9) into equation (33), and assuming that the weighing functions for a node are identical to the interpolation functions used to define the approximate solution $\hat{h}$ (Galerkin method), we get

$$\frac{\gamma}{\mu}\int\int\int_D N_j(x,y,z)\,(\nabla\cdot([k]\cdot\nabla\hat{h}^e))\,dD = 0 \qquad (34)$$

where we have assumed that the specific weight and the viscosity of the fluids are constant within each domain D_1 and D_2.

Because the second derivative of the approximate solution is not defined for most type of elements, Green's theorem can be used to reduce the order of the derivatives of $\hat{h}^e$ appearing in equation (34). The Green's theorem states:

$$\int\int\int_D F(\nabla\cdot\vec{G})\,dD = \int\int_A F(\vec{G}\cdot\hat{n})\,dA - \int\int\int_D \vec{G}\cdot\nabla F\,dD \qquad (35)$$

where D = the problem domain,

A = the area of the boundary of such domain, and

$\hat{n}$ = a unit vector normal to the surface A.

Defining $\vec{F} = N_j$, and $\vec{G} = [k]\nabla\hat{h}^e$, then equation (34) can be written as

$$\frac{\gamma}{\mu}\int\int\int_D N_j \nabla\cdot[k]\cdot\nabla\hat{h}^e\, dD =$$

$$\frac{\gamma}{\mu}\int\int_A N_j [k]\cdot\nabla\hat{h}^e\cdot\hat{n}\, dA \; - \; \frac{\gamma}{\mu}\int\int\int_D [k]\cdot\nabla\hat{h}^e\cdot\nabla N_j\, dD \; = \; 0 \qquad (36)$$

Substituting equation (27) into equation (36), we get

$$\frac{\gamma}{\mu}\int\int\int_D [k]\cdot\left(\sum_{i=1}^{m}\nabla N_i\right)\cdot\nabla N_j h_i\, dD \; = \; \frac{\gamma}{\mu}\int\int_A N_j[k]\cdot\left(\sum_{i=1}^{m}\nabla N_i\right)\cdot\hat{n}\, h_i\, dA \qquad (37)$$

or

$$\frac{\gamma}{\mu}\sum_{i=1}^{m}\sum_{j=1}^{m}\int\int\int_D \nabla N_i\cdot[k]\cdot\nabla N_j h_i\, dD \; = \; \frac{\gamma}{\mu}\sum_{i=1}^{m}\sum_{j=1}^{m}\int\int_A [k]\cdot\nabla N_i h_i\, dA \qquad (38)$$

where m is the number of nodes in the mesh.

There is no systematic way of developing reasonable interpolation functions N_i for the approximate function $\hat{h}$. The basic principle of the finite element method is that the interpolation functions N_i can be defined piecewise over subregions of the domain called finite elements, and that over any subdomain, the interpolation functions N_i can be chosen to be very simple functions such as polynomials of low degree. These interpolation functions must be continuous throughout the problem domain. Therefore, we can write equation (38) as made by the contribution of all the elements that form the mesh. In this way, equation (38) can be rewritten as

$$\sum_{e=1}^{NE} \left[\sum_{i=1}^{n}\sum_{j=1}^{n} \frac{\gamma}{\mu} \int\int_{D^e}\int \nabla N_i^e \cdot [k] \cdot \nabla N_j^e \, h_i \, dD^e\right] = \sum_{e=1}^{NE} \left[\sum_{i=1}^{n}\sum_{j=1}^{n} \frac{\gamma}{\mu} \int\int_{A^e} [k] \cdot \nabla N_i^e \, h_i \, dA^e\right] \tag{39}$$

where NE = the number of elements,

D^e = element domain,

A^e = area of the boundary of the element domain, and

n = the number of nodes per element.

The term inside the area integral can be identified as the groundwater flux across the element's surface. For elements on the exterior of the mesh, this term is used to represent specified rates of groundwater flow (Neumann boundary conditions). This term will be positive if water is entering the mesh, and will be zero if no flow is specified. For elements in the interior of the mesh, this term for adjacent elements will have opposite signs, canceling out its contribution for nodes the two elements share (Figure 5). We will refer to this term as the flux vector F_i^e. Equation (39) can now be written as

$$\sum_{e=1}^{NE} \left[\frac{\gamma}{\mu} \sum_{i=1}^{n} \sum_{j=1}^{n} \left(\int\int_{D^e} \int \nabla N_i^e \cdot [k] \cdot \nabla N_j^e \, dD^e \right) h_i \right] = \sum_{e=1}^{NE} F_i^e \qquad (40)$$

For a general element, equation (40) can be written as

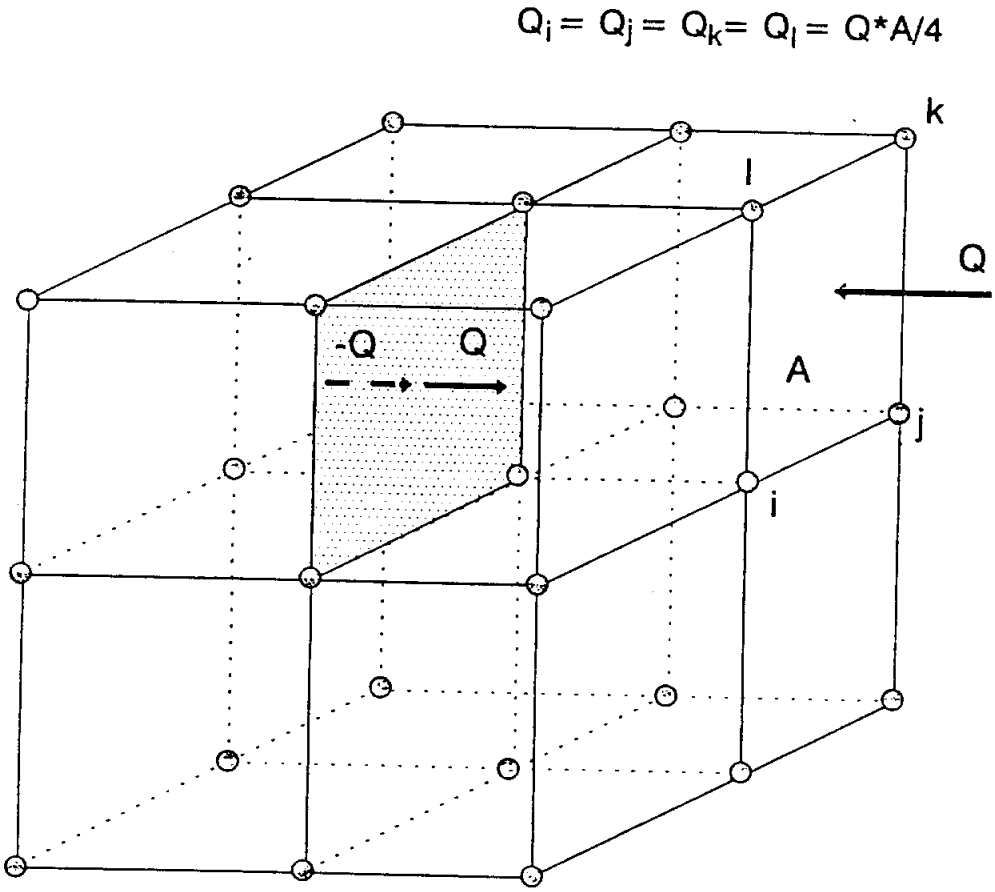

Figure 5. Fluxes through the internal and external faces of the elements with respect to the mesh.

$$\sum_{i=1}^{n}\sum_{j=1}^{n}\frac{\gamma}{\mu}\left(\int\int_{D^e}\int \nabla N_i^e\cdot[k]\cdot\nabla N_j^e\,dD^e\right)h_i \;=\; F_i^e \qquad (41)$$

Although the whole domain can be anisotropic and heterogeneous, the medium within the element is anisotropic but homogeneous, and equation (40) can be written in matrix form as

$$\left[\frac{\gamma}{\mu}\int\int_{D^e}\int\begin{bmatrix}\frac{\partial N_1}{\partial x} & \frac{\partial N_1}{\partial y} & \frac{\partial N_1}{\partial z}\\ \cdot & \cdot & \cdot\\ \cdot & \cdot & \cdot\\ \cdot & \cdot & \cdot\\ \frac{\partial N_n}{\partial x} & \frac{\partial N_n}{\partial y} & \frac{\partial N_n}{\partial z}\end{bmatrix}\begin{bmatrix}k_x & 0 & 0\\ 0 & k_y & 0\\ 0 & 0 & k_z\end{bmatrix}\begin{bmatrix}\frac{\partial N_1}{\partial x} & \cdot\cdot & \frac{\partial N_n}{\partial x}\\ \frac{\partial N_1}{\partial y} & \cdot\cdot & \frac{\partial N_n}{\partial y}\\ \frac{\partial N_1}{\partial z} & \cdot\cdot & \frac{\partial N_n}{\partial z}\end{bmatrix}dx\,dy\,dz\right]\begin{Bmatrix}h_1\\ \cdot\\ \cdot\\ \cdot\\ \cdot\\ h_n\end{Bmatrix}=\begin{Bmatrix}F_1\\ \cdot\\ \cdot\\ \cdot\\ \cdot\\ F_n\end{Bmatrix} \qquad (42)$$

where k_x, k_y, and k_z are the permeabilities in the x, y, and z directions inside the element. Note that the supraindex for

the element e has been suppressed to simplify the notation. In a more simplified way, equation (42) can be written as

$$\underset{n*n}{[M_{ij}]}\ \underset{n*1}{\{h_i\}} = \underset{n*1}{\{F_i\}} \tag{43}$$

where $[M_{ij}]$ is the big matrix defined in equation 42. The contribution of each element, gives rise to the general system of equation

$$\underset{m*m}{[M]}\ \underset{m*1}{\{h_i\}} = \underset{m*1}{\{F_i\}} \tag{44}$$

where

$$\underset{m*m}{[M]} = \sum_{e=1}^{NE} \underset{n*n}{[M^e]} \tag{45}$$

and

$$\underset{m*1}{\{F\}} = \sum_{e=1}^{NE} \underset{n*1}{\{F^e\}} \tag{46}$$

where n is the number of nodes per element, and m is the total number of nodes in the mesh. An example is shown in Figure 6 of the assemblage of the global matrix from the element matrices, for a three elements, and three nodes per element system. How each element contributes to the global matrix can be seen.

In equation (42), after the interpolation functions are defined, the integration must be done for all the elements that form the mesh. The interpolation functions must be continuous along the boundary between adjacent elements, but their first derivatives do not have to be continuous. The interpolation functions should be defined in such a way that makes the solution converges to the true solution as the number of nodes and elements in the mesh increase. The value

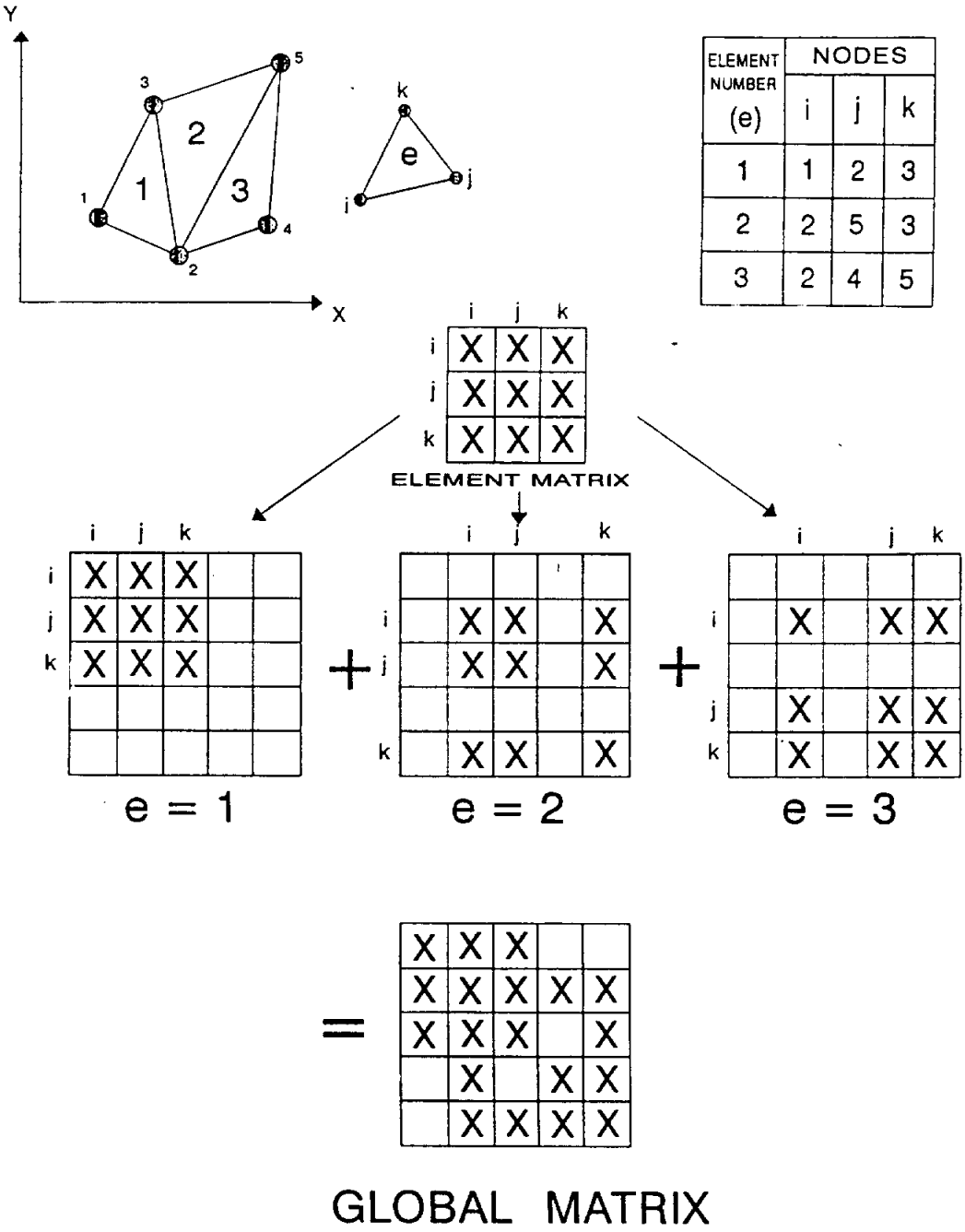

Figure 6. Example of the assemblage of the global matrix from the element matrices.

of all the element interpolation functions sum to one at every point within the element.

In this research work, eight nodes hexahedron isoparametric elements are used. The order of the polynomials used for the shape and interpolation functions are the same.

The integrations in equation (42) are performed numerically. The numerical integration procedure is greatly simplified if the interpolation functions and their derivatives for each node are defined using a local coordinate system. In a local coordinate system, a point within an element is assigned using a coordinate system origin attached to the element (Figure 7). These interpolation functions and their derivatives at each node of the element are given by (Istok, 1989).

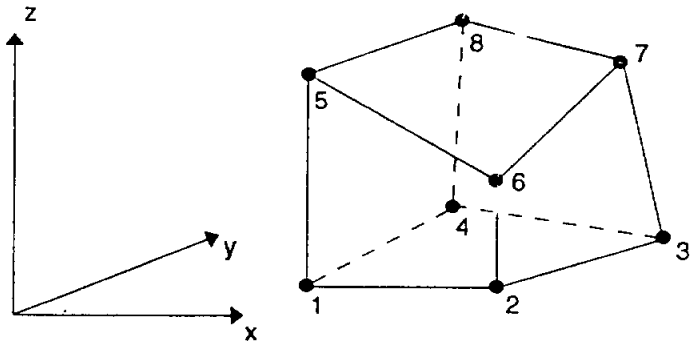

GLOBAL SYSTEM

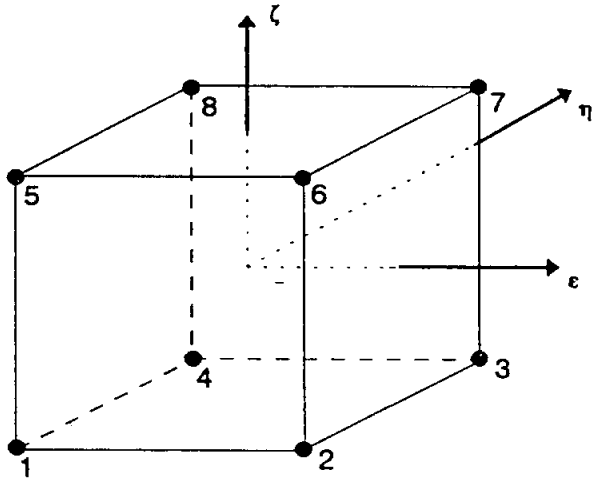

LOCAL SYSTEM

Figure 7. Definition of global and local coordinate systems for the elements.

$$N_i = \frac{1}{8}(1+\varepsilon_i\varepsilon)(1+\eta_i\eta)(1+\zeta_i\zeta)$$

$$\frac{\partial N_i}{\partial \varepsilon} = \frac{\varepsilon_i}{8}(1+\eta_i\eta)(1+\zeta_i\zeta)$$

$$\frac{\partial N_i}{\partial \eta} = \frac{\eta_i}{8}(1+\varepsilon_i\varepsilon)(1+\zeta_i\zeta) \qquad (47)$$

$$\frac{\partial N_i}{\partial \zeta} = \frac{\zeta_i}{8}(1+\varepsilon_i\varepsilon)(1+\eta_i\eta)$$

where the coefficients ϵ_i, η_i, and ζ_i for each node i are given in Table 1.

TABLE 1

Node i	1	2	3	4	5	6	7	8
ϵ_i	-1	1	1	-1	-1	1	1	-1
η_i	-1	-1	1	1	-1	-1	1	1
ζ_i	-1	-1	-1	-1	1	1	1	1

The matrix $[M^e]$ from equation (42) can now be written in term of the local coordinate system as

$$[M^{\gamma}] = \frac{\gamma}{\mu}\int_{-1}^{1}\int_{-1}^{1}\int_{-1}^{1}\begin{bmatrix} \frac{\partial N_1}{\partial \varepsilon} & \frac{\partial N_1}{\partial \eta} & \frac{\partial N_1}{\partial \zeta} \\ . & . & . \\ . & . & . \\ . & . & . \\ \frac{\partial N_8}{\partial \varepsilon} & \frac{\partial N_8}{\partial \eta} & \frac{\partial N_8}{\partial \zeta} \end{bmatrix}[J^{-1}]^T\begin{bmatrix} k_x & 0 & 0 \\ 0 & k_y & 0 \\ 0 & 0 & k_z \end{bmatrix}[J^{-1}]\begin{bmatrix} \frac{\partial N_1}{\partial \varepsilon} & . & . & \frac{\partial N_8}{\partial \varepsilon} \\ \frac{\partial N_1}{\partial \eta} & . & . & \frac{\partial N_8}{\partial \eta} \\ \frac{\partial N_1}{\partial \zeta} & . & . & \frac{\partial N_8}{\partial \zeta} \end{bmatrix}|J|\,d\varepsilon\,d\eta\,d\zeta \tag{48}$$

where the Jacobian [J] is defined as

$$[J] = \begin{bmatrix} \frac{\partial N_1}{\partial \varepsilon} & . & . & . & \frac{\partial N_8}{\partial \varepsilon} \\ \frac{\partial N_1}{\partial \eta} & . & . & . & \frac{\partial N_8}{\partial \eta} \\ \frac{\partial N_1}{\partial \zeta} & . & . & . & \frac{\partial N_8}{\partial \zeta} \end{bmatrix}\begin{bmatrix} x_1 & y_1 & z_1 \\ . & . & . \\ . & . & . \\ . & . & . \\ x_8 & y_8 & z_8 \end{bmatrix} \tag{49}$$

and the inverse of the Jacobian is given by

$$[J^{-1}] = \frac{1}{|J|}\begin{bmatrix} \frac{\partial y}{\partial \eta} & -\frac{\partial x}{\partial \eta} & \frac{\partial z}{\partial \eta} \\ -\frac{\partial y}{\partial \varepsilon} & \frac{\partial x}{\partial \varepsilon} & -\frac{\partial z}{\partial \varepsilon} \\ \frac{\partial y}{\partial \zeta} & -\frac{\partial x}{\partial \zeta} & \frac{\partial z}{\partial \zeta} \end{bmatrix} \qquad (50)$$

where |J| is the determinant of the Jacobian, which should be positive in order to assure a proper transformation. If the determinant of the Jacobian is zero, it indicates that the volume of the considered element has degenerated into a plane or an area. If it is negative, it indicate that the element has been turned inside out. Geometrically, a positive value of |J| gives the ratio of volumes between the real element volume and the transformed one.

The derivatives of each element in equation (50) are

$$\frac{\partial x}{\partial \varepsilon} = \sum_{i=1}^{8} x_i \frac{\partial N_i}{\partial \varepsilon} \quad ; \quad \frac{\partial x}{\partial \eta} = \sum_{i=1}^{8} x_i \frac{\partial N_i}{\partial \eta} \quad ; \quad \frac{\partial x}{\partial \zeta} = \sum_{i=1}^{8} x_i \frac{\partial N_i}{\partial \zeta}$$

$$\frac{\partial y}{\partial \varepsilon} = \sum_{i=1}^{8} y_i \frac{\partial N_i}{\partial \varepsilon} \quad ; \quad \frac{\partial y}{\partial \eta} = \sum_{i=1}^{8} y_i \frac{\partial N_i}{\partial \eta} \quad ; \quad \frac{\partial y}{\partial \zeta} = \sum_{i=1}^{8} y_i \frac{\partial N_i}{\partial \zeta} \qquad (51)$$

$$\frac{\partial z}{\partial \varepsilon} = \sum_{i=1}^{8} z_i \frac{\partial N_i}{\partial \varepsilon} \quad ; \quad \frac{\partial z}{\partial \eta} = \sum_{i=1}^{8} z_i \frac{\partial N_i}{\partial \eta} \quad ; \quad \frac{\partial z}{\partial \zeta} = \sum_{i=1}^{8} z_i \frac{\partial N_i}{\partial \zeta}$$

where x_i, y_i, and z_i are the coordinates of the element nodes with respect to the real coordinate system. Details about the mathematics of the element transformation are given in Becker et al., 1981.

The numerical integration process is carry out using a direct formula, derived from the method of Gauss quadrature, which in three dimensions can be stated as (Dhatt and Touzot, 1984)

$$\int_{-1}^{1}\int_{-1}^{1}\int_{-1}^{1} f(\varepsilon,\eta,\zeta)\, d\varepsilon\, d\eta\, d\zeta = \sum_{i=1}^{r} w_i\, f(\varepsilon_i,\eta_i,\zeta_i) \qquad (52)$$

This formula is capable of integrating monomials $\epsilon^i\eta^j\zeta^k$ exactly, provided that $i+j+k \leq m$, where m is the maximum order of the monomials. From the definition of the interpolation functions (equations 47), it is shown that the resulting monomials inside the integral in equation (48) are not greater than three, therefore, m=3 was considered appropriate for the present model. The order m, the number of integration points r, the coordinates ϵ_i, η_i, and ζ_i, and the weight used in this model are given in Table 2.

TABLE 2

Order m	Number of Integration Points r	Coordinates ϵ_i	η_i	ζ_i	weight w_i
3	6	1	0	0	4/3
		-1	0	0	
		0	1	0	
		0	-1	0	
		0	0	1	
		0	0	-1	

Mean Permeabilities for the Elements

One of the main capabilities of the model is that it can handle very anisotropic and heterogeneous media.

As it was shown in the scheme of solution, during the iterative process, the location of both the interface and the phreatic surface are shifted from their initial location to a new location dictated by the boundary conditions given by equations (11) and (14). During this process, the mesh is recalculated, and there will be elements that can intersect more than one layer with different geologic characteristics. In the finite element approach, values of permeabilities in x, y, and z directions must be assigned to each element. A new methodology was developed to evaluate what is called a weighted permeability for each element. This method consist of taking one element at a time, finding in which layer, each of the nodes of the considered element is located. Then the four faces of the element parallel to x and y directions are considered separately, as it is shown in Figure 8. For each of these faces, equivalent thicknesses b_i are calculated in such

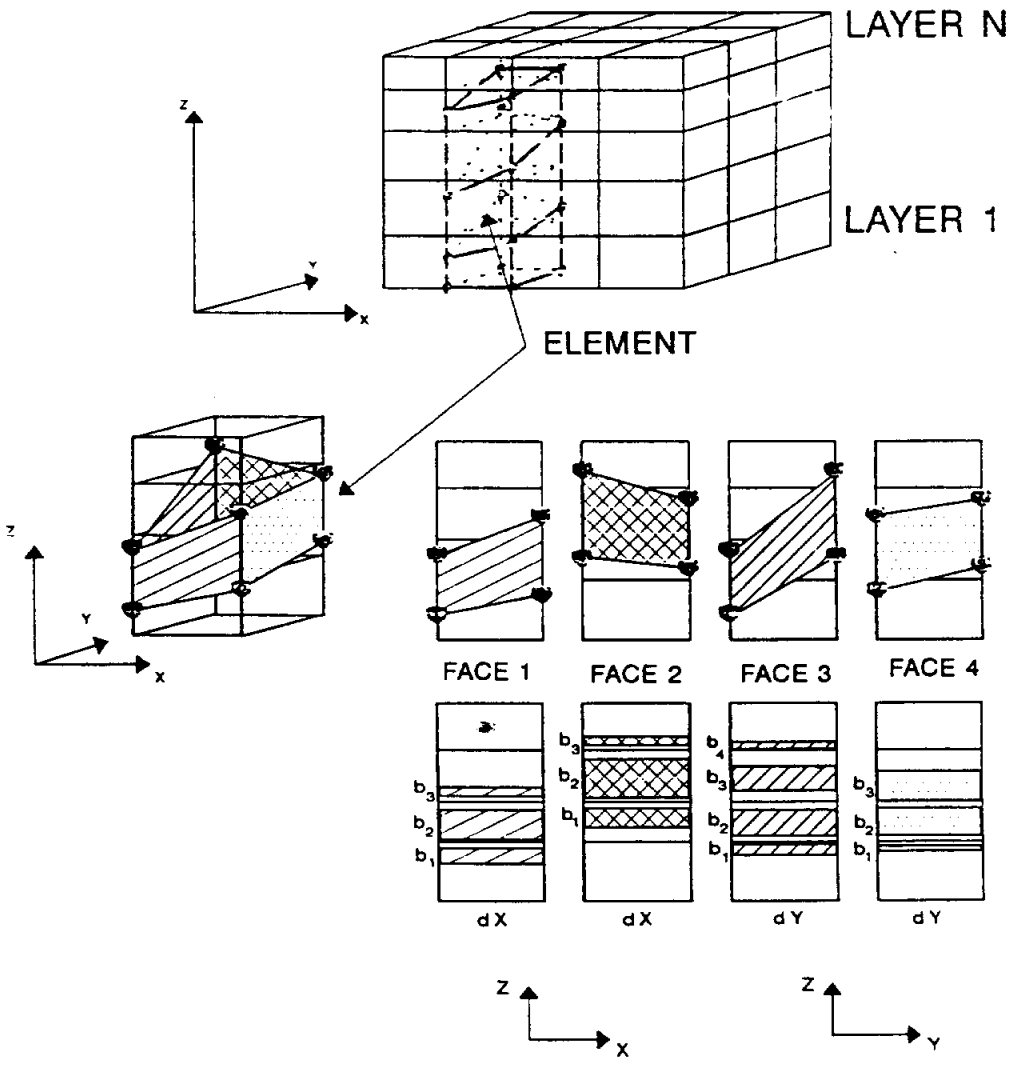

Figure 8. Definition of the faces of an element, used to calculate the weighted permeability of the element.

a way that the area b_i*d, where d can be either dx or dy, is equal to the intersection area between the face and each of the layers. After the areas are determined for each face, then the horizontal and vertical permeabilities are calculated using the relations for equivalent permeability for flow parallel to the layers, and for equivalent permeability for flow perpendicular to the layers, respectively.

$$k_H = \frac{\sum_i^{NL} k_{Hi} b_i}{\sum_i^{NL} b_i} \quad ; \quad k_V = \frac{\sum_i^{NL} b_i}{\sum_i^{NL} \frac{b_i}{k_{Vi}}} \qquad (53)$$

where NL = number of intersected layers of each face,

k_H = horizontal permeability (x or y, depending upon which face is being considered), and

k_V = permeability in the z direction.

Finally, the permeability in the x direction for each element is evaluated as the mean value of the permeabilities calculated for faces 1 and 2. Similarly, the permeability in

the y direction is evaluated as the mean value of the permeabilities calculated for the faces 3 and 4. The permeability in the z direction for each element is evaluated as the mean value of the permeabilities in the z direction calculated for the four faces.

Automatic Mesh Generation

One cumbersome aspect of the application of the finite element method to solve a specified problem is the preparation of the input data. The input data consist of a description of the element mesh topology. The node numbers and the coordinates of the node points, along with the element numbers and the node numbers associated with each element, have to be provided to the computer program. This process is normally tedious if it is done by hand, even for small grid. When working with three-dimensional models, this task takes on major proportions, because the finite element mesh in these cases normally contains hundred or thousands of nodes.

In the specific case of the model developed in this research, the automatic mesh generation became necessary, because during the iterative process used to find the solution of the problem, the water table and the interface have to move in order to accomplish the boundary conditions imposed on them. The water table and the interface are represented by surfaces made of nodes, and when these nodes change their

positions, the rest of the nodes of the mesh also move. This means that the mesh can contract or expand accordingly with the new locations of the water table and the interface.

A simple automatic mesh generation algorithm was developed, in order to handle the situation already mentioned. Although several types of three-dimensional elements can be used to develop three-dimensional grids, the simple linear parallelepiped element was used, because it makes the calculation of the mean permeability of each element easier, when it intersects more than one layer.

The algorithm with different values of increments along the three coordinates axes will generate the grid as shown in Figure 9. For simplicity, the nodes are allowed to move only along the z coordinate. In the case of constant density model, a parameter called LIMIT was introduced, to tell the program that the nodes below the plane of nodes given by this parameter will remain at the same original location during the iterative process. This is advantageous in the case we know that the drawdown of the water table will not reach the z coordinates values of the plane of nodes given by the LIMIT

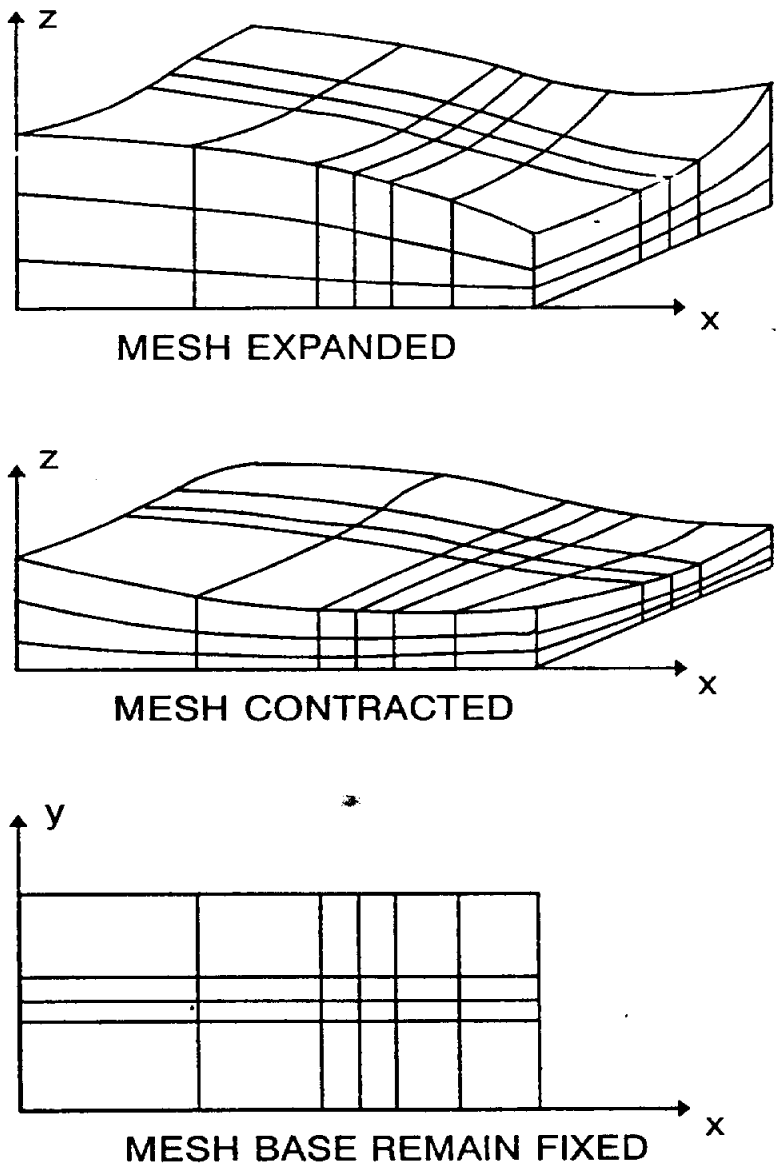

Figure 9. Automatic mesh generation.

parameter. In this way, the permeabilities of the elements located below this plane do not have to be recalculated, making the permeabilities values of these element more accurate, and saving execution time. In two densities mode, this parameter is not used because of the presence of the interface.

IMPLEMENTATION OF THE THEORY

Boundary Conditions

The theoretical statement of the boundary conditions were discussed in the theoretical development section. In this section, how the different types of boundary conditions can be handled with the finite element method will be discussed.

Dirichlet Boundary Conditions

Dirichlet boundary conditions refers to a boundary condition in which the values of the variable, in this case the piezometric head, is assigned to some points on the boundary of the problem domain. Because we are using the iterative Gauss-Seidel method to solve the resulting system of equations, the equations whose head values are known, are simply excluded from the iterations. To accomplish this process, a code (HEADCODE) is defined. Specifically, for those nodes in which the piezometric head is known, HEADCODE≥2, the

corresponding equation is excluded from the iterations.

Neumann Boundary Conditions

Neumann boundary condition refers to a boundary condition in which the values of the derivatives of the variable or fluxes are assigned to some of the nodes (eg. wells) or faces of the elements (eg. recharge or infiltration).

In the case we are simulating wells, the screened area of the well is simulated as a group of nodes, such that the sum of the flux values assigned to each node is equal to the flux value assigned to the well (Figure 10). In finite element, these fluxes values are easily assigned to each node. In equation (40), we showed that the right hand side vector (F_i) represents a flux vector in which each of its components is the flux representative of each of the nodes. Similar to the Dirichlet boundary condition case, a code (in this case, FLUXCODE) is defined. Specifically, for those nodes in which the flux is known, FLUXCODE≥2, then the corresponding flux vector component is assigned. For those nodes with no flux,

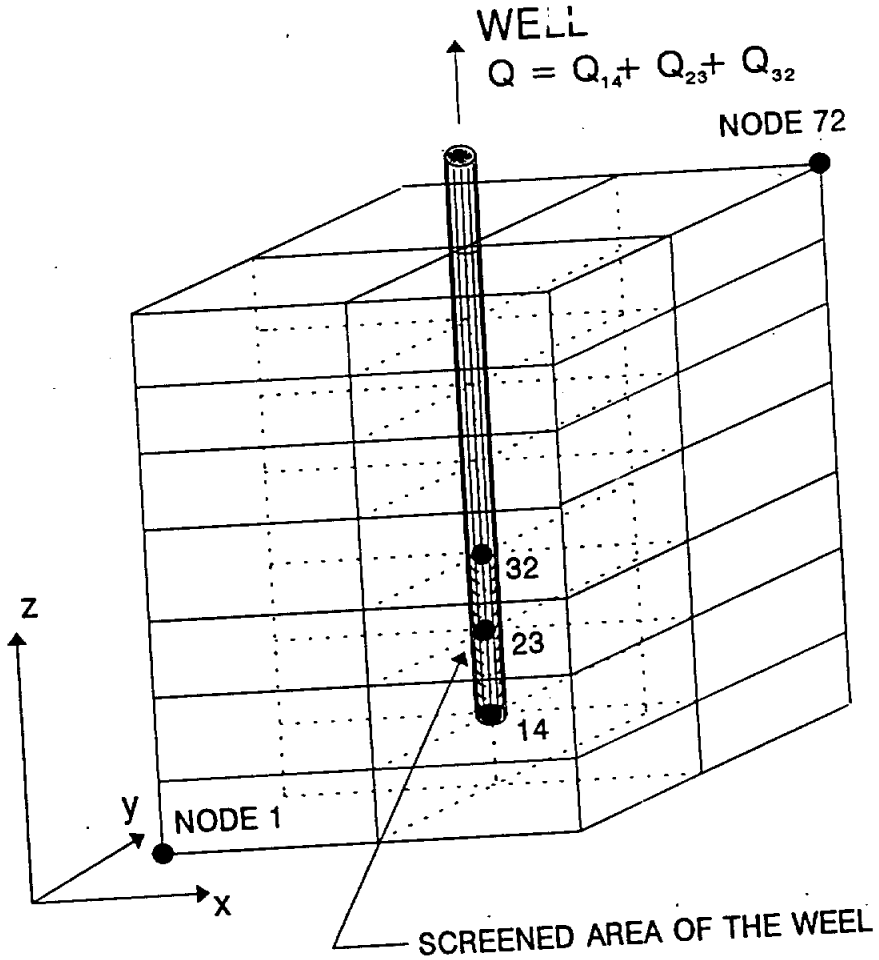

Figure 10. Representation of a well in the model.

then FLUXCODE=0 is assigned.

In the case we are simulating recharge or infiltration values, the treatment is a little different. This is because infiltration values are normally given values of length per unit time, per unit area. Therefore, these values have to be convert to flux values on the nodes. This is accomplished by multiplying the infiltration value (units L/T) of a specific element of the mesh by the corresponding area, and then the resulting value is divided by 4 which is the number of nodes that define one face of the hexahedrical element used in the model.

The introduction of flux and infiltration boundary conditions is done by subroutine Ensam.

When boundaries like the water table and the interface are considered, special treatment is required because these are boundaries where Dirichlet and Neumann boundary conditions are specified. The treatment of these boundaries is explained in the section about iterative process.

Iterative Process

From the Theoretical Development section, Development of the Governing Equations, it was found that the piezometric head variable appears in the boundary condition equations. On the other hand, the problem can not be solved unless the location of the water table and the interface, and the boundary conditions on them are known. This fact makes it necessary to use an iterative procedure to find the solution of the problem. Mathematically, the two boundary conditions on the water table, equations (14) and (15), and the two boundary conditions on the interface, equations (11) and (13), compensate the lack of information on the location of these boundaries, making the problem solvable.

In the iterative procedure, the location of the water table is updated in each step. An initial estimate for the location of this surface is first introduced. The water table is then considered as a stream surface (impermeable boundary), with unknown head distribution. The distribution of the piezometric head in the interior of the domain, and on its

boundary is calculated. This lead to values for the piezometric head at the water table and at the interface nodes. The head values on the water table can then be compared with the elevation of those points. These values, especially at the beginning of the process, will not be the same, and a new position for the water table can be assumed taking $z=h_1$ (equation 14). This process continue until the absolute values of the differences between the old and the new locations of the water table be less than some specified error. After each iteration, the water table is shifted to its new location, then the mesh is recalculated, and the permeabilities of the elements are evaluated again.

After the water table reaches the final location, the piezometric head values of those nodes that represent the interface, are used together with the boundary conditions on the interface, equations (24) and (25), to calculate the interface location under the dynamic conditions present in the system.

The evaluation of the location of the interface in the way already explained, is valid only for small changes in the

elevation of the interface. This is because the location of the interface is not updated each time the location of the water table is updated. Nevertheless, because of small variations on the water table which normally produce high variations on the interface, it is expected that the internal values of the piezometric head inside the domain should not change too much, making the approach a good approximation to evaluate the interface location.

Pointer Matrix and Gauss-Seidel Algorithm

Computer memory is used very inefficiently if all coefficients of the matrix M are really stored, because most of them are zeros. In fact, a coefficient in the position described by row i and column j is different from zero only if nodes i and j occur jointly in at least one element. When hexahedrons with eight nodes are used to represent the element, a specific node can be surrounded by no more than 26 other nodes, as it is shown in Figure 11. Therefore, adding an additional position for the considered node itself, no more than 27 elements on each row of the matrix are different from zero. Thus, most of the memory is used to store zeros, and most of the calculations involve multiplications by zero.

A pointer matrix (Bear and Verruijt, 1987) is a matrix of integers describing the position of the nonzeros in the matrix, and can be used to eliminate most of the waste of memory and computation time.

For the hexahedral elements mentioned before, each interior node is connected with other 26 nodes. If the grid has N nodes or degrees of freedom, then the pointer matrix

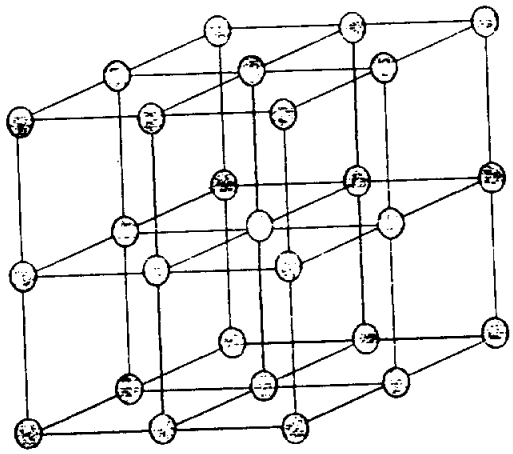

SURROUNDING NODES= 26

LOCATION FOR THE NODE ITSELF= 1

LOCATION FOR {f} ON THE ROW= 1

NUMBER OF COLUMS FOR
MATRICES [K]$_{ss}$ AND [POINTER] = 26

LINEAR HEXAHEDRONS ELEMENTS

Figure 11. Elements represented by hexahedrons with eight nodes, and showing that one node can be surrounded by no more than 26 other nodes.

will be a matrix of N rows and 28 columns, 26 columns for the surrounding nodes, 1 for the node itself, and the last column is used to store the number of nonzero elements of each row.

Once the pointer matrix has been generated, the nonzero coefficients of the matrix M can be store in a matrix of the same size than the pointer matrix, in which the last column is used to store the vector of data or flux vector F. Figure 12 shows an example of using a pointer matrix to reduce the size of a general matrix $[K]_{old}$, building an equivalent smaller matrix $[K]_{new}$. Using the pointer matrix, the memory requirement is greatly reduced, specially for large systems. If we are dealing with a system of 10000 nodes, and one degree of freedom per node, represented by a square matrix of size 10000 by 10000 (Figure 13), and assuming that a real number uses 4 bytes, and an integer number 2 bytes, then the total memory requirement for the original matrix M is $10,000*10,000*4 = 4*10^8$ bytes. Using the pointer matrix, the total memory would be $10,000*28*4 = 1.12*10^6$ bytes for the new matrix M, and $10,000*28*2 = 5.6*10^5$ bytes for the pointer matrix, giving a total of $1.68*10^6$ bytes for both matrices. The use of the pointer matrix in this case represents a reduction in memory

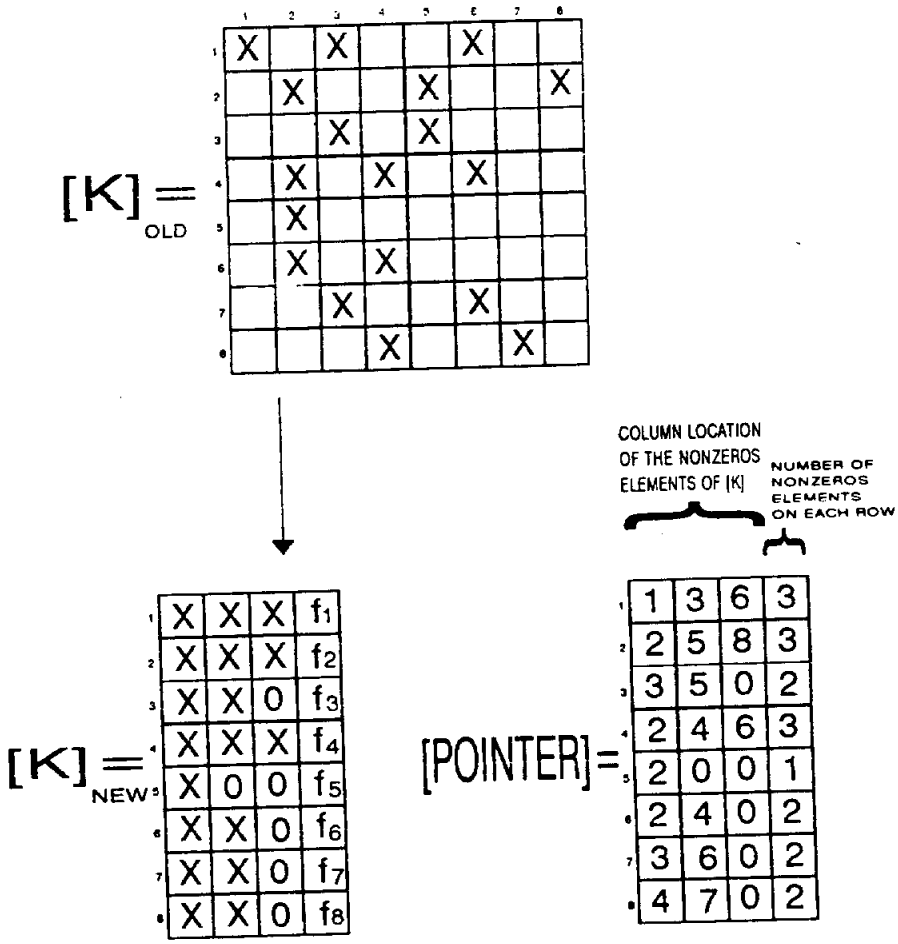

Figure 12. Example of using a pointer matrix to reduce the size of a general matrix $[K]_{old}$.

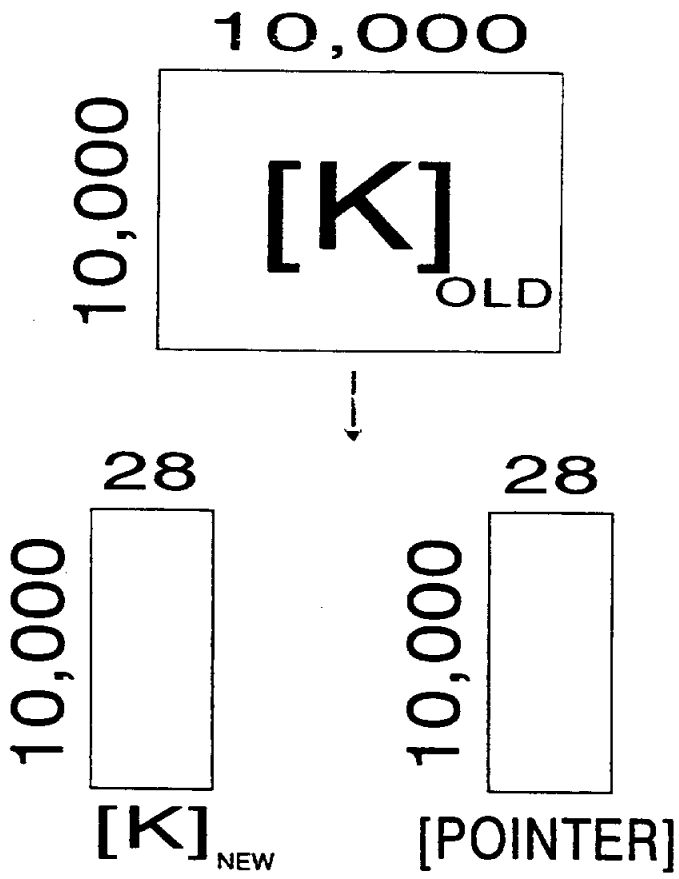

Figure 13. Representation of the matrix $[K]_{old}$ of size 10000*10000, the pointer matrix [POINTER], and the reduced matrix $[K]_{new}$.

requirements of about 99.58%. Additionally, computation time is also saved because most of the multiplications by zeros are not done.

The pointer matrix is built only from the data given by the connectivity matrix NG(number of elements, number of nodes per element), and assigning the number of columns of this matrix NP, which in our case, as was already explained is 28. This task is done by the subroutine Pointer.

The Gauss-Seidel method is used together with the pointer matrix to build the algorithm of solution of the resulting system of equations. Details about this method and its behavior for the different types of systems of equations that can be solved are given by Carnahan et al., 1969.

RESULTS OF MODEL TESTING

The model was run to achieve three objectives, verification, sensitivity analysis, and application. The accuracy of the model was tested using analytical solutions of simple cases for several conditions. This verification process confirmed that the model works properly. The sensitivity of the model to various input parameters was also tested. The major parameters examined were grid spacing, errors of the solution process, and the relative sizes of the element sides. Finally, the model was run for the Dove Creek area, in order to determine an appropriate distribution and pumping rates of a set of wells for brine recovery to avoid the brine seep through the ground surface.

Model Verification

The purpose of verifying a model is to show that it will properly simulate physical situations. Known responses under specific conditions are given by analytical solutions and

experimental data. For flow through porous media, analytical solutions are usually solutions to simple problems, such as homogeneous and isotropic media, one or two dimensional problems with simple boundaries. Experimental data sets are usually more complex.

The model developed for constant density of the water was verified using existing analytical solutions for flow between two line sources, leaky aquifer, and flow to a well.

Flow Between Two Line Sources

The flow between two line sources was run for the rectangular dam shown in Figure 14. The piezometric head on the left and right sides of the dam were kept constant at 10 m and 4 m, respectively. The piezometric head distribution in this problem does not depend on the hydraulic conductivity of the medium. The analytical solution is given by Mariño and Luthin, 1982. The grid used for the finite element simulation consisted of thirteen nodes on the x direction and eleven nodes on the z direction. Although five nodes were used along

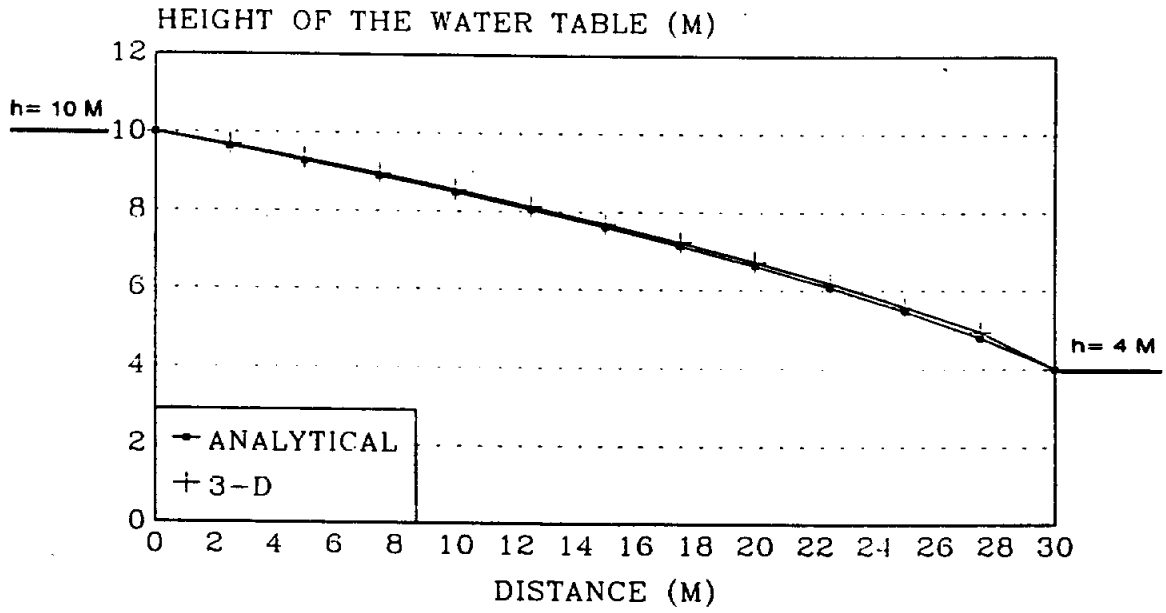

Figure 14. Flow between two line sources through an unconfined aquifer without recharge.

the y direction, only two nodes were necessary because there is no flow in the y direction. The two solution matched very well.

Figure 15 shows the water table distribution for the previous problem, but in this case, a constant recharge rate of 0.4 m/s was introduced. The analytical solution for this problem is given by Mariño and Luthin, 1982. With the velocity option of the model, a mass balance was checked, giving an error of 1 %. Introduction of the recharge term retard the final solution under the same error condition used to stop the iterative processes. The recharge problem required 30 % more computer time than the non recharge problem.

The model was also tested against an analytical solution for flow between two line sources, when the impermeable bottom is inclined. The same grid was used as in the previous cases except the constant head boundary conditions on the left and the right sides were changed to 20 m and 5 m, respectively (Figure 16). The analytical solution for this one-dimensional problem is given by Mariño and Luthin, 1982.

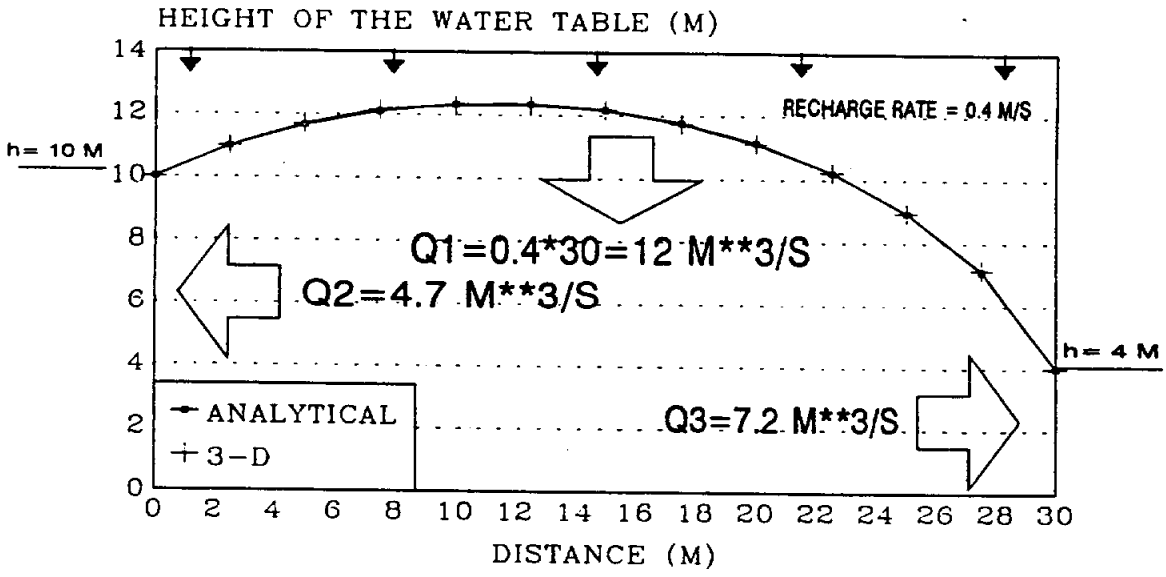

Figure 15. Flow between two line sources through an unconfined aquifer with recharge.

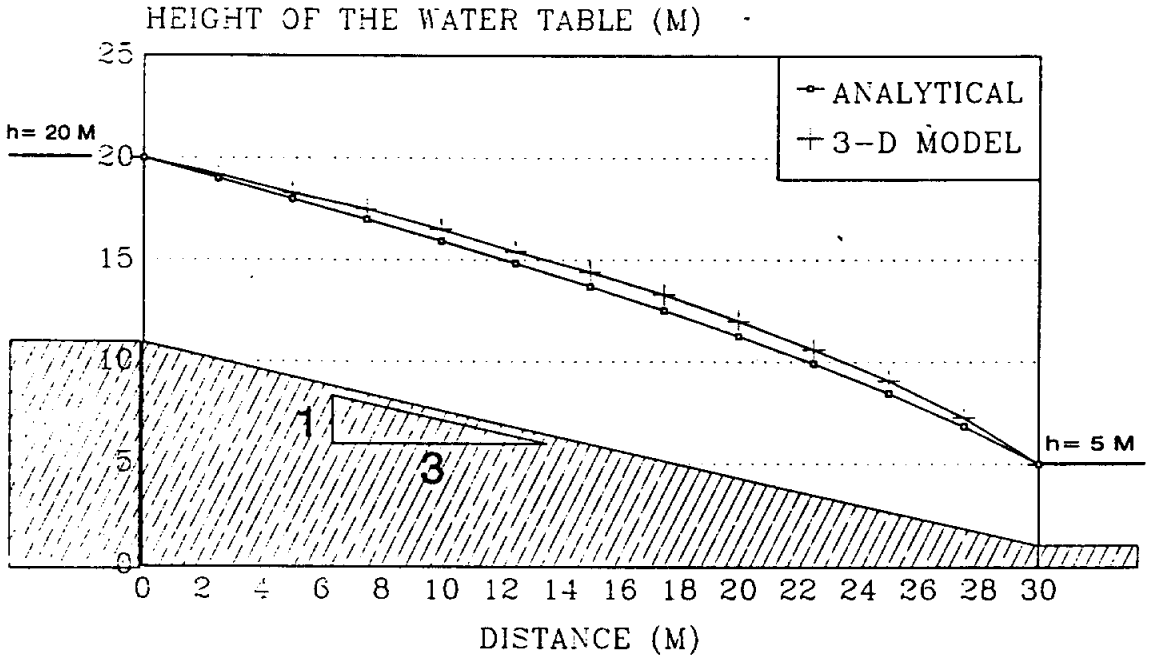

Figure 16. Flow between two line sources through an unconfined aquifer with inclined impermeable bottom.

The final verification of the model for flow between two line sources was for a leaky unconfined-confined aquifer with recharge, shown in Figure 17, for which an analytical solution is also given by Mariño and Luthin, 1982. In this case, a grid with 11 nodes along x axis, 11 nodes along z axis, and 5 nodes along y axis was used. A low permeable layer 2 m thick separates the confined and unconfined aquifers. The rest of the parameters used are given in Figure 17. From this figure it can be seen that the analytical and numerical solutions match very well.

Flow to a Well

In order to verify the model under pumping conditions, a flow to a well problem was chosen. The analytical solution for this problem considering infiltration is also given by Mariño and Luthin, 1982. The problem consist of a well pumping 0.1894 m^3/s from an unconfined isotropic and homogeneous aquifer 30 m thick, and hydraulic conductivity of 0.001 m/s. Due to the cylindrical symmetry of this problem, only one fourth of the

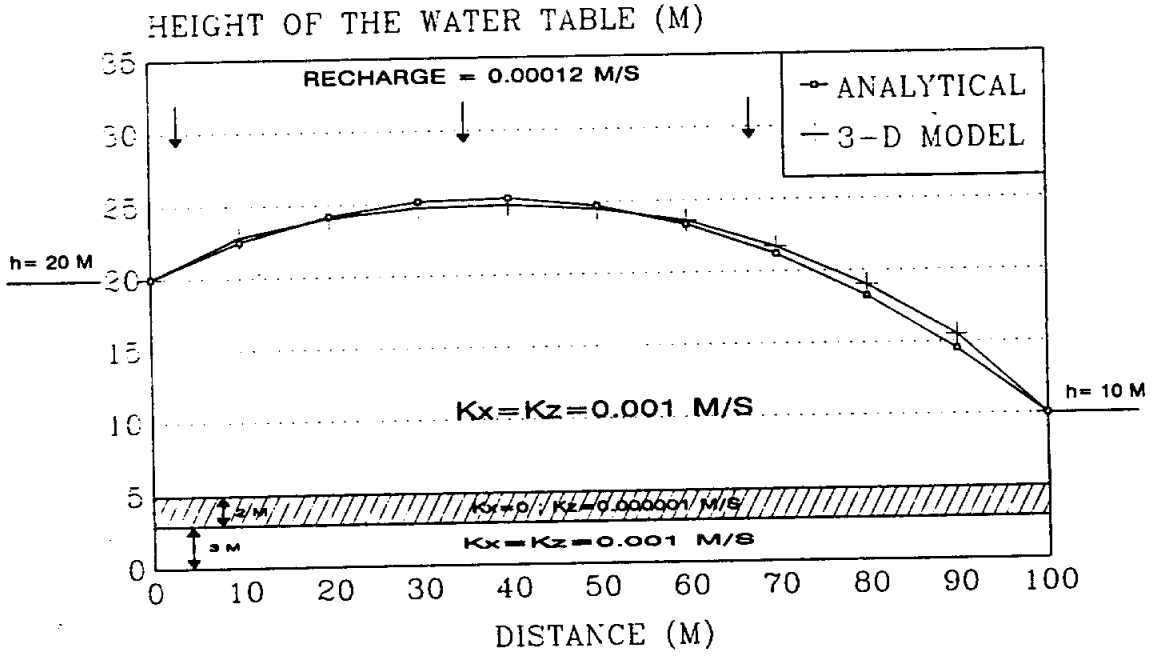

Figure 17. Flow between two line sources through a leaky unconfined-confined aquifer with recharge.

area around the well was simulated as shown in Figure 18. Fluxes through sides A and B were specified as zero, while a constant head of 30 m was specified at sides C and D. The results of the analytical and numerical solutions for infiltration values of zero and 0.0000002 m/s are shown in Figure 19.

The previous analytical and numerical solutions prove the applicability of the numerical model for the cases already mentioned.

Two Density Model

The two density model was tested against an analytical solution for a single well pumping water from a fresh water aquifer which is underlain by a denser salt water, and separated by an abrupt interface. Bear, 1979, used the method of small perturbations to study the time dependent interface upconing. His results are in agreement with field studies carry out by Schmorak and Mercado, 1961. His solution is valid only for relatively small interface rises, approximately less

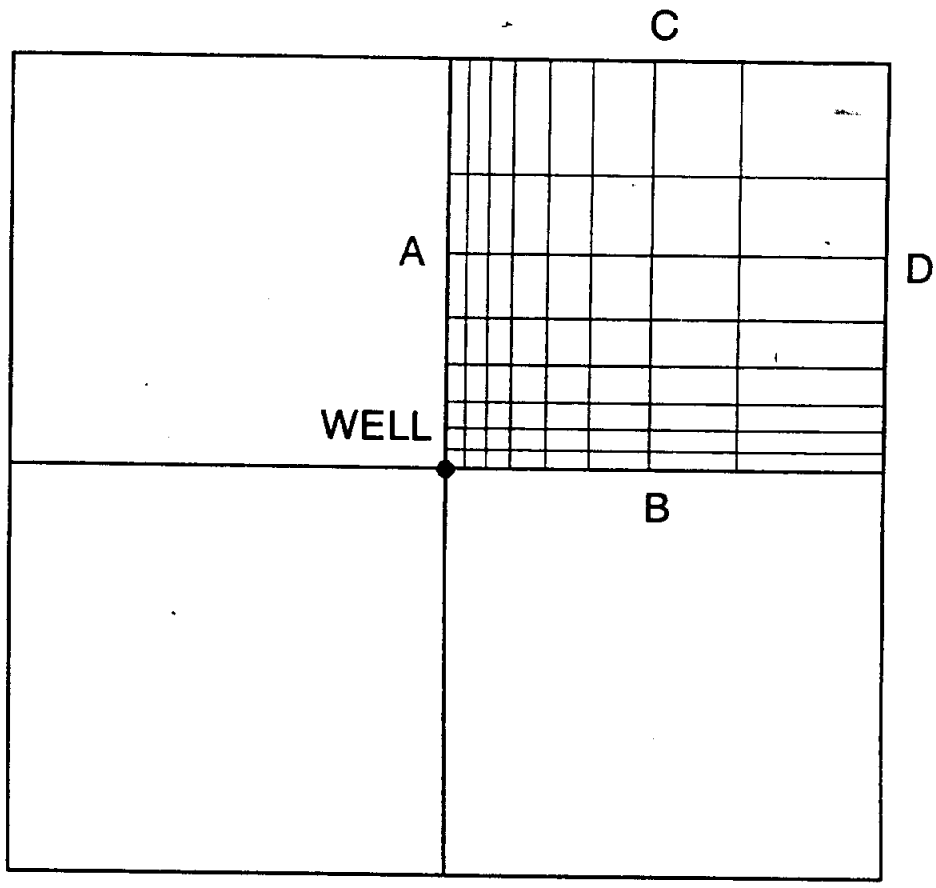

Figure 18. Horizontal part of the grid used to simulate the flow to a well.

than 1/3 the distance from the initial interface to the sink. For steady state conditions, his solution reduces to

$$\xi(r) = \frac{\gamma_f \, Q}{2\pi K (\gamma_s - \gamma_f)(r^2+d^2)^{1/2}} \qquad (54)$$

where γ_f and γ_s are the specific weight of fresh and salt water, respectively, Q is the pumping rate of the well, and K is the hydraulic conductivity of the medium. The elevation of the interface (ξ) with respect to its original location, the elevation difference (d) between the original interface location and the screened area of the well, and the radial distance (r) from the well, are shown in Figure 20.

The simulation consisted of a well pumping fresh water from an aquifer 34 m thick, underlain by salt water, and separated by a sharp interface. The screened length of the well was 1 m, and located between 15 m and 16 m below the original water table. The other parameters used and the analytical and numerical solutions are shown in Figure 21. The finite element grid consisted of 11 nodes along x axis, 11 nodes along y axis, and 9 nodes along z axis. The separation between the nodes from the well to the edges of the grid were

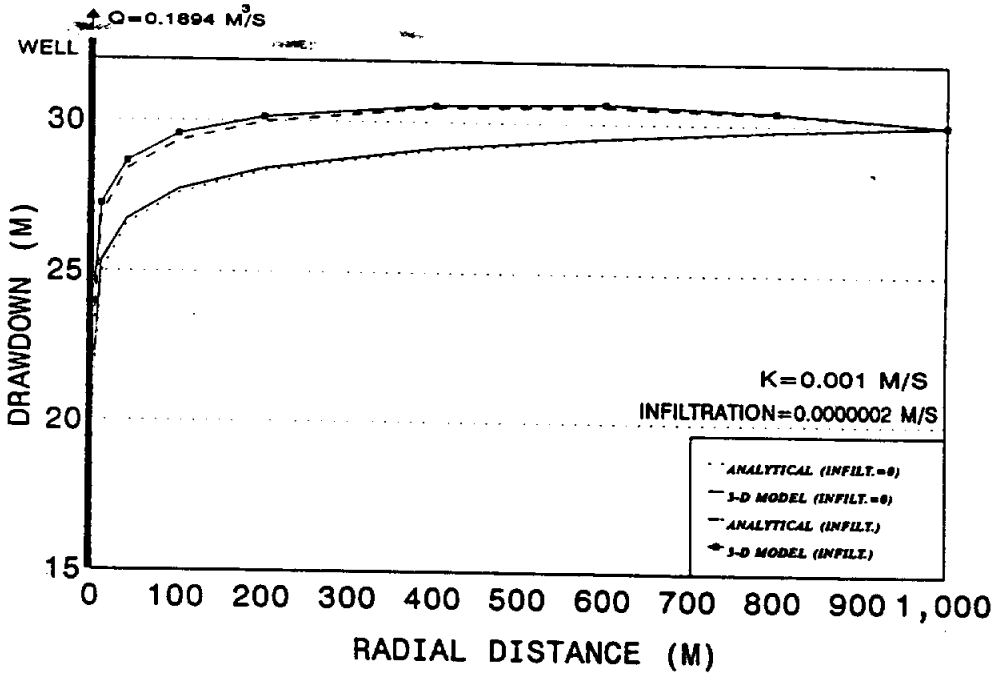

Figure 19. Flow to a well in an unconfined aquifer.

than 1/3 the distance from the initial interface to the sink. For steady state conditions, his solution reduces to

$$\xi(r) = \frac{\gamma_f \, Q}{2\pi K (\gamma_s - \gamma_f)(r^2+d^2)^{1/2}} \qquad (54)$$

where γ_f and γ_s are the specific weight of fresh and salt water, respectively, Q is the pumping rate of the well, and K is the hydraulic conductivity of the medium. The elevation of the interface (ξ) with respect to its original location, the elevation difference (d) between the original interface location and the screened area of the well, and the radial distance (r) from the well, are shown in Figure 20.

The simulation consisted of a well pumping fresh water from an aquifer 34 m thick, underlain by salt water, and separated by a sharp interface. The screened length of the well was 1 m, and located between 15 m and 16 m below the original water table. The other parameters used and the analytical and numerical solutions are shown in Figure 21. The finite element grid consisted of 11 nodes along x axis, 11 nodes along y axis, and 9 nodes along z axis. The separation between the nodes from the well to the edges of the grid were

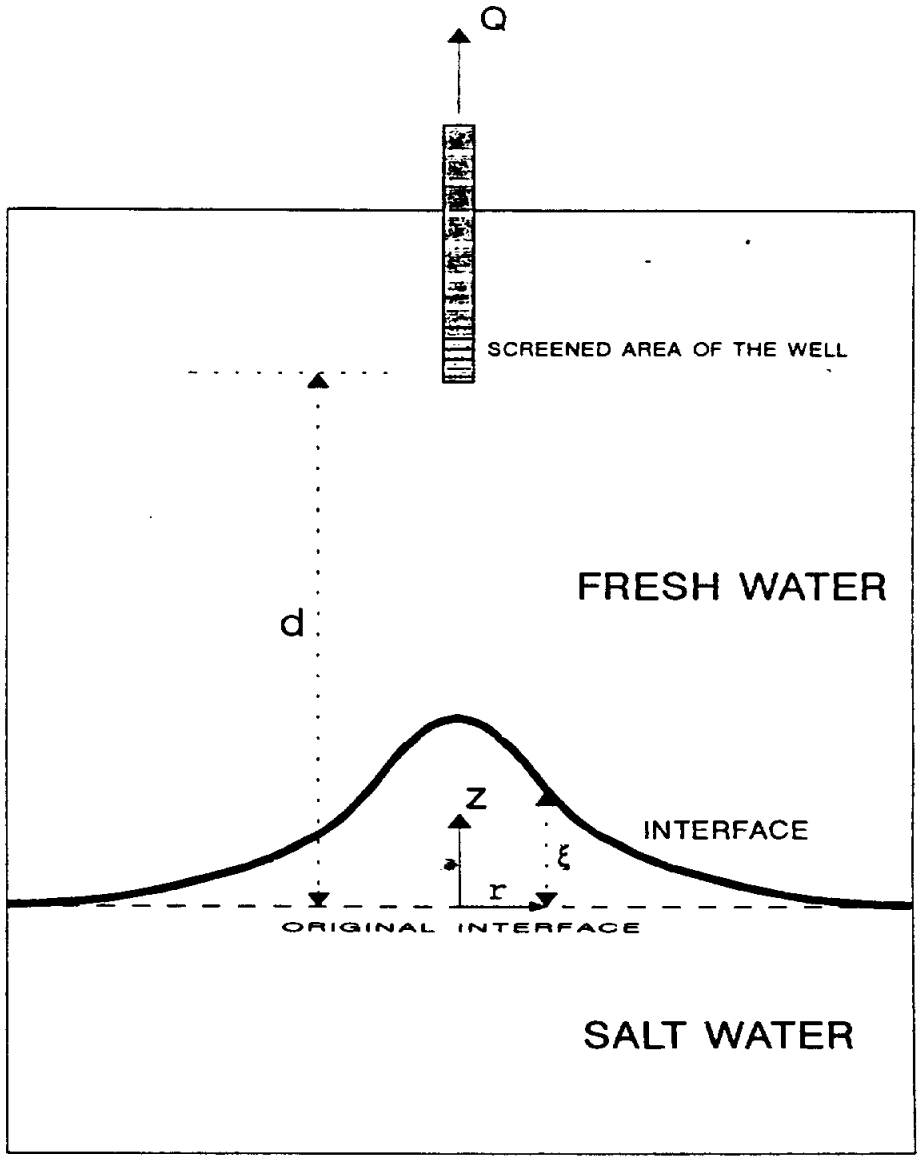

Figure 20. Definition of variables for the upconed interface formula derived by Bear, 1979.

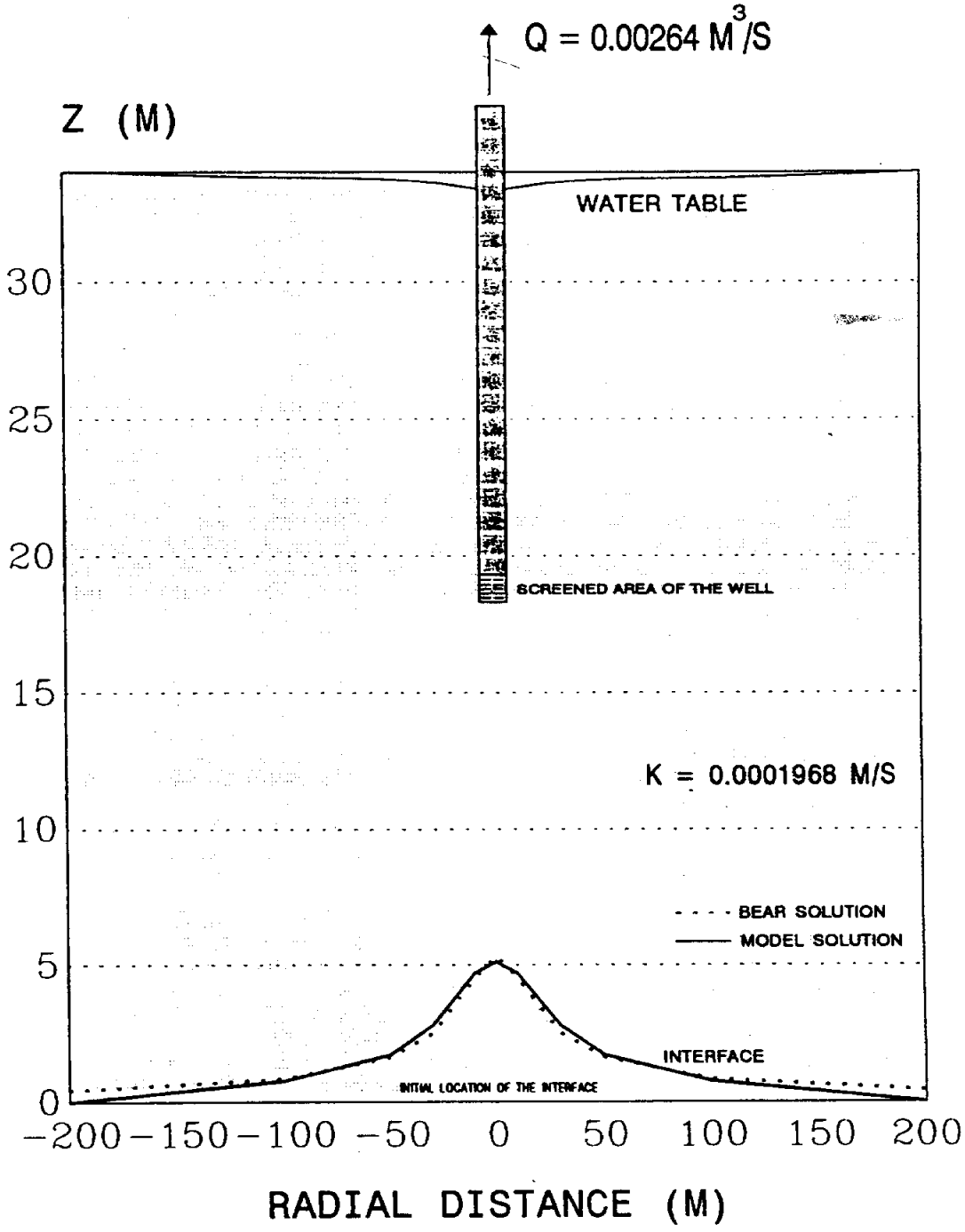

Figure 21. Upconed interface results.

10, 20, 20, 50, and 100 meters. Both curves match very well except at the left and right sides where there is a small difference because Bear's solution is for an infinite horizontal aquifer.

Sensitivity Analysis

The sensitivity of a model to input parameters should be known and should reflect the response to a change in physical properties found in nature. The input parameters investigated are the grid spacing, the error values used to stop the iterative Gauss-Seidel solution process, and the relative sizes of the element sides.

The flow to a well problem was used to examine the effects of these three parameters. The simulated aquifer consists of four layers with the hydraulic conductivities values expressed in the Figure 22. The dimensions of the simulated aquifer are 4,000 ft along x axis, 4,000 ft along y axis, and 55 ft thick. Water is pumped from the second and third layers at a constant rate of 0.12 cfs. Two different grids were used for the simulations. One grid consisted of 11 nodes along x axis, 11 nodes along y axis, and 9 nodes along z axis. The distance between nodes along x axis, and y axis measured from the well, located at the center, were 100, 200, 200, 500, and 1,000 ft. The other grid consisted of 17 nodes along x axis, 17 nodes

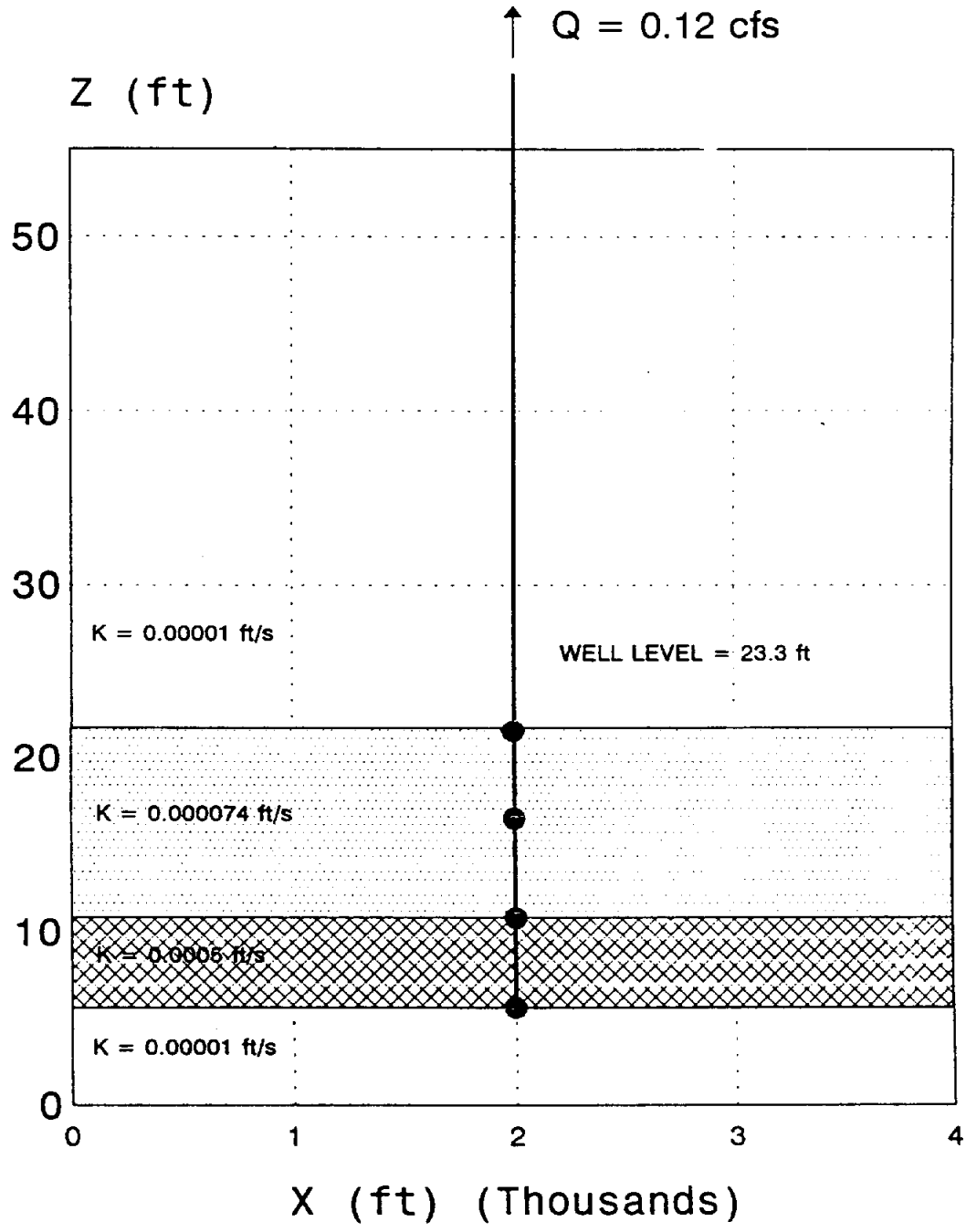

Figure 22. Definition of parameters for the flow to a well problem used in the sensitivity analysis.

along y axis, and 9 nodes along z axis. The distance between the nodes along x axis and y axis for this case were 50, 100, 150, 200, 250, 500, and 500 ft. The magnitude of the errors (difference in piezometric head of the new value and the value from the previous iteration in each node) used to stop the iterative Gauss-Seidel procedure were 0.01, 0.001, and 0.0001.

The results of the different runs are shown in Figure 23. Physically, this is a symmetric problem, because the pumping well is located at the center of the horizontal part of the grid. Nevertheless, curves c and d do not show such symmetric behavior. These curves were obtained using different grids but equal iteration errors (E=0.01)* On the other hand, curves a and e show similar symmetric behavior, even though curve a was obtained from a denser grid than curve e. The error chosen for these two curves was equal to 0.0001. These results show that the solution has a strong dependence on the magnitude of the error used to stop the iterative Gauss-Seidel solution process. Also, we noted that the solution does not depend strongly on the two kind of grids used. The magnitude of the drawdown is also affected by the grid spacing, and the size of

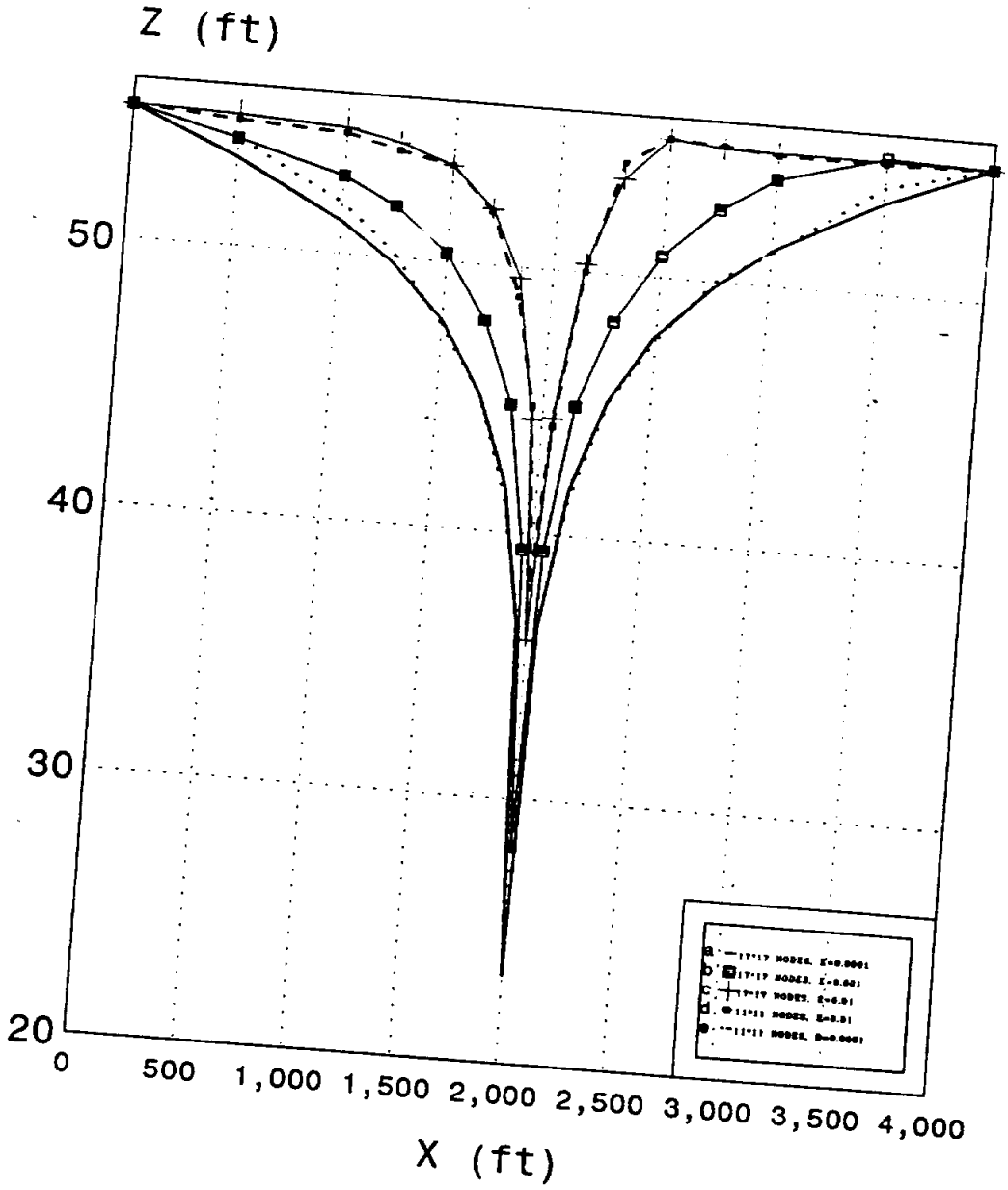

Figure 23. Results of the flow to a well problem used in the sensitivity analysis.

the error used. Curve b was obtained using an error equal to 0.001, which is between the error used for the extreme cases a and e, and c and d.

During the assembly process of the element matrix, the element integral must be solved. These integral are solved using the numerical method known as Gauss quadrature, in which one of the steps is the evaluation of the volume of the elements. Because this task is performed numerically, problems can appear if the relative sizes of the sides of the element are too different. This is the case when we are dealing with very thin layers that must be represented by elements whose areal dimensions are much larger than the vertical dimension. For the flow to a well problem already considered, the vertical dimension of the thinner elements was changed, reducing their values from 10 ft. The minimum z size for an element found before getting a floating point exception error was 5 ft, and the maximum x and y dimensions were 500 ft. Therefore, for this problem, if an element has an areal extension of 500 ft by 500 ft, then the minimum thickness of that element cannot be less than 5 ft.

APPLICATION OF THE MODEL TO THE NATURAL SALT POLLUTION ON THE BRAZOS RIVER

The Brazos River is a major source of water in Texas; however, natural salt springs and seeps in the upper Brazos River basin (Figure 24) discharge significant quantities of sodium chloride, calcium sulfate and other dissolved solids into the river, thereby reducing the downstream water quality. Salt springs and seeps could be controlled using recovery wells to lower the piezometric surface or water table, and deep injection wells to dispose of the brine.

Rather than developing a single, large project to control natural salt pollution in the Brazos River, it will probably be more cost effective to control the pollution in stages. Each salt spring or seep is unique and will require a unique solution. As salt pollution control technology is developed, it can be applied at other sites. One of the sites with largest potential benefit cost ratio seems to be the Dove Creek area on Salt Croton Creek, which is the area of concern for the application of the model developed in this work.

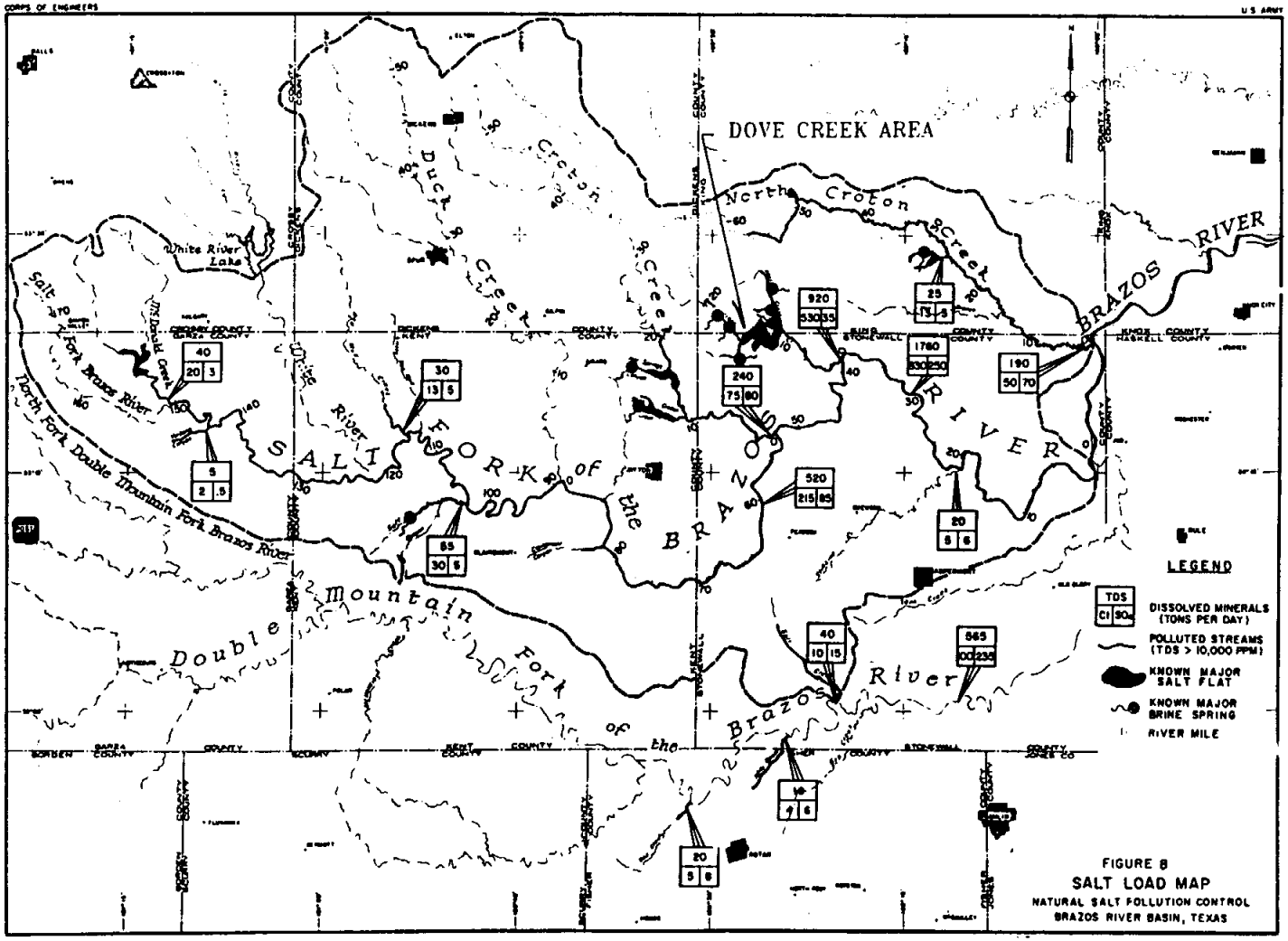

Figure 24. Salt load, salt flat, and major brine springs in the upper Brazos River, Texas.

The average daily load on the Brazos River at Possum Kingdom Reservoir is 1,000 tons of chloride. The average daily chloride load from Salt Croton Creek is about 500 tons or 50 % of the chloride at Possum Kingdom Reservoir. The average discharge on Salt Croton Creek is 5.6 cfs. The base flow ranges from 0.5 to 2.0 cfs and contributes approximately 330 tons of chloride per day. A properly designed system of recovery wells in the Dove Creek area, potentially reduce the chloride loading at Possum Kingdom Reservoir by 40 to 50 % by pumping and injecting approximately two cfs of brine.

Lowering the hydrostatic head in the salt water aquifer will eliminate the discharge from the springs and seeps. Reversing the hydraulic gradient at the surface so that the direction of percolation is downward, will also eliminate the build-up of salt at the surface of the salt flat. The project would reduce the salt load on the Brazos River, both during low flows when the salt contribution is primarily from springs and seeps and during flood flows when the contribution is from removal of the white salt layer at the surface of the salt flat.

Geology

Rocks of the Permian Age crop out in the Croton Creek and Dove Creek areas (Figure 25). The formation consist mainly of beds of shale, sandstone, gypsum and dolomite. The westward regional dip is about 25 ft per mile and is opposite to the regional ground surface slope.

The Childress dolomite member of the Grayburg formation crops out in the bluffs of Dove Creek flat and the canyons of Dove and Haystack Creeks (McMillion, 1958). The thickness in the outcrop area ranges from 9 to 13 ft and a similar thickness range is recorded or reported in logs of wells west of Dove Creek flat. On the outcrop, this rock member consists predominantly of gypsum and dolomite, and in the subsurface is predominantly of anhydrite and dolomite (McMillion, 1958).

Fresh water in contact with anhydrite will result in hydration to gypsum. It is not chemically possible for sodium chloride brine to alter anhydrite to gypsum when the temperature is greater than 67° F. Unless the brine had recently saturated the rocks, gypsum should not be found below the interface between fresh and groundwater and brine (Keys

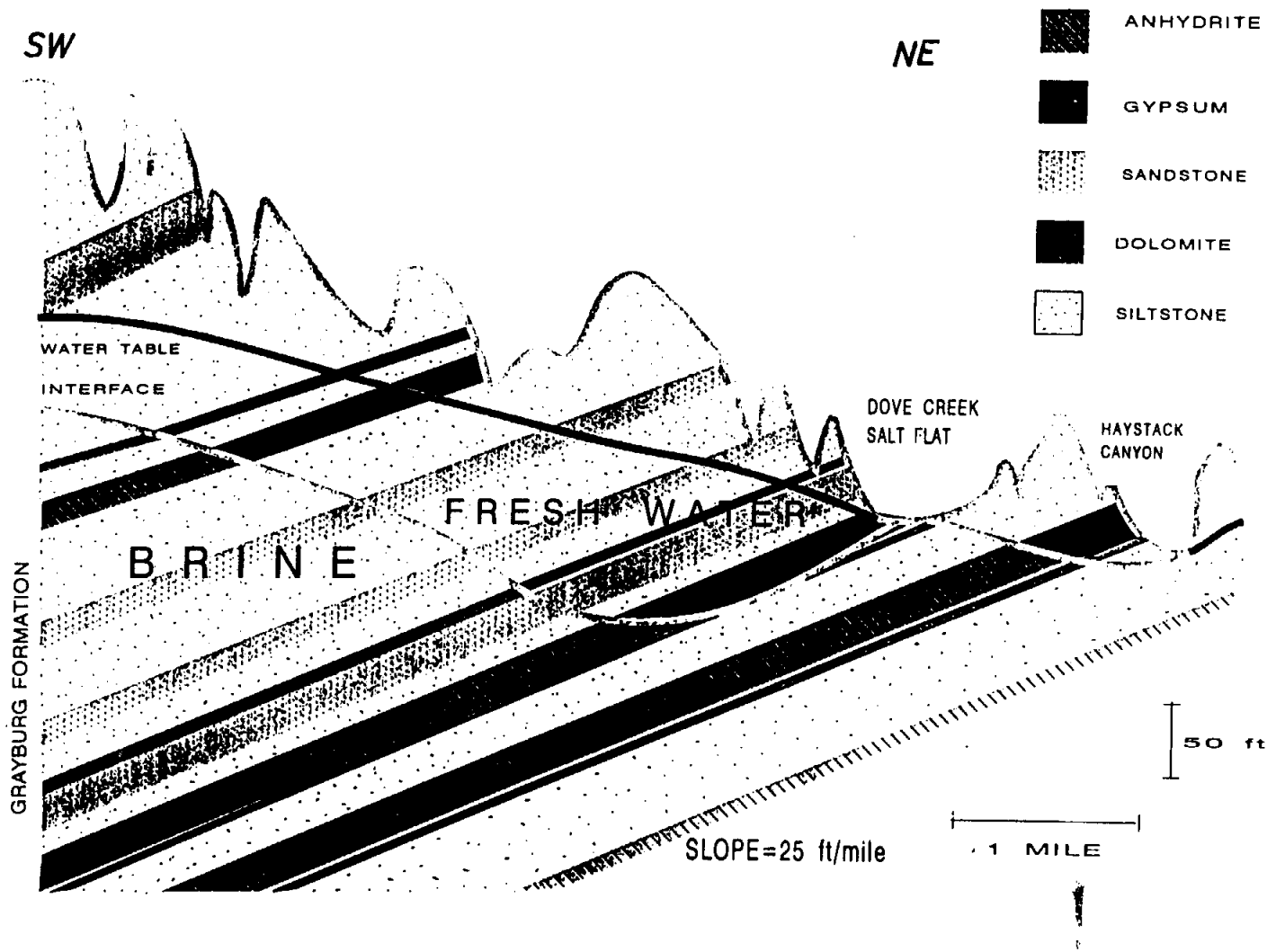

Figure 25. Section SW - NE, showing the rocks of the Permian Age that crop out in the Dove Creek Salt Flat and Haystack Canyon.

and MacCary, 1973). The amount of anhydrite found above the interface probably depends on the rate and depth of weathering.

Lying immediately below the Childress member is banded red and green gypsiferous clay of the Dog Creek formation. The clay is laminated, jointed, generally friable and conchoidally fractured. On the floor of Dove Creek flat, salt water saturated clay is hard, tough and resistant (McMillion, 1958).

Lying above the Childress member is the sandy-textured redbed strata of the Grayburg formation. The redbed strata that crops out in the northeastern Kent County consist of red, poorly consolidated, very fine-grained sand and silt and locally poorly cemented sandstone and siltstone interbedded with gypsum. Halite beds ranging in thickness from 4 to 75 ft are present in the subsurface (McMillion, 1958). Near surface halite beds have been removed by dissolution with fresh groundwater from precipitation.

Groundwater

The groundwater in the study areas occurs under both unconfined and confined conditions. Over most of the area, a shallow fresh water layer overlies saline water. Because of the low permeability of the sediments, the water table follows closely the steep gradients of the ground surface. The water table is generally encountered at depths ranging from 30 to 60 ft below the ground surface. The relatively fresh water is mainly calcium sulfate type that has total dissolved solids from 2,000 to 5,000 mg/l and extends to depths very near the floor level of the creeks and salt flats. Below this depth, the water becomes salty and within a vertical distance of several feet changes to chloride type brine with dissolved solids more than 200,000 mg/l. The water table intersects the land surface along many of the streams. Fresh water seeps occur near the head of Haystack Creek in southwest King County, while salt water seeps occur in the Croton Creek area in northeastern Kent County at Hot Springs and Short Croton flat (McMillion, 1958).

The brine-fresh water interface is a thin transition zone that lies between the fresh water above and the brine below. The position of the interface is shown in Figure 25. In general, the interface transects lithologic units and is not related to stratigraphy or structure. The shape of the interface is closely related to the thickness of the overlying fresh water. The depth of the interface below the land surface is greatest where the thickness of the fresh water is the greatest. The depth of the interface below the land surface is generally least where the thickness of the freshwater is the smallest (Stevens and Hardt, 1965).

The bodies of brine and fresh water are in hydraulic continuity, their pressures near the interface are very nearly equal as it was stated in the theoretical part of this work. Therefore, if a well is screened just below the interface, the brine would rise approximately to the water table, if the brine had the same density as the fresh water. However, the brine in the area of interest has a relative density of 1.2, then it would rise in such a well to a level somewhat below that of the water table. If the vertical components of flow are neglected, the height to which the brine would rise above

the interface, is the thickness of the fresh water zone multiplied by the ratio of the density of fresh water to that of the brine. By adding this height to the altitude of the interface at representative points, Stevens and Hardt, 1965, computed the piezometric surface of the brine shown in Figure 26. The movement of brine is enhanced by solution openings in the gypsum and by fractures in both the gypsum and anhydrite. Anhydrite exists below the brine-fresh water interface, while gypsum exists near the land surface.

The source of the water for the springs and seeps along Croton Creek is apparently precipitation on the upland area to the west where sandy soils are favorable for recharge. The lateral movement of the unconfined groundwater is generally to the east under a hydraulic gradient which appears to conform reasonably with the topographic slope. The saline conditions of the water at the springs and seeps probably result from the percolating water leaching halite from the Grayburg strata as it flows from the recharge area to the points of discharge. Sinkholes apparently resulting from the dissolution of halite occurs in the recharge area to the west. When precipitation

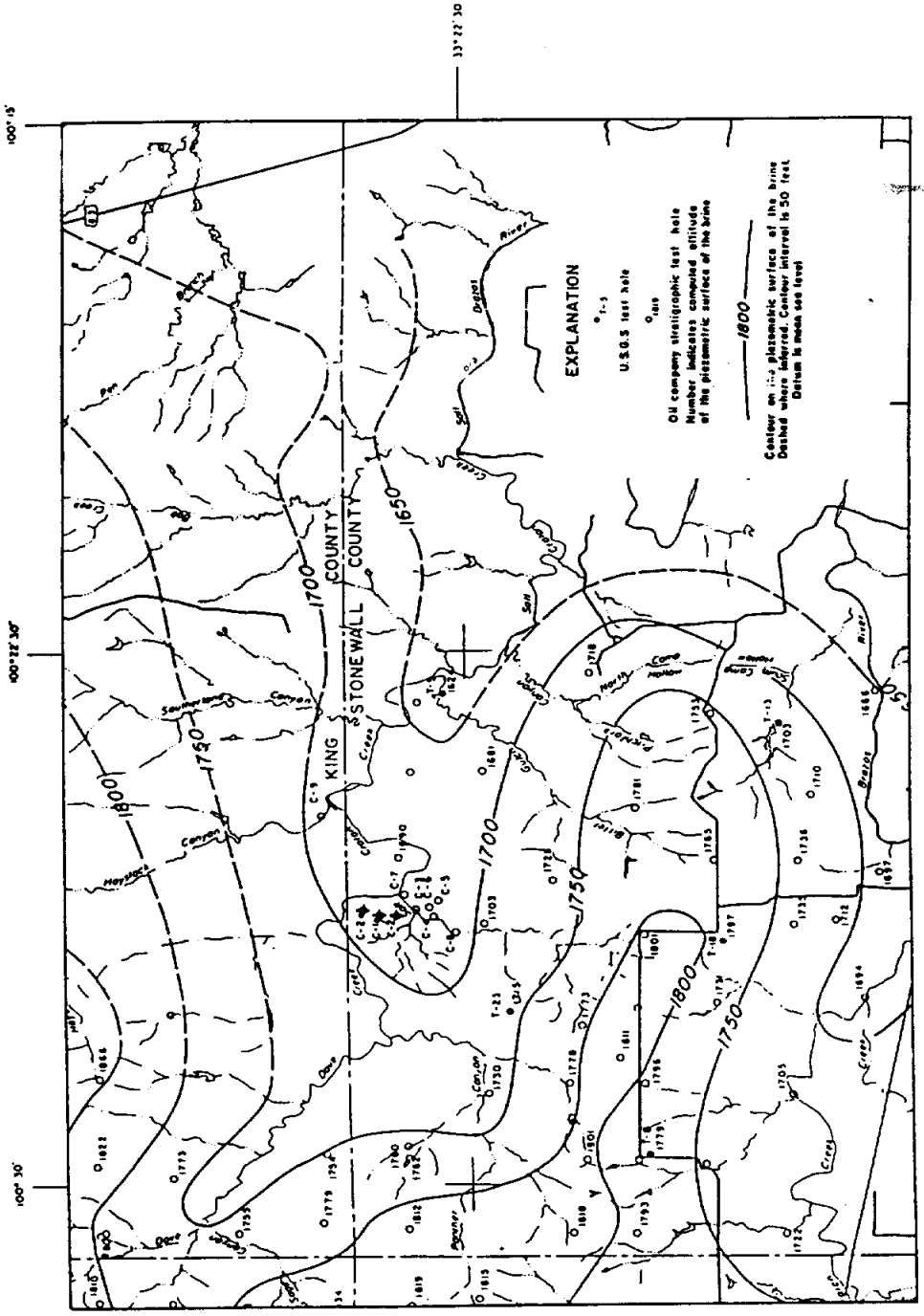

Figure 26. Piezometric surface of the brine.

increases on the recharge area, the saline discharge along Croton Creek also increases (McMillion, 1958).

The artesian system that discharges saline water at Dove Creek flat is hydrologically complex and the source of recharge is unknown. Aerial photography of the Dove Creek flat area did not reveal any sinkholes (Baker, Hughes and Yost, 1964). It might be that the solution channels in the Childress are connected hydraulically with the unconfined groundwater aquifer up the topographic slope to the west of Dove Creek flat and form an artesian conduit through which saline water moves up dip to discharge points in the flat. On the outcrop of the Childress, the anhydrite has been altered to gypsum. The groundwater movement has been restricted in this zone because the fractures have been closed by the expansion of the gypsum (McMillion, 1958).

The source of the water discharging in the Dove Creek area might also be regional upflow of deep brine.

The Dove Creek salt study conducted by Mason-Johnston and Associates (1955) indicates the flow of brine is through thin layers of badly broken shale and seams of gypsum. Borings taken in the study indicate that the layers transmitting brine

are in the upper Dog Creek formation. No flow of brine was observed in one of the boring taken in Haystack Canyon. The borings taken in Dove Creek salt flat indicated several zones of brine flow. The zones were described generally as fractured red and green shale or broken gypsum several feet thick.

Halite - Dissolution Brine and Deep Basin Brine

Brines that originate in the local area from dissolution of halite by recharge precipitation can be expected to exhibit chemical characteristics similar to halite. Cation exchange between sodium in the water and calcium in the shale cause deep-basin brines to have a sodium to chloride ratio smaller than that in halite. The weight ratio of bromide to chloride and iodide to chloride can also be used to distinguish between the brine types when the chloride concentration is greater than 10,000 mg/l (Richter and Kreitler, 1986).

Richter and Kreitler (1986) studied the geochemistry of salt spring and shallow subsurface brines in the Rolling Plains area of Texas. They classified the brines into three groups: A, B and C based on the weight ratio of ions. Halite-

dissolution brines were in group A and deep-basin brines were in group C. Group B brines were a combination of halite-dissolution brine and deep-basin brine. Springs in the Dove Creek area were group B brines.

Hydraulic Conductivity of Porous Layers

Pressure tests were conducted by Mason-Johnston and Associates (1955) at borings C-1, C-2, and C-2A (see Figure 26). During the test, water was pumped into the boring. The flow rate and pressure at the ground surface was recorded. A casing and packer were used in the boring so that water was injected into a specific layer or seam. The tests were of short duration and only lasted for a few minutes. Using the Theis equation, the pump-in test can be utilized to estimate the hydraulic conductivity of the formation. Since the tests were conducted for a very short duration, the hydraulic conductivity computed is representative of only a small area around the boring. The values of hydraulic conductivity can be expected to show large variations. The computed values of hydraulic conductivity are listed in Table 3 and range from 12

to 320 gpd/ft^2. The maximum transmissivity was at boring C-2 and was 1540 gpd/ft.

Flow net analysis of the brine aquifer indicates that the hydraulic conductivity of the aquifer increases near the discharge zone and tnat hydraulic conductivity measurements of the formation taken several miles from the Dove Creek discharge zone will not be representative values for the design of the recovery system. The artesian spring located at boring C-4 was reported in 1961 to be discharging 90 gpm (Baker, Hughes and Yost, 1964)a, which indicates a high hydraulic conductivity at that location.

An exploration hole drilled about a mile northwest of Dove Creek salt flat tapped a brine aquifer at elevation 1655. Water discharged into the air to a height of 43 ft above the ground (1770 ft) for a period of 40 hours. The period of flow and the artesian head indicates that the aquifer is very permeable and extends over a large area(Baker, Hughes and Yost, 1964).

Table 3. Computed values of Hydraulic conductivity.

Test Hole	Depth to Top (ft)	Seam Thickness (ft)	Hydraulic Conductivity (ft/s)	Transmissivity (ft^2/s)
C-1	61.7	21.8	0.000021	
	85.0	7.0	0.000049	0.0008
C-2	14.0	4.5	0.00037	
	94.5	8.8	0.000064	
	108.0	5.0	0.000087	0.0027
C-2A	51.0	2.5	0.00056	0.0014
C-4	55.0	17.0	0.00310	0.0527

Evaluation of a Recovery Wells System for the Brine - Part I

In order to properly design a system of recovery wells, the number of wells used, their location and pumping rates must be determined. As a preliminary study, it was considered convenient to know the behavior of the groundwater system under different array of wells, pumping rates and permeabilities of the rocks.

From previous analytical analysis and physical considerations not presented in this work, it was decided to simulate an area of 11000 ft along the W-E direction by 22500 ft along the S-N direction, using only one array of ten pumping wells. The relative location of the simulated area is shown in Figure 27. The horizontal part of the grid used consisted of 31 nodes along the x direction, and 117 nodes along the y direction, as it is shown in Figure 28. These nodes are more concentrated around the wells where the larger gradients of the piezometric head are expected to occur. The ten wells used are equally separated 1500 ft from each other. Along the vertical direction, nine nodes were used, and seven different layers were considered. 32643 nodes and 27840

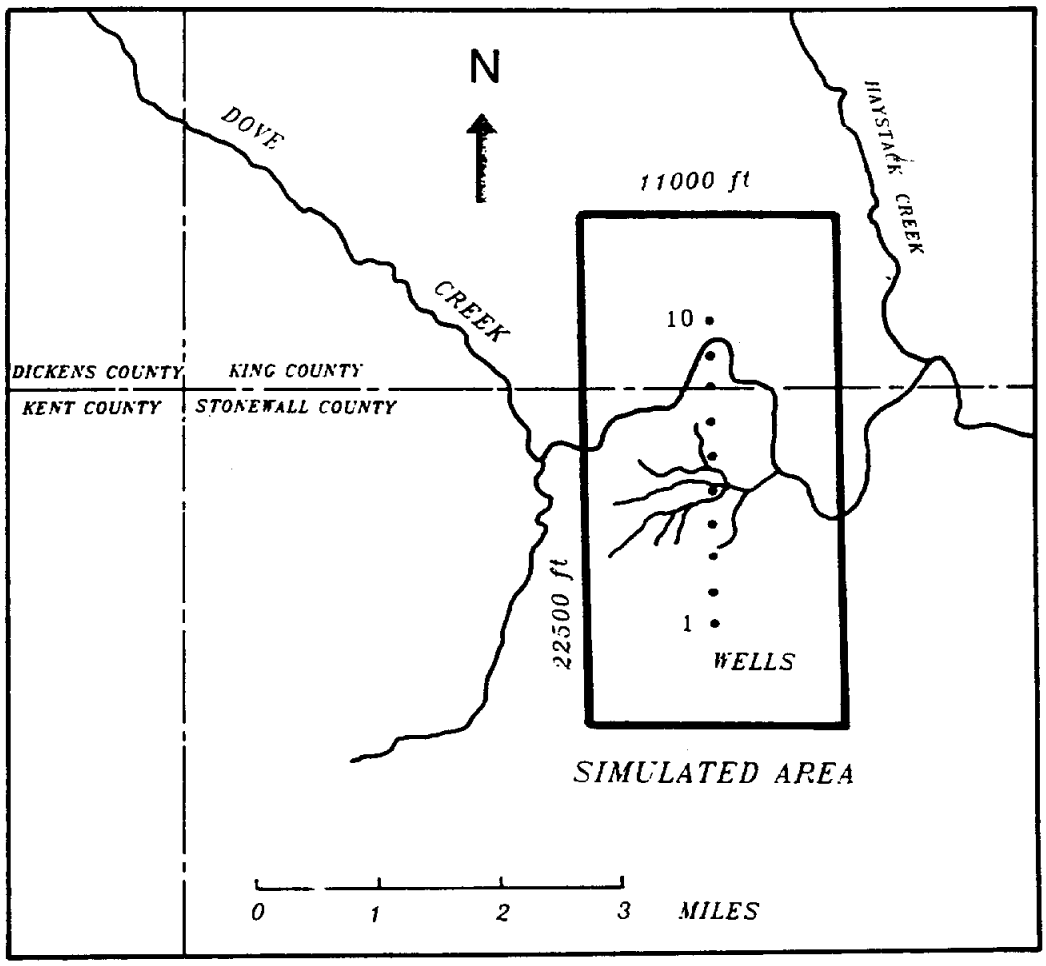

Figure 27. Location of the simulated area.

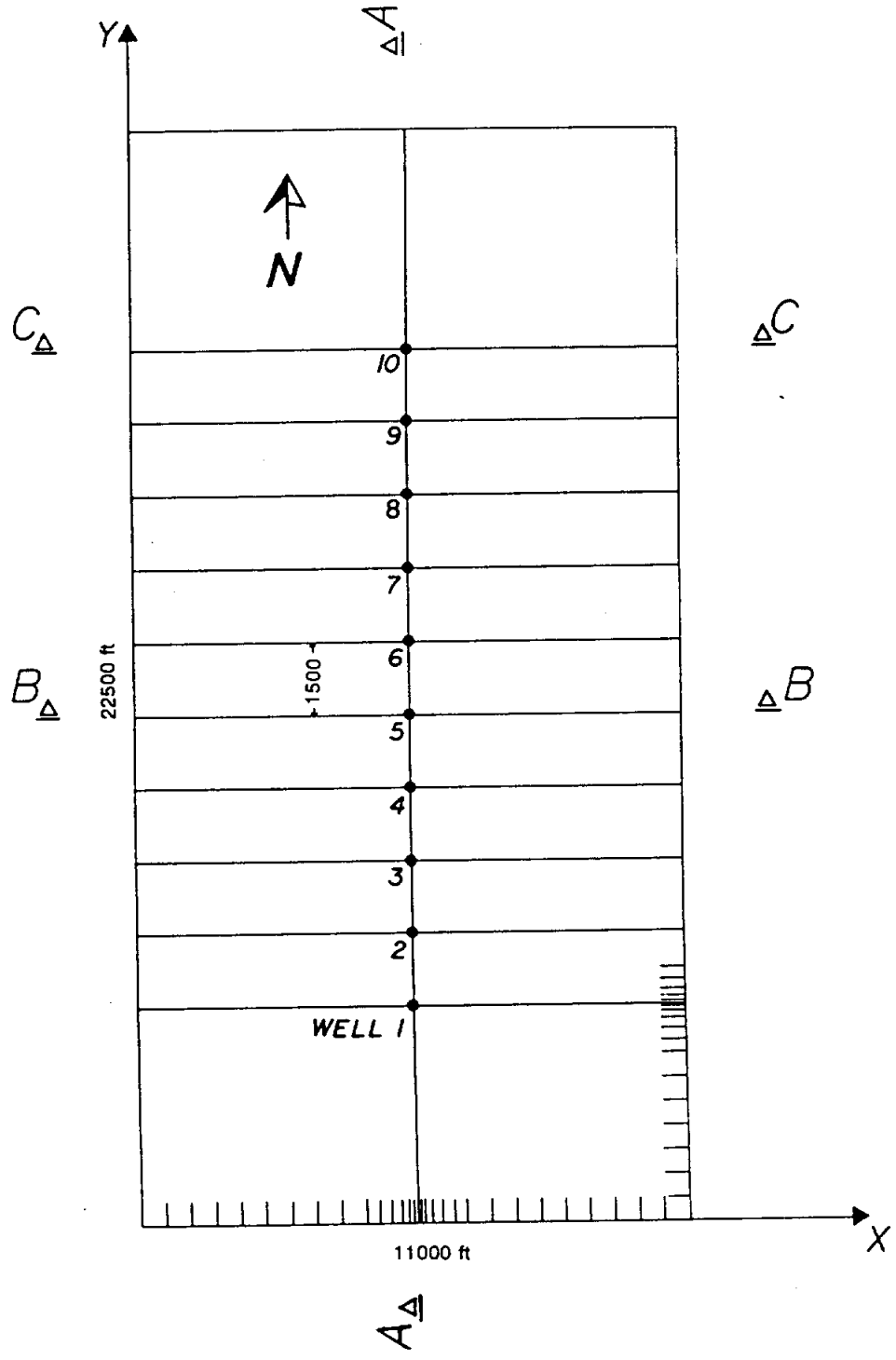

Figure 28. Horizontal profile of the grid used in the simulation, showing the location of the wells used.

elements were used to build the grid for this simulation. All the wells were screened in the lowest Gypsum and Dolomite layers, as it is shown in Figure 29. The five nodes below the top of the screened area of the wells remain fixed in the space during the iterative process to relocate the water table, while the elevation of the four nodes above the top of the screened area of the wells can vary during this iterative process.

Constant piezometric head values were imposed on the lateral boundaries of the grid used. These values of the piezometric head were taken from Figure 26.

The first test of the model was a simple calibration procedure. The purpose of this test was to compare the piezometric surface obtained from the map shown in Figure 26, with the piezometric surfaces obtained from the model without pumping wells, and for several hydraulic conductivity conditions. From the results shown in Figure 30, it can be seen that the piezometric surface obtained from isotropic layers (condition A) matches well with the surface obtained from the map. The piezometric surface obtained when the hydraulic conductivity in the z direction is ten times smaller

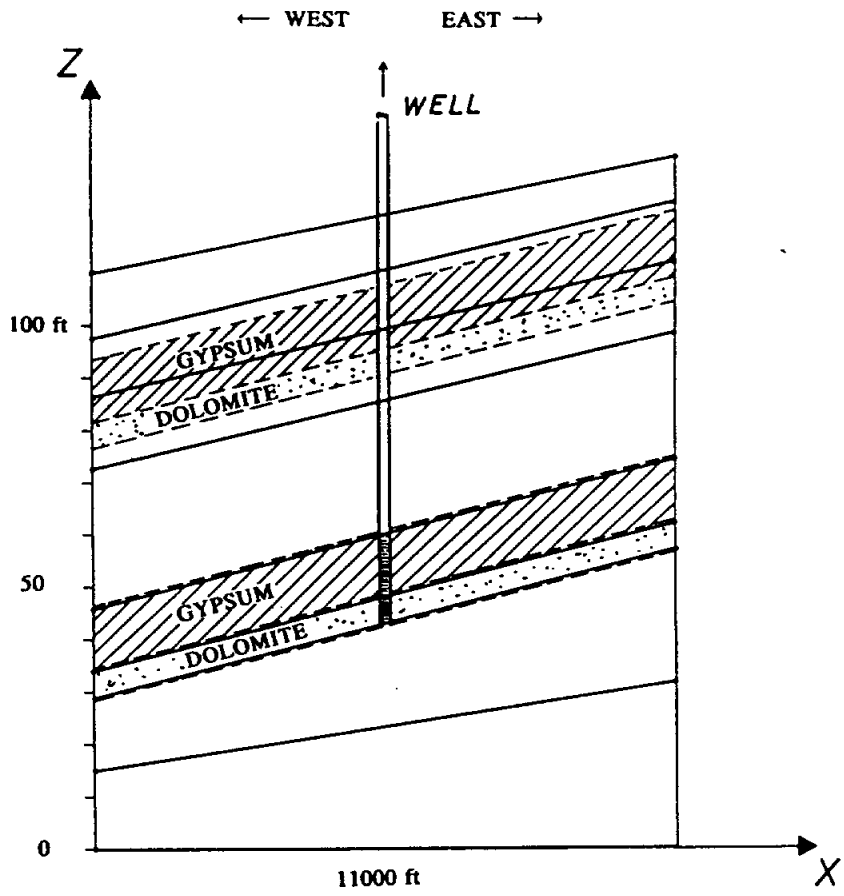

ADD 1600 ft TO THE ELEVATION, TO GET THE ELEVATION ABOVE SEA LEVEL.

Figure 29. Vertical profile of the grid used in the simulation, showing a representative well screened in the lower Gypsum and Dolomite layers.

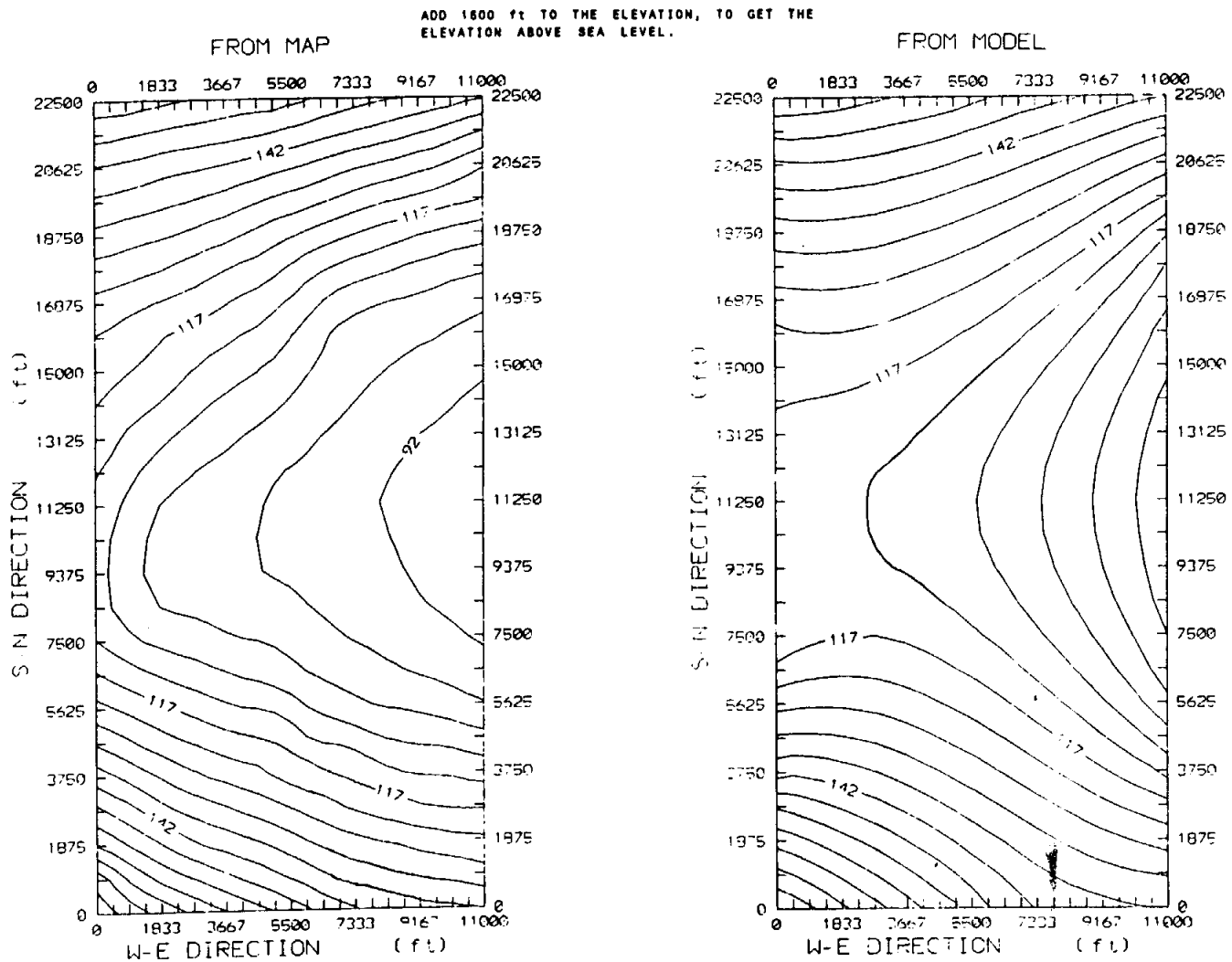

Figure 30. Piezometric head curves obtained from a piezometric head map and from the model.

than that in the x direction (condition B), does not matches very well with that obtained from the map. In this last case, the piezometric surface goes up relative to the piezometric surface for the isotropic layers case. This behavior is expected from the flow net theory for anisotropic media (see Cedergren, 1967).

These results indicate that the real hydraulic conductivity values along the z direction are not much different than those in the x and y directions.

The second test consisted of the evaluation of the drawdown under several pumping conditions, when the hydraulic conductivity on each layer were considered constant along the three coordinate directions (isotropic layers). The results shown in Figure 31, indicate that the maximum possible pumping rate from all the wells was 1.05 cfs, and occurs when each well is pumping at the rates indicated in Figure 31 for Q=variable. The maximum drawdown is determined when a piezometric head value reaches the top of the screened area of a well.

Because the model has to relocate the four nodes along the z direction between the top of the screened area and the

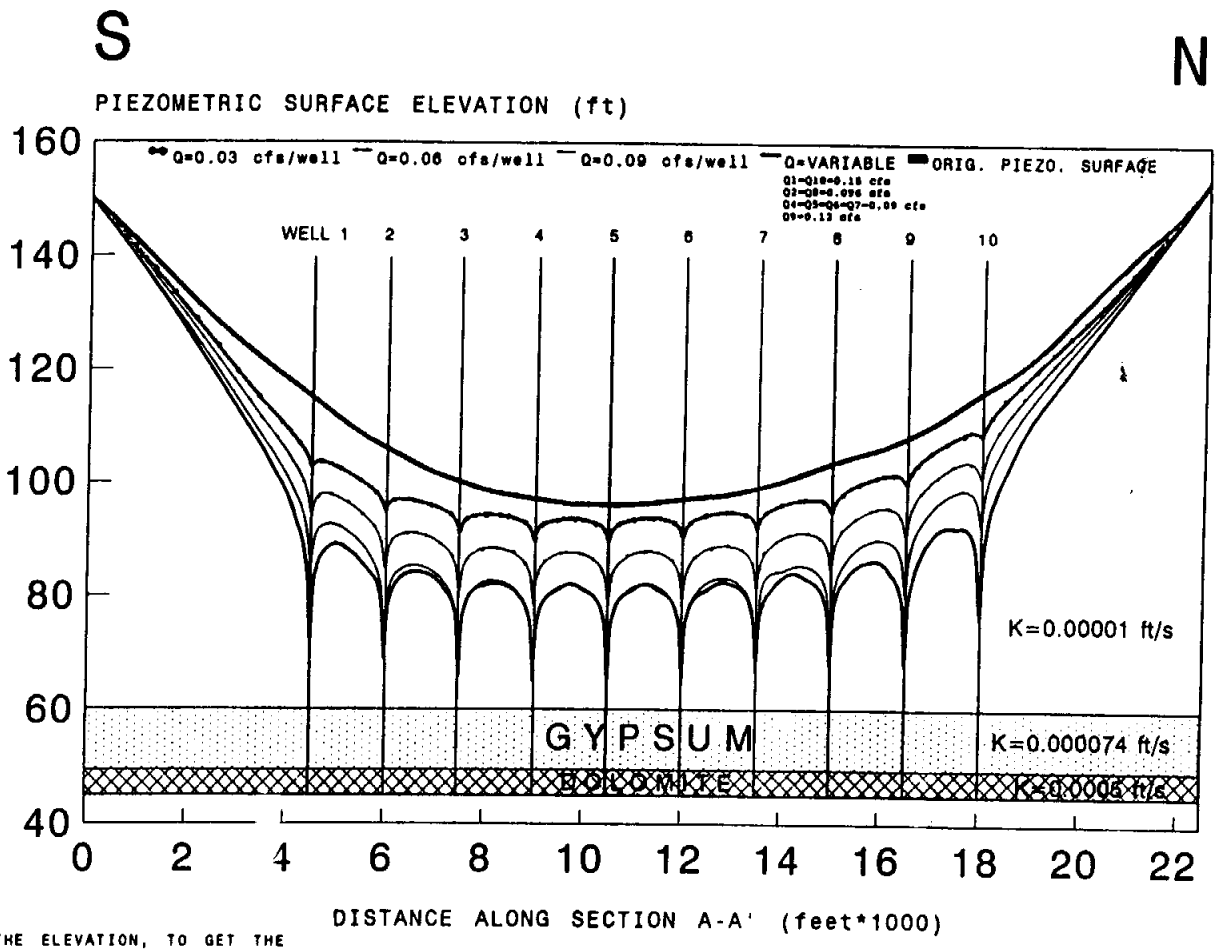

Figure 31. Drawdown along the wells under several pumping rates, and isotropic but heterogeneous layers.

lowest piezometric head value, the model does not allow the piezometric head surface to reach the top of the screened area of the wells. If this occurs, the program stop and gives an execution error code. In this case, the maximum drawdown must be found from the previous iteration results. Since the thickness of the elements can not be zero, the spacing of the variable elevation nodes between the water table and the top of the well screen can not be zero. For this reason, the real maximum drawdown could be a little higher than that shown in Figure 31. From this arguments, it is estimated that the maximum pumping rate from all the wells could be approximately 1.2 cfs. The previous arguments about the maximum drawdown also apply for the following results.

The third test was to evaluate the effect of reducing the hydraulic conductivity along the z direction by a factor of 10 with respect to those along the x and y direction. The results shown in Figure 32 indicate that the drawdown is greater near the center of the line of wells than at the end wells, as it is expected. Theoretically, the drawdown is inversely proportional to the thickness of the aquifer. In Figure 33,

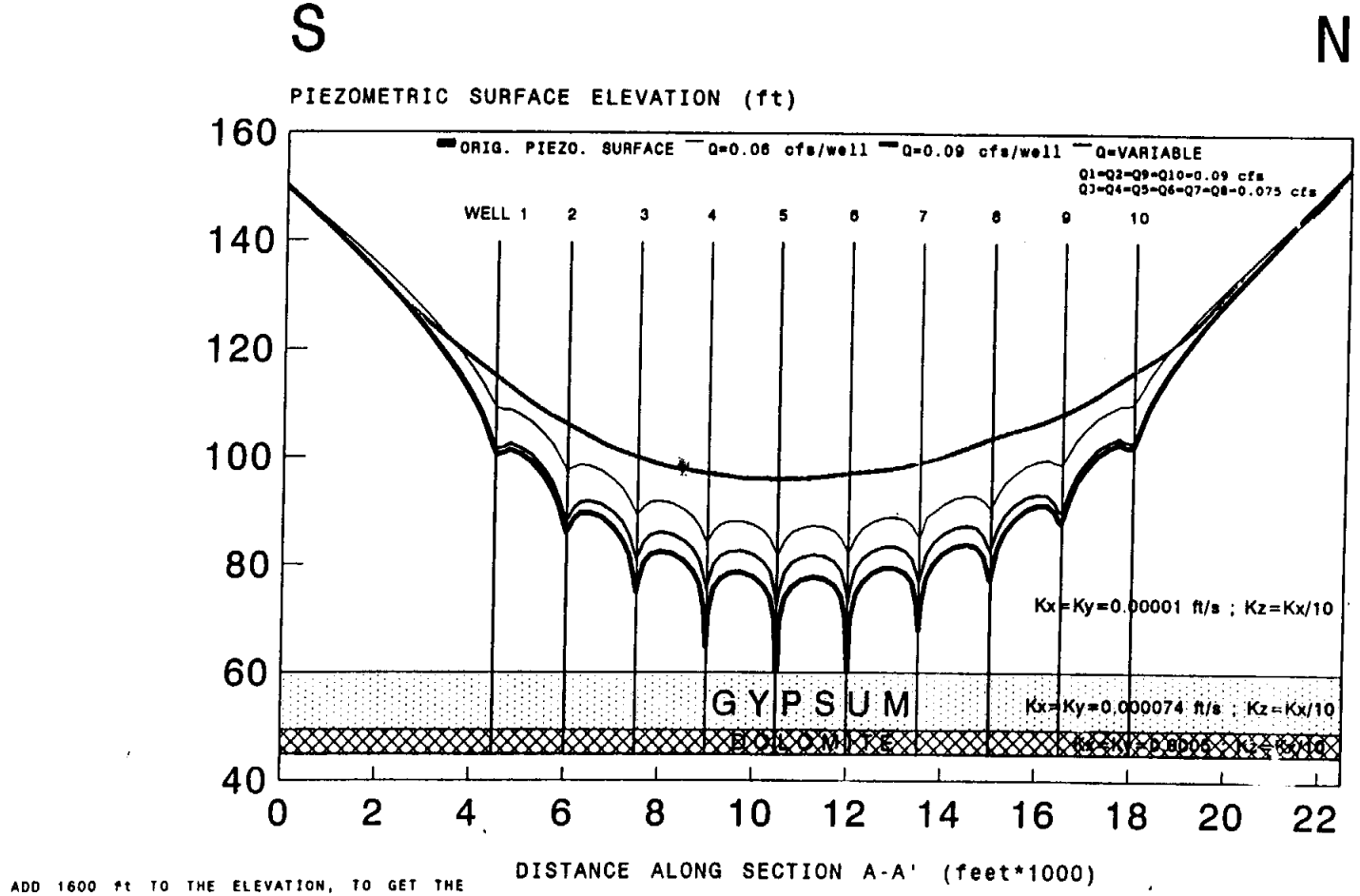

ADD 1600 ft TO THE ELEVATION, TO GET THE ELEVATION ABOVE SEA LEVEL.

Figure 32. Drawdown along the wells under several pumping rates, and permeability in the z direction reduced by a factor of ten of the permeabilities in the x and y directions.

the drawdown curves from the second and third test are compared, when each well is pumping at a rate of 0.06 cfs.

The fourth test consisted of reducing the hydraulic conductivity used in the third test by a factor of two. The results for different pumping rates are shown in Figure 34. For these conditions, the maximum possible pumping rate from the system of wells is estimated in 0.7 cfs. In Figure 35, a comparison for the same pumping rate per well conditions, and the same hydraulic conductivity values used in tests two and four is presented. It can be seen how the maximum drawdown occurs near the center of the line of wells, corresponding to the case of lower hydraulic conductivity.

Figures 36 and 37 show the same results from test two, three, and four, but now along cross sections oriented in the W-E direction and passing by wells 5 and 10, respectively. From these figures it can be seen that the piezometric head gradient is reversed east of the wells.

For the values of hydraulic conductivity used in this analysis, more than 10 recovery wells will be required to eliminate the natural salt pollution in the Dove Creek area. To eliminate the natural salt springs and seeps in the Dove

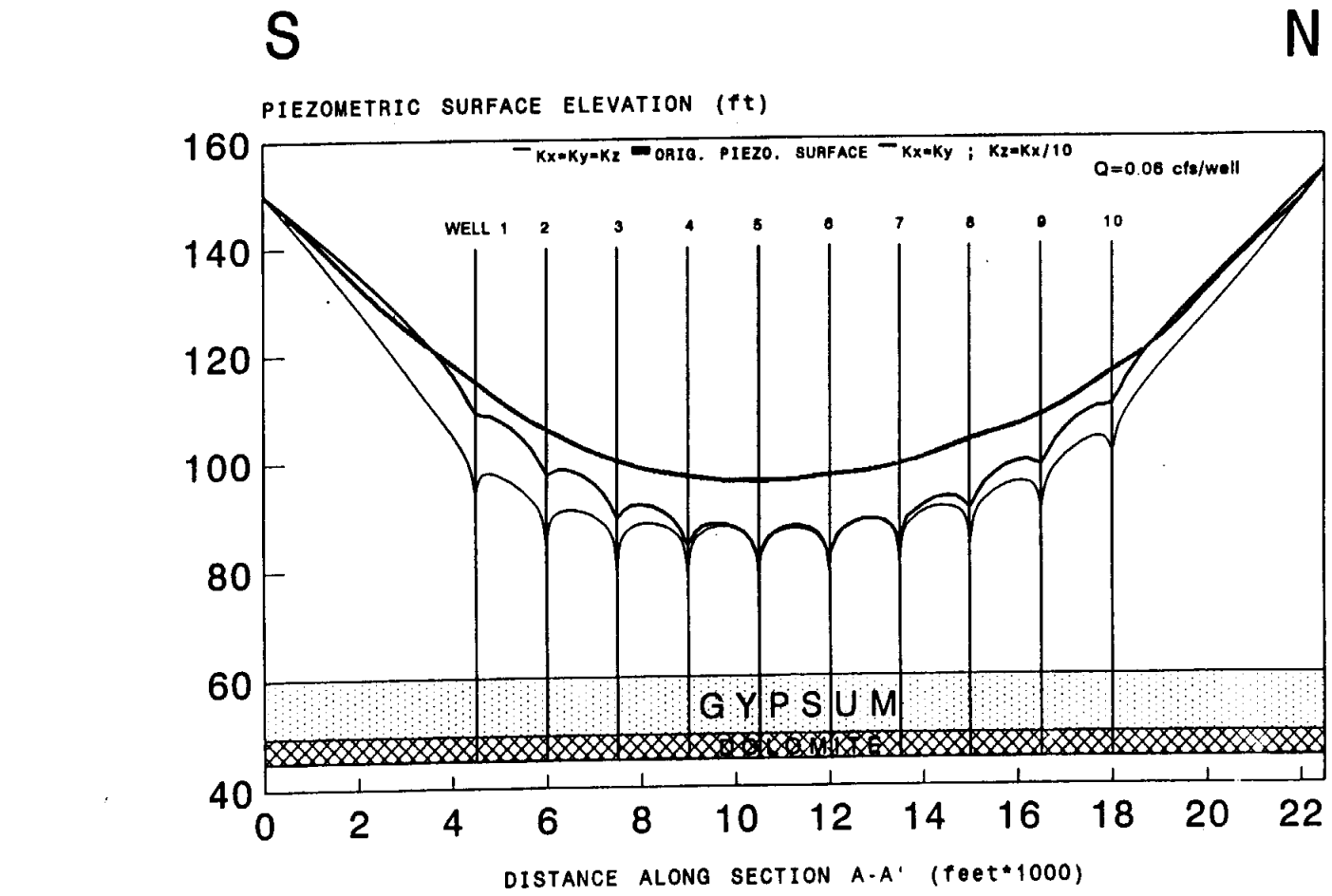

Figure 33. Comparison of the drawdown along the wells under the same pumping rate, when $K_x=K_y=K_z$ and when $K_x=K_y$, and $K_z=K_x/10$.

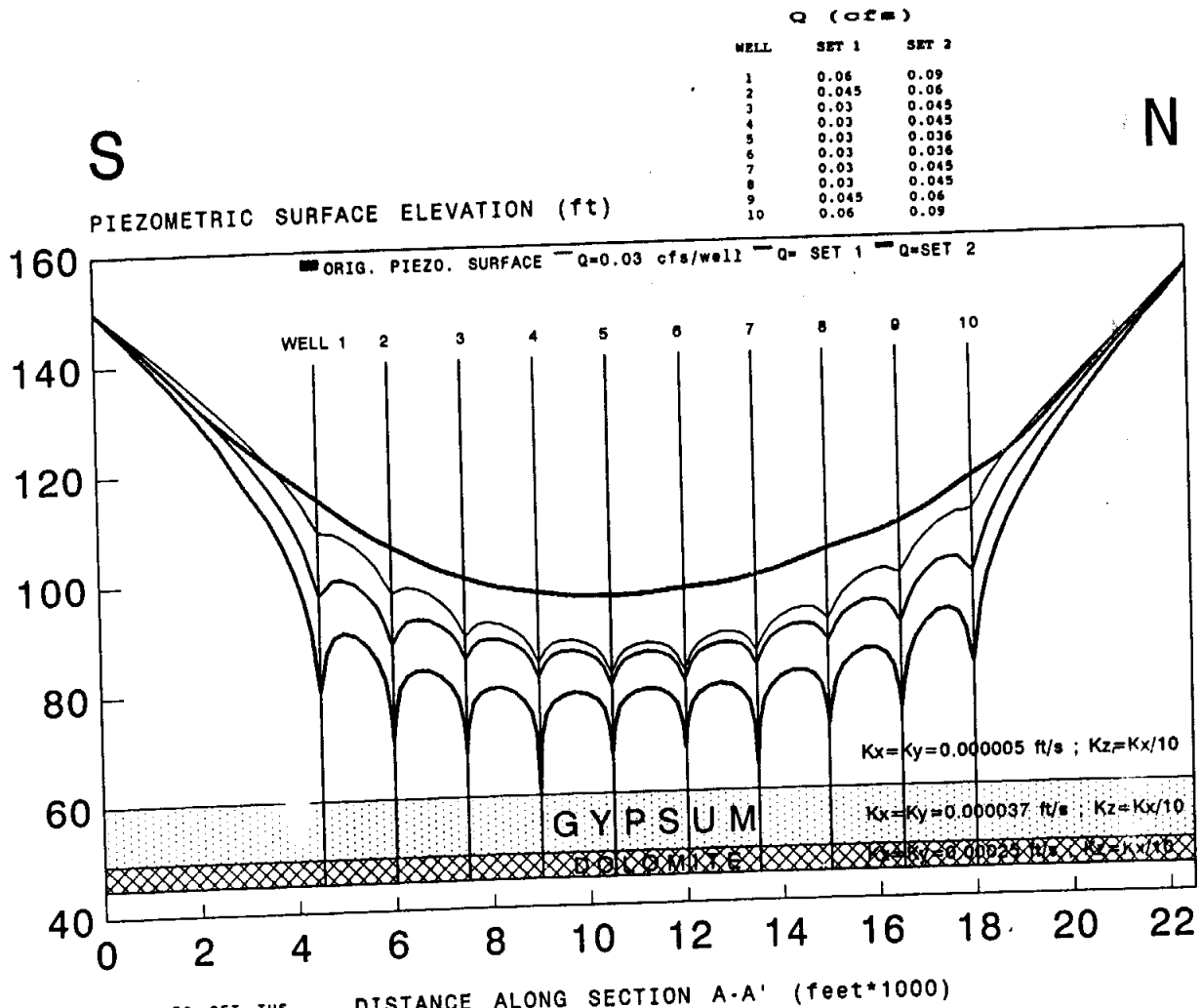

ADD 1600 ft TO THE ELEVATION, TO GET THE ELEVATION ABOVE SEA LEVEL.

Figure 34. Drawdown along the wells under several pumping rates, and permeabilities values reduced to one half of the values shown in Figure 32.

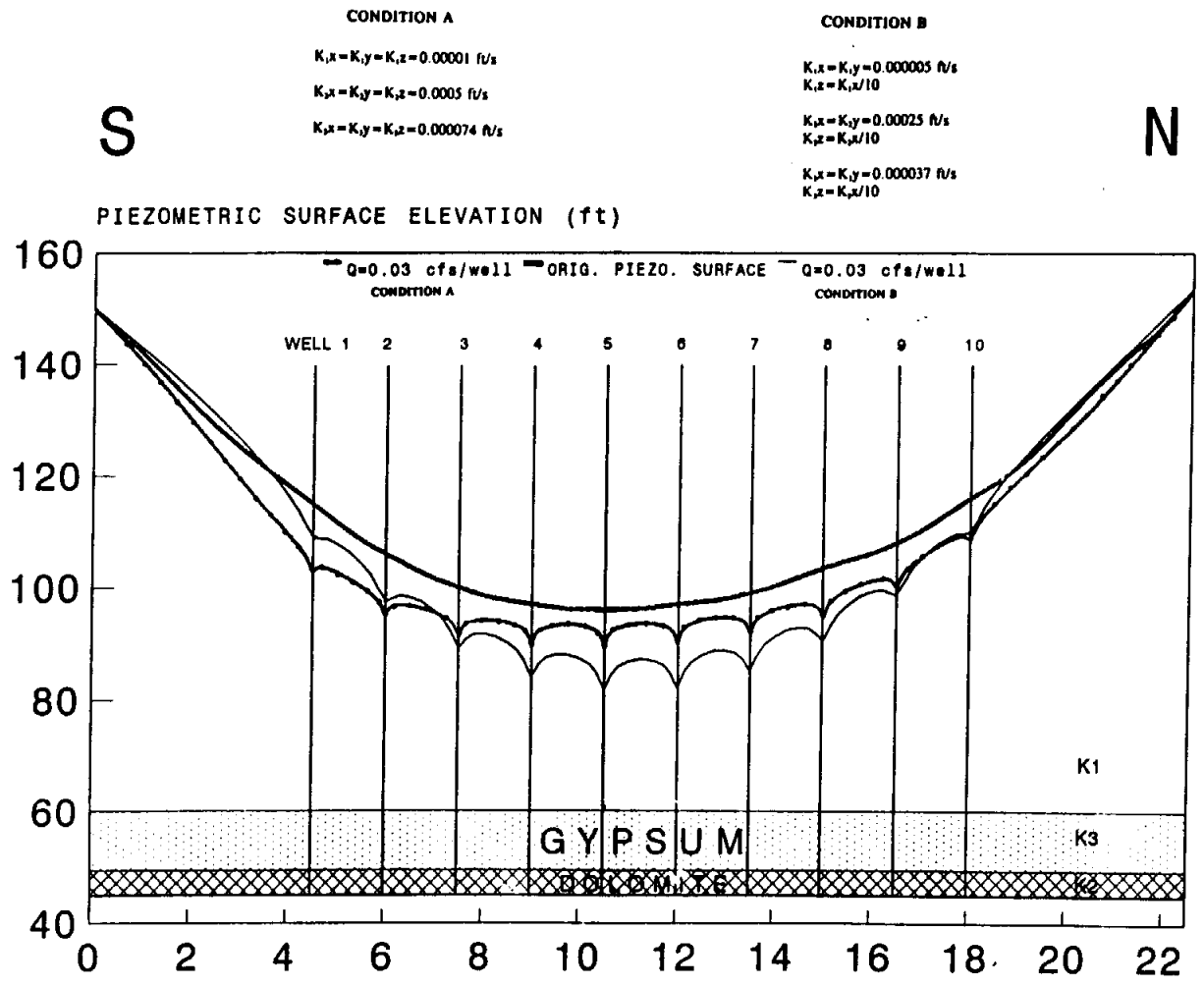

ADD 1600 ft TO THE ELEVATION, TO GET THE ELEVATION ABOVE SEA LEVEL.

Figure 35. Comparison of the drawdown along the wells under the same pumping rate and two different permeability conditions.

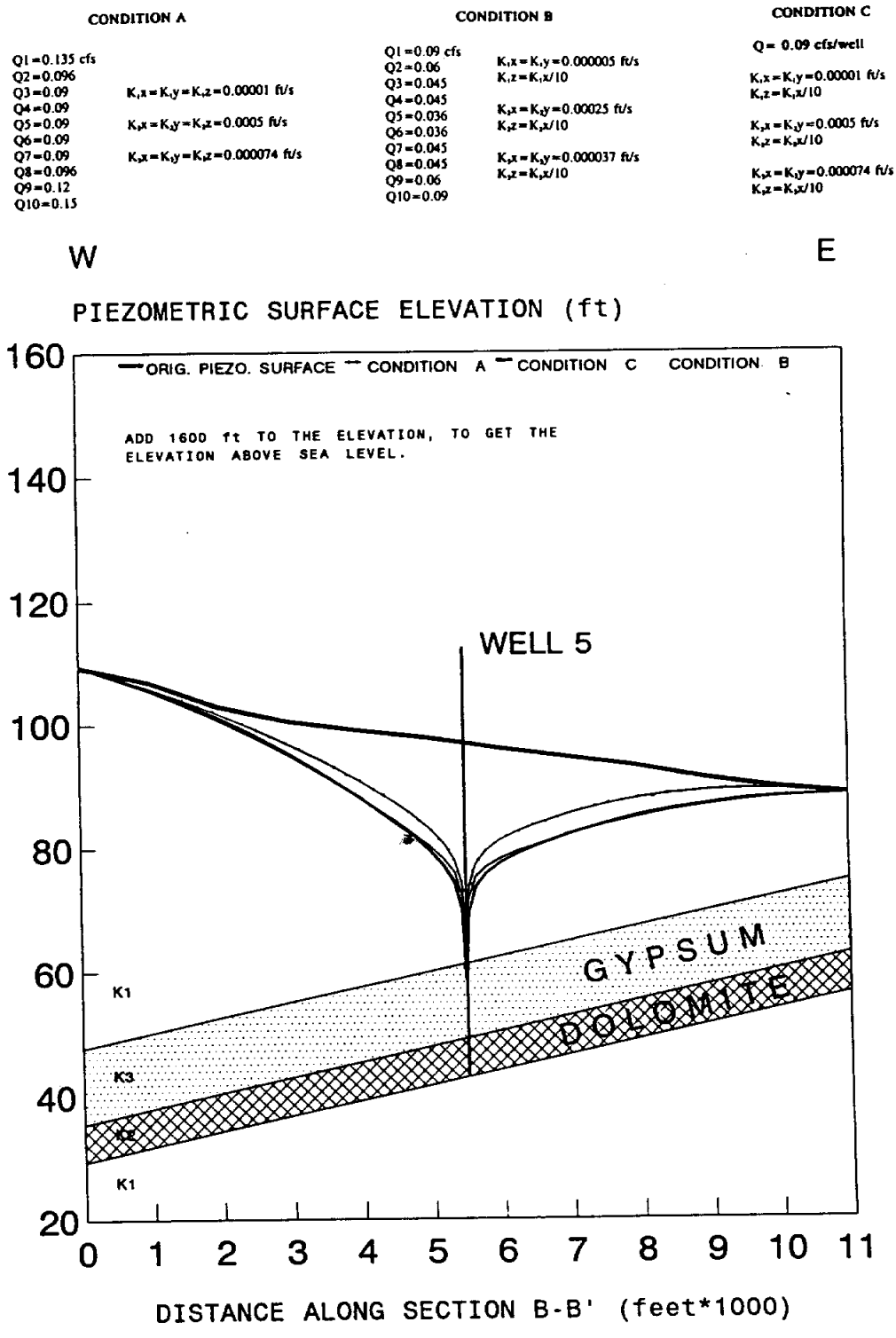

Figure 36. Drawdown along the section B-B' for different pumping rates and permeabilities conditions.

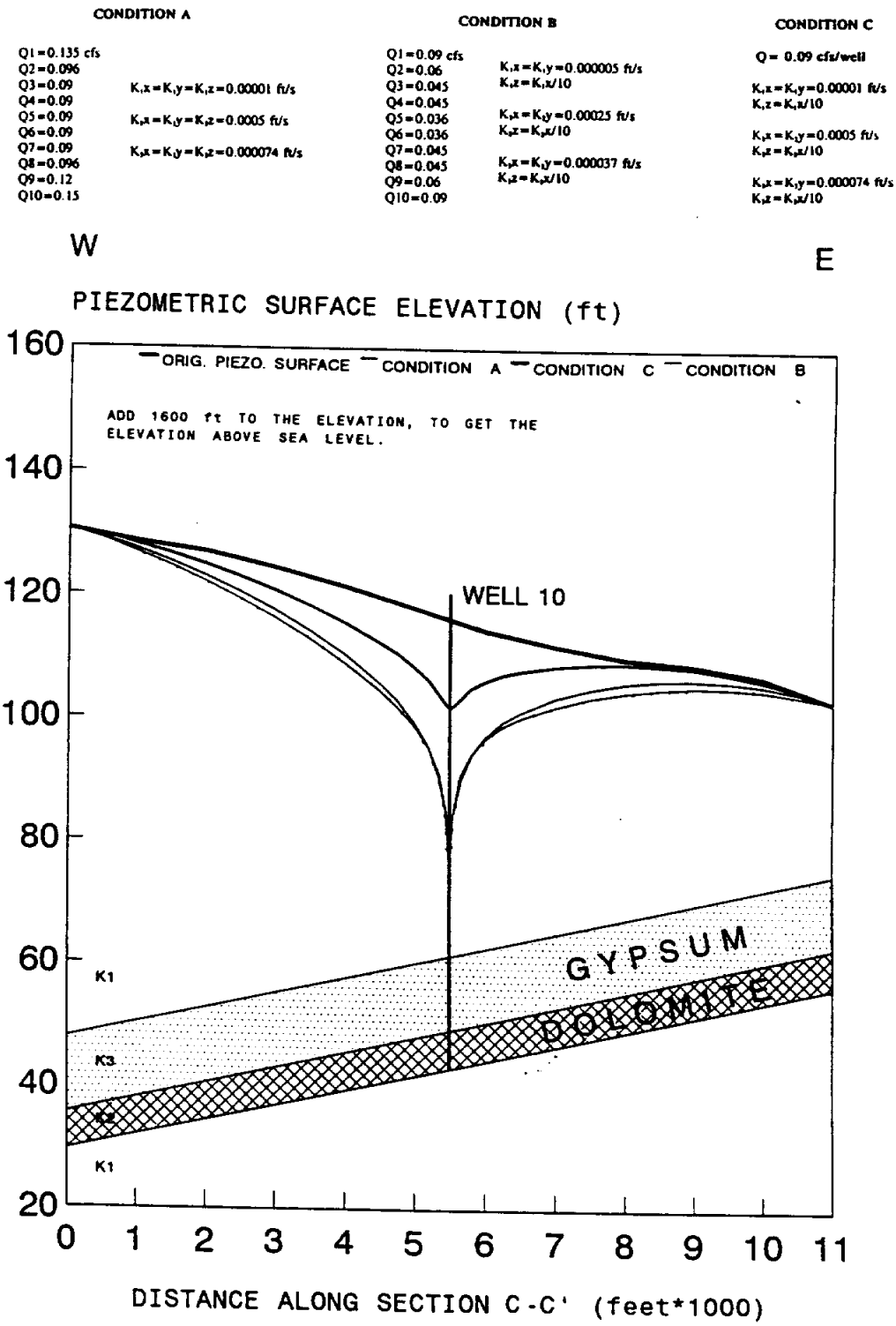

Figure 37. Drawdown along the section C-C' for different pumping rates and permeabilities conditions.

Creek area, it will be necessary for the pumping rate of the recovery system to be at least 2 cfs of brine.

Evaluation of a Recovery Wells System for the Brine - Part II

From the analysis of the model results in the part I, it was decided to extend the area simulated in westward direction. In part II of the analysis the area simulated was 15000 ft in W-E direction and 22500 in S-N direction. The location of the problem domain is shown in the Figure 38. Each horizontal layer of the grid consisted of 39 nodes in the X direction and 105 nodes in the Y direction. Of the 9 nodes or layers in the Z direction, 5 nodes remained fixed in elevation during the iterative solution process. The screened portion of each well consisted of 3 nodes. The horizontal grid with relative location of wells is shown in Figure 39. The vertical grid was considered to consists of 5 layers. In the first simulation of part II, the upper brine aquifer is not considered to be permeable medium, and is assigned a permeability of 0.00001 ft/sec. As shown in Figure 40, the well is screened only in the lower brine aquifer. The lower brine aquifer consists predominantly of anhydrite and dolomite, and is assumed to have a uniform thickness of 17 ft.

The application of model considered the non-homogeneous nature of the brine aquifer. The permeability of the aquifer

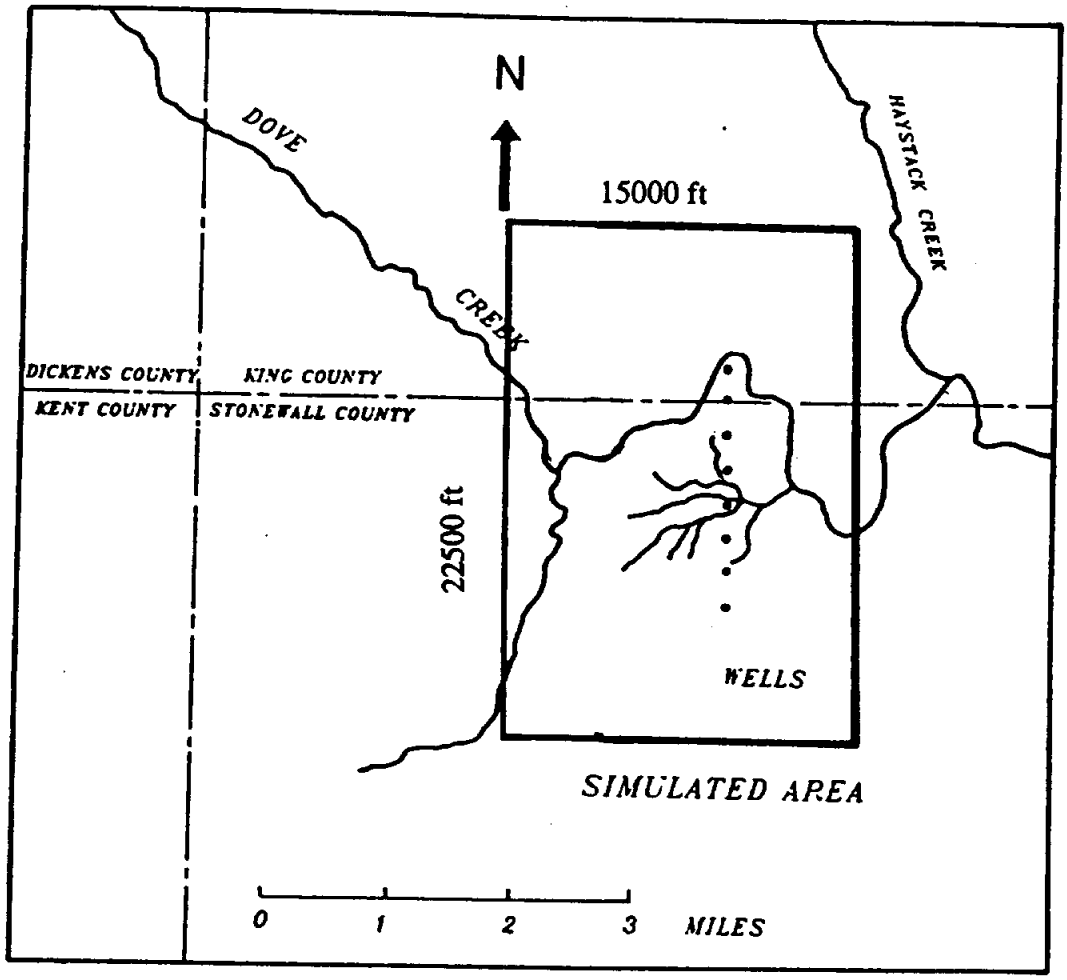

Figure 38. Location of the simulated area for expanded model.

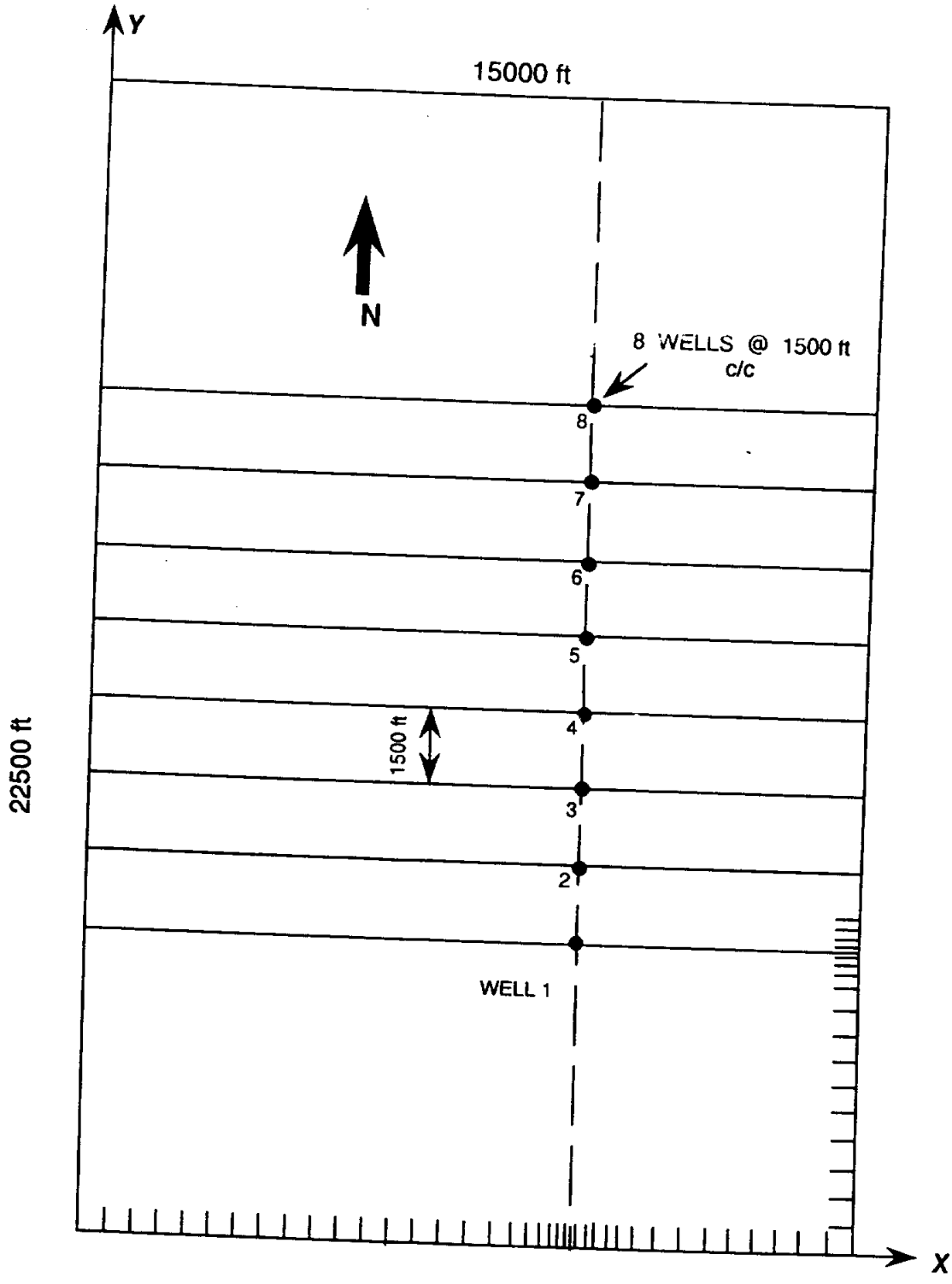

Figure 39. Simulated area in the Dove Creek region, showing the location of wells and horizontal grid for expanded model.

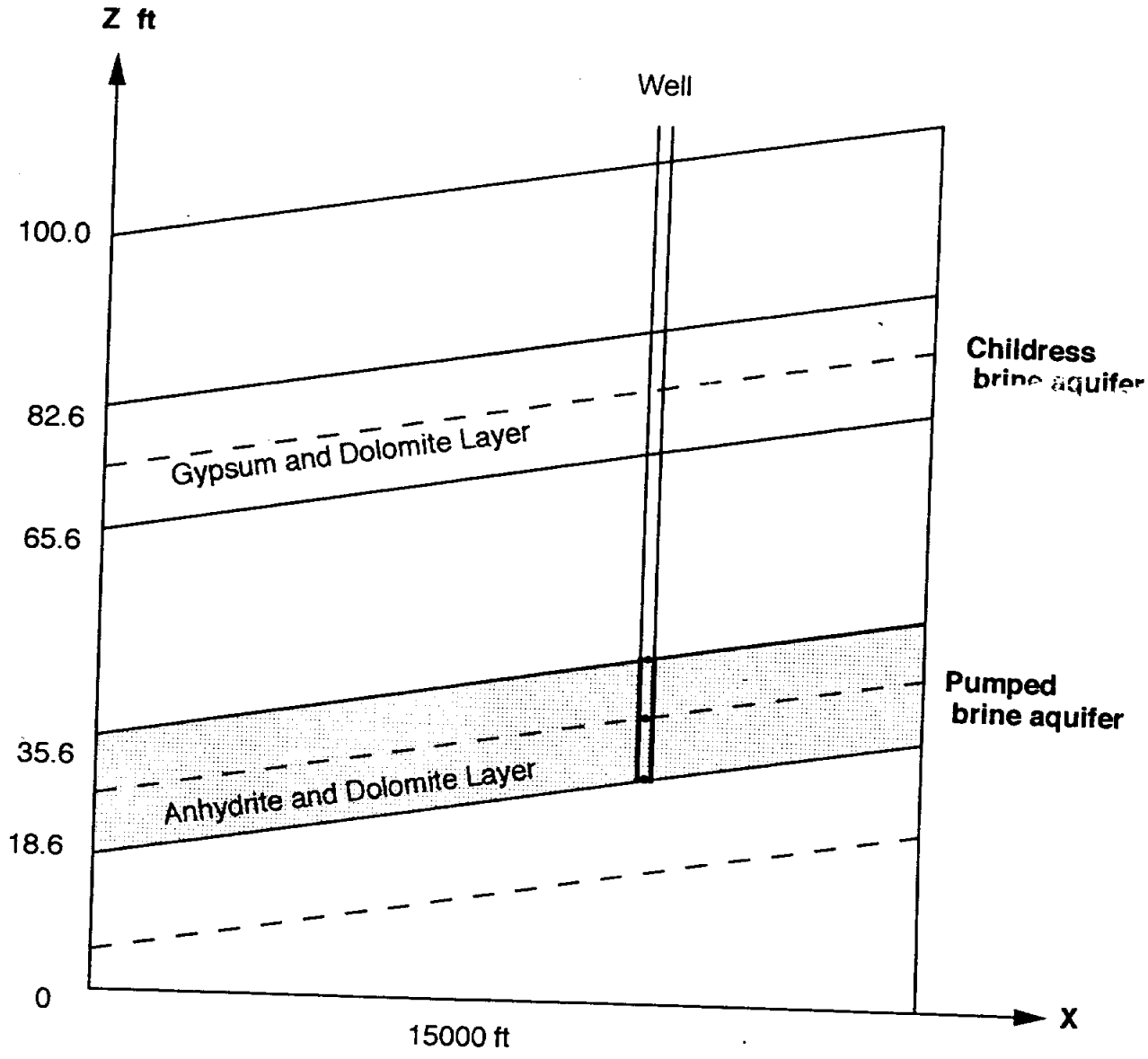

ADD 1600 ft TO THE ELEVATION TO GET THE ELEVATION ABOVE MEAN SEA LEVEL

Figure 40. Vertical profile of the expanded grid used in the simulation.

from which discharge is obtained is not treated as constant. The flow net analysis of the brine aquifer based on the contour maps of piezometric surface(Stevens and Hardt, 1965) indicated that the permeability of the medium increases towards to discharge zone. The permeability computed from the pressure tests conducted by Mason-Johnson and Associates(1955) vary. The results from pressure tests at borings C-1, C-2, and C-2A show a large variation. The artesian spring located at boring C-4 indicates high hydraulic conductivity at that region. Using the steady state Thiem equation, and for a constant discharge of 90 gpm the permeability of the aquifer was computed to be 0.00310 ft/sec.

As shown in Figure 41, the brine aquifer was considered to consist of different zones with different permeabilities. An area 6000 ft by 4000 ft in the discharge zone was considered to have permeability of 0.00155 ft/sec, one half of the magnitude computed at test boring C-4. An area 8000 ft by 15000 ft surrounding the discharge zone was assumed to have the average permeability(0.000096 ft/sec) of the data obtained from the observation wells C-1, C-2, and C-2A. The remaining area simulated by the model was assigned a permeability of

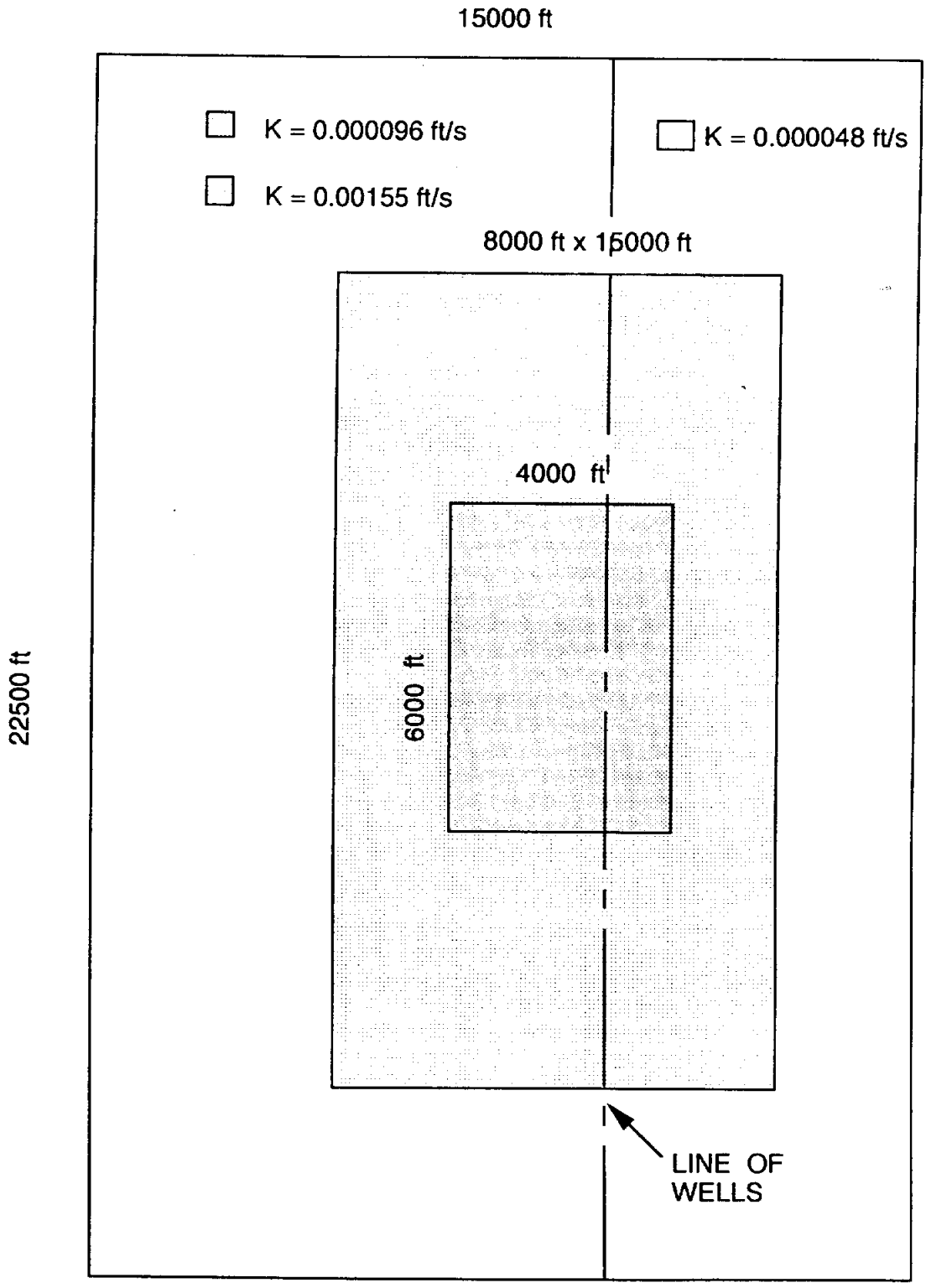

Figure 41. The brine aquifer for expanded model with different permeability regions.

half of the average value of data from the test wells(0.000048 ft/sec).

As a calibration measure, the area was first simulated without the pumping wells. As shown in Figure 42, the computed piezometric surface for equilibrium condition, matches well with the one obtained from map(Stevens and Hardt, 1965). The results obtained in this case are more compatible with the available data than those obtained in the part I, where the aquifer is considered to be homogeneous.

A number of simulation runs were made with the model changing the number of wells and well pumping rates. It was determined that 8 wells spaced at 1500 ft interval would yield a discharge of 2 cfs and would be adequate to stop the flow of the natural brine seeps and springs in the area from discharging into Dove Creek. A N-S profile of the water surface with and without pumping is shown in Figure 43. The pumping rate at the wells could be increased if necessary because the drawdown at the wells is above the top of the well screen. The piezometric surface of the brine with 8 recovery wells in operation is shown in Figure 44. Streamlines showing the flow of brine towards the recovery wells were added to the

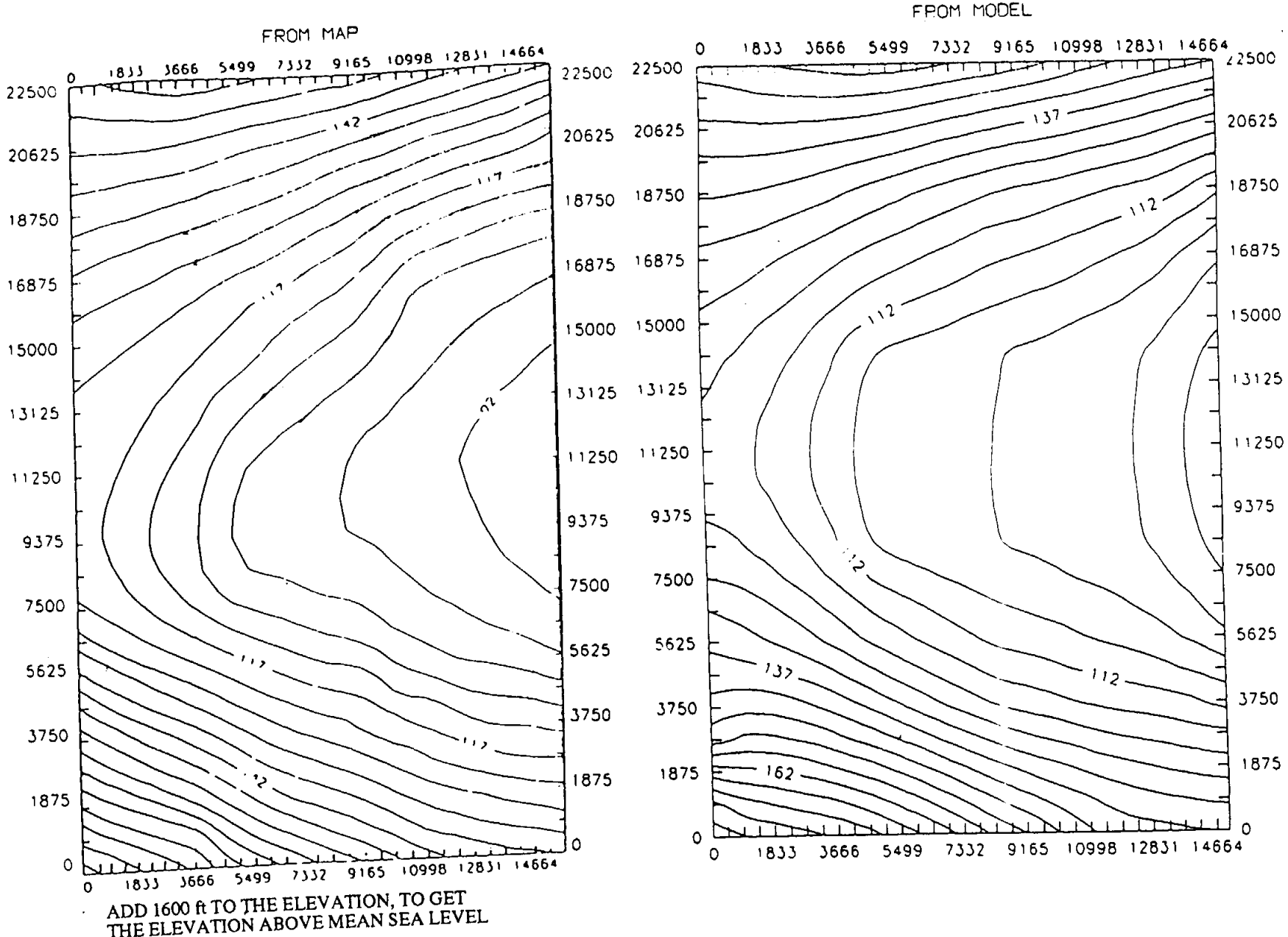

Figure 42. Piezometric head contours from Map and Model for expanded model.

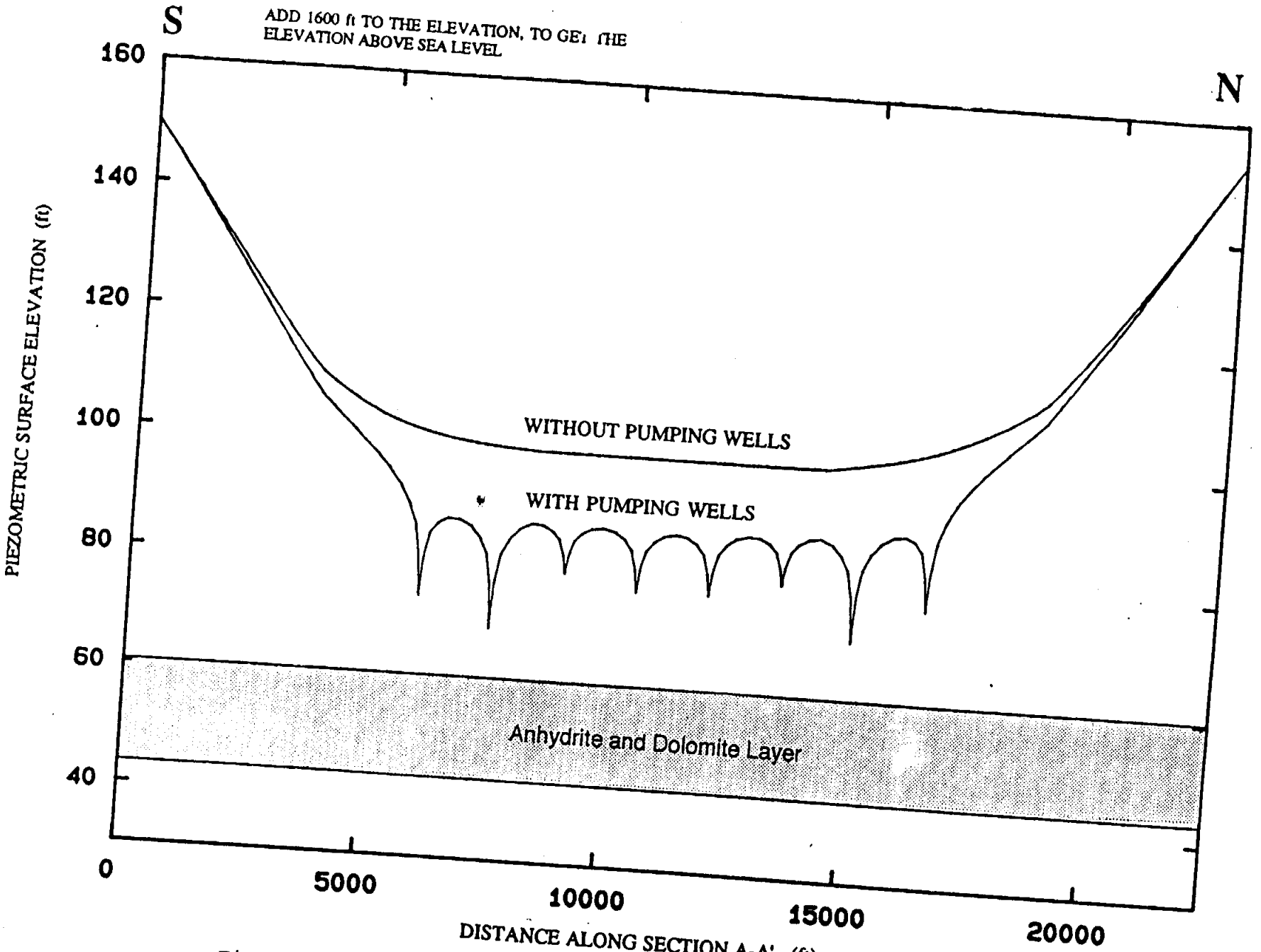

Figure 43. Profile of Drawdown along the wells with and without pumping wells for expanded model.

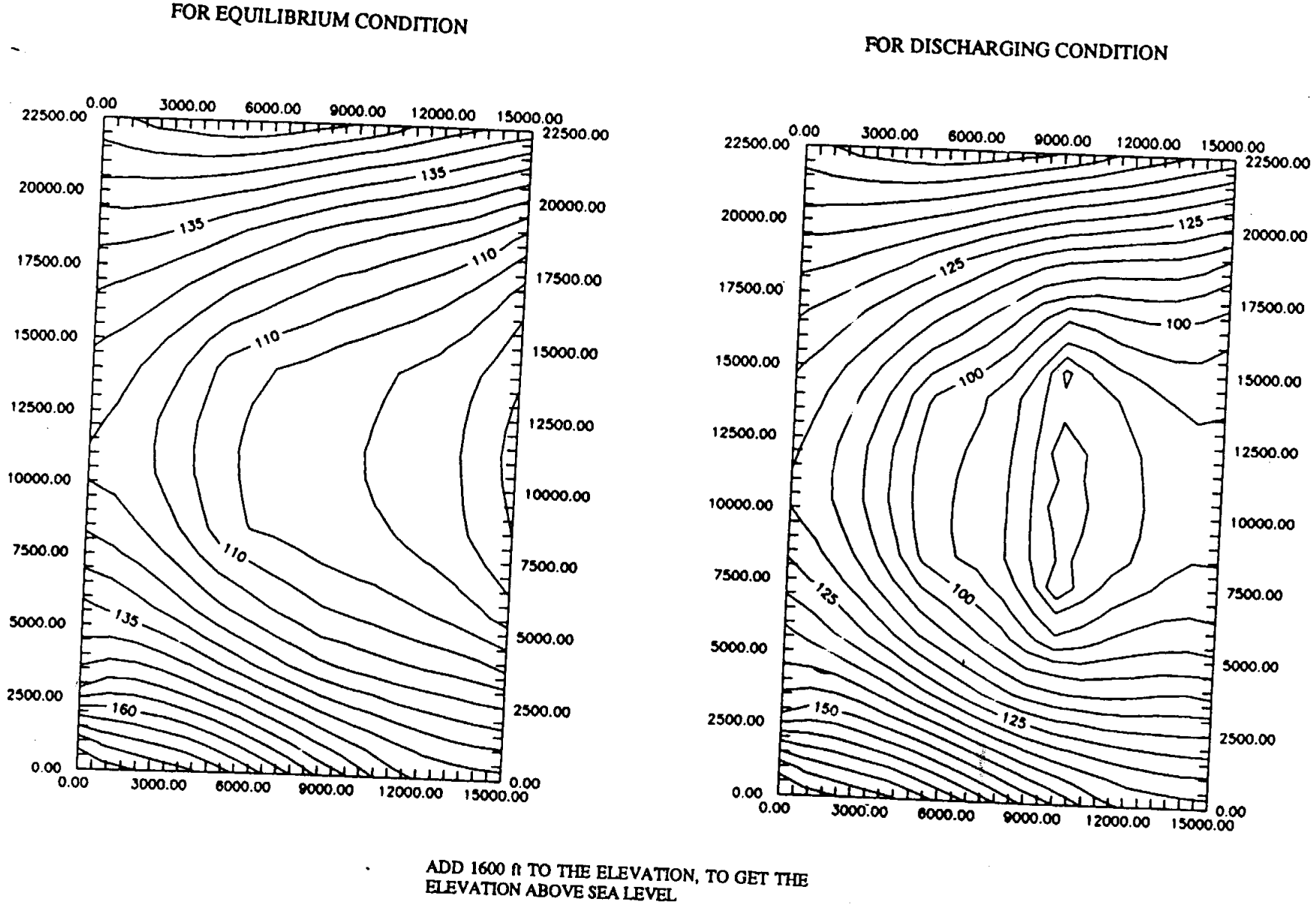

Figure 44. Piezometric head curves obtained for equilibrium and discharging conditions for expanded model.

plot of piezometric surface by hand and is shown in Figure 45. The stream line analysis indicate that a pumping rate of 2 cfs is adequate to prevent the natural salt pollution in the Dove Creek area.

Simulation with two Brine aquifers

Two brine aquifers exist in the Dove Creek area. As shown in the Figure 46, the wells are screened only in the lower brine aquifer. The upper brine aquifer is the Childress member of the Grayburg and consists of predominantly gypsum(where in contact with fresh water) and dolomite. The thickness of the Childress varies between 9 and 19 ft(McMillion,1958). The vertical grid was considered to consists of 5 layers. The upper brine aquifer was considered as one isotropic layer of uniform thickness of 17 ft. In the previous simulations of the area, the permeability of Childress aquifer is not taken into consideration. To evaluate the effect of vertical permeability of the medium and contribution of the Childress brine aquifer to the discharge, a simulation run is made by assigning the Childress aquifer a significant permeability(0.000048 ft/sec).

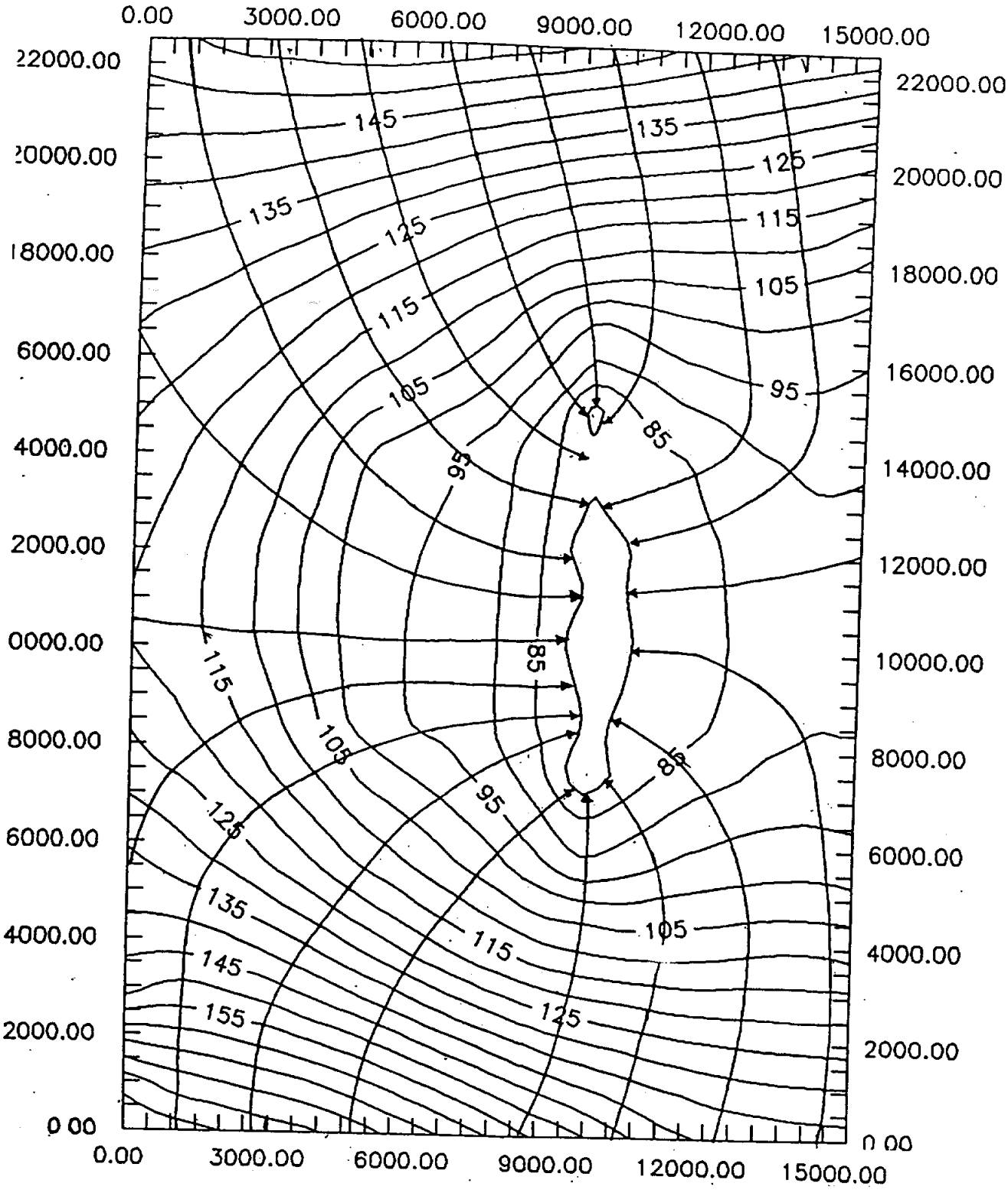

ADD 1600 ft TO THE ELEVATION, TO GET THE ELEVATION ABOVE SEA LEVEL

Figure 45. Contour map of piezometric surface for expanded model with stream lines of brine flow.

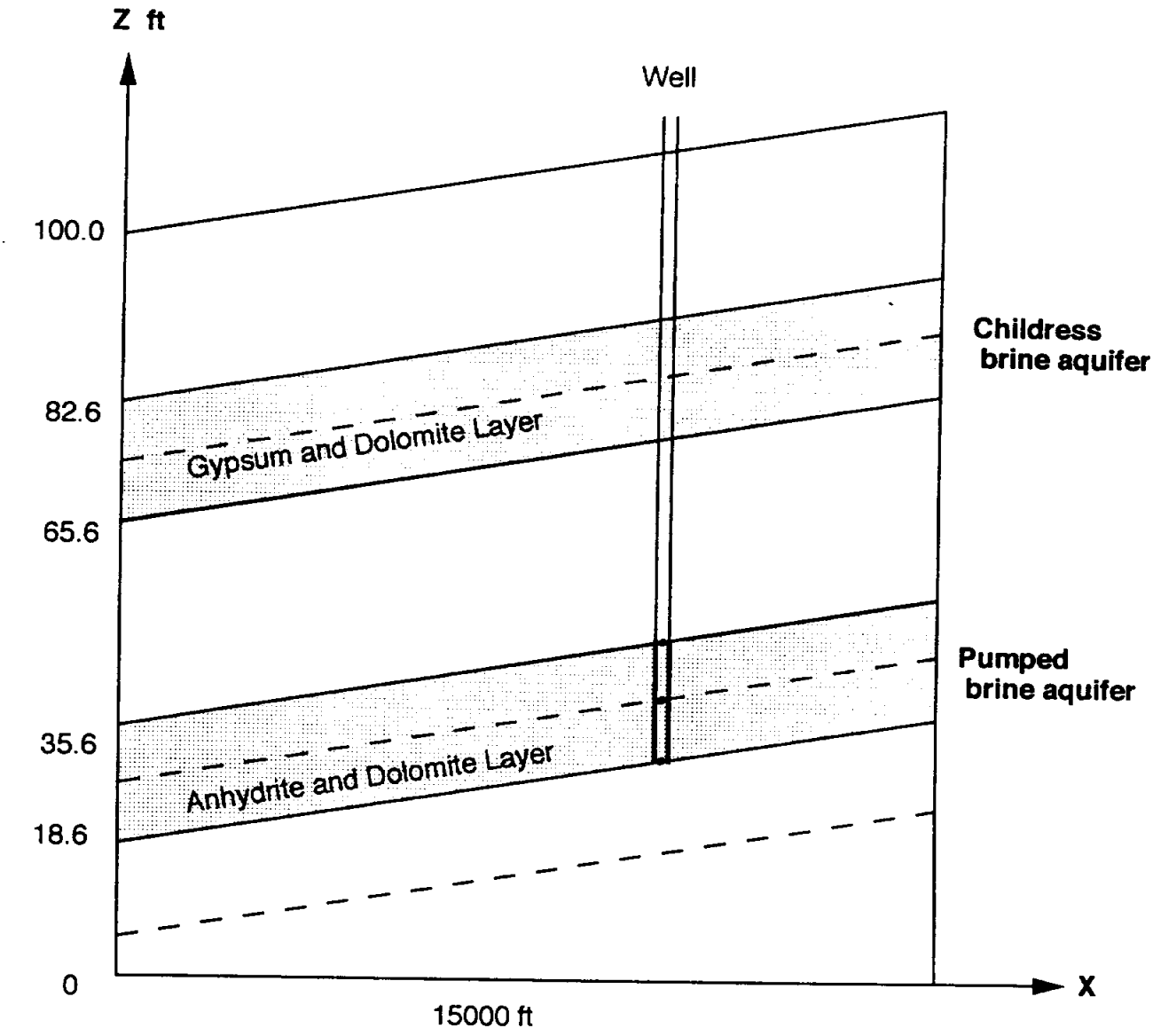

Figure 46. Vertical part of the grid used for simulation with two brine aquifers.

The results obtained indicate that the upper brine aquifer will also contribute to the discharge from the recovery well system. Figure 47 shows a N-S profile of the water table through the line of recovery wells for a steady state discharge of 2 cfs, with one and two brine aquifers. Considering two brine aquifers the pumping rate could be increased if necessary. However, the objective of the recovery system is to prevent the natural salt seeps and springs with a minimum brine recovery. Figure 48 shows the contours of piezometric surface of brine, with one and two brine aquifers under discharging conditions. From the analysis of the results in this simulation, it is shown that the Childress aquifer will also contribute to the discharge of the recovery wells. This simulation represents the best estimates of aquifer conditions in the Dove Creek area. Figure 49 shows the piezometric contour map of the area considering eight recovery wells pumping at a rate of 2 cfs considering two brine aquifers. Under these conditions a pumping rate of more than 2 cfs is required for 100 percent capture of the brine.

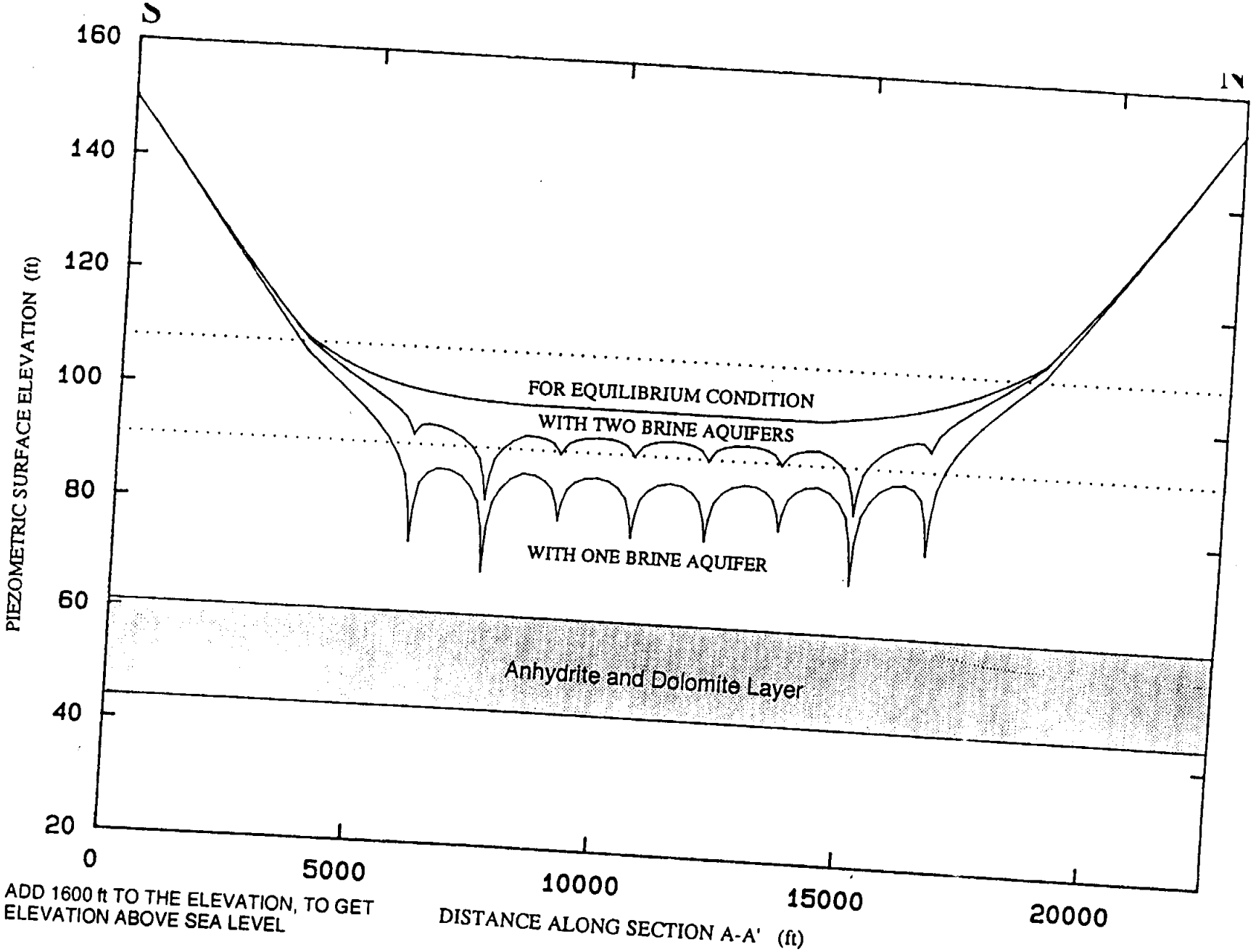

Figure 47. Drawdown along wells with two and one brine aquifers.

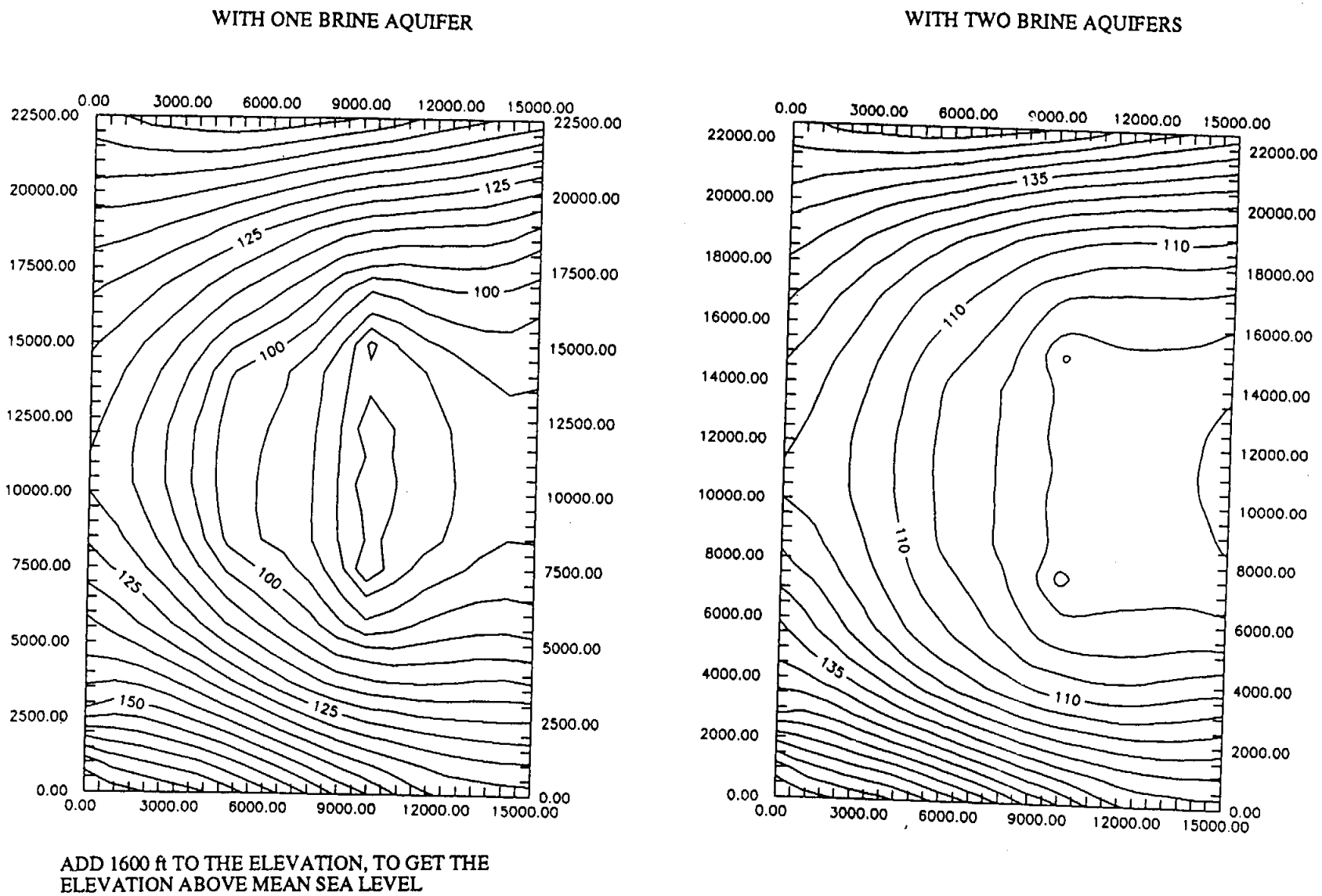

Figure 48. Piezometric head curves obtained with one and two brine aquifers.

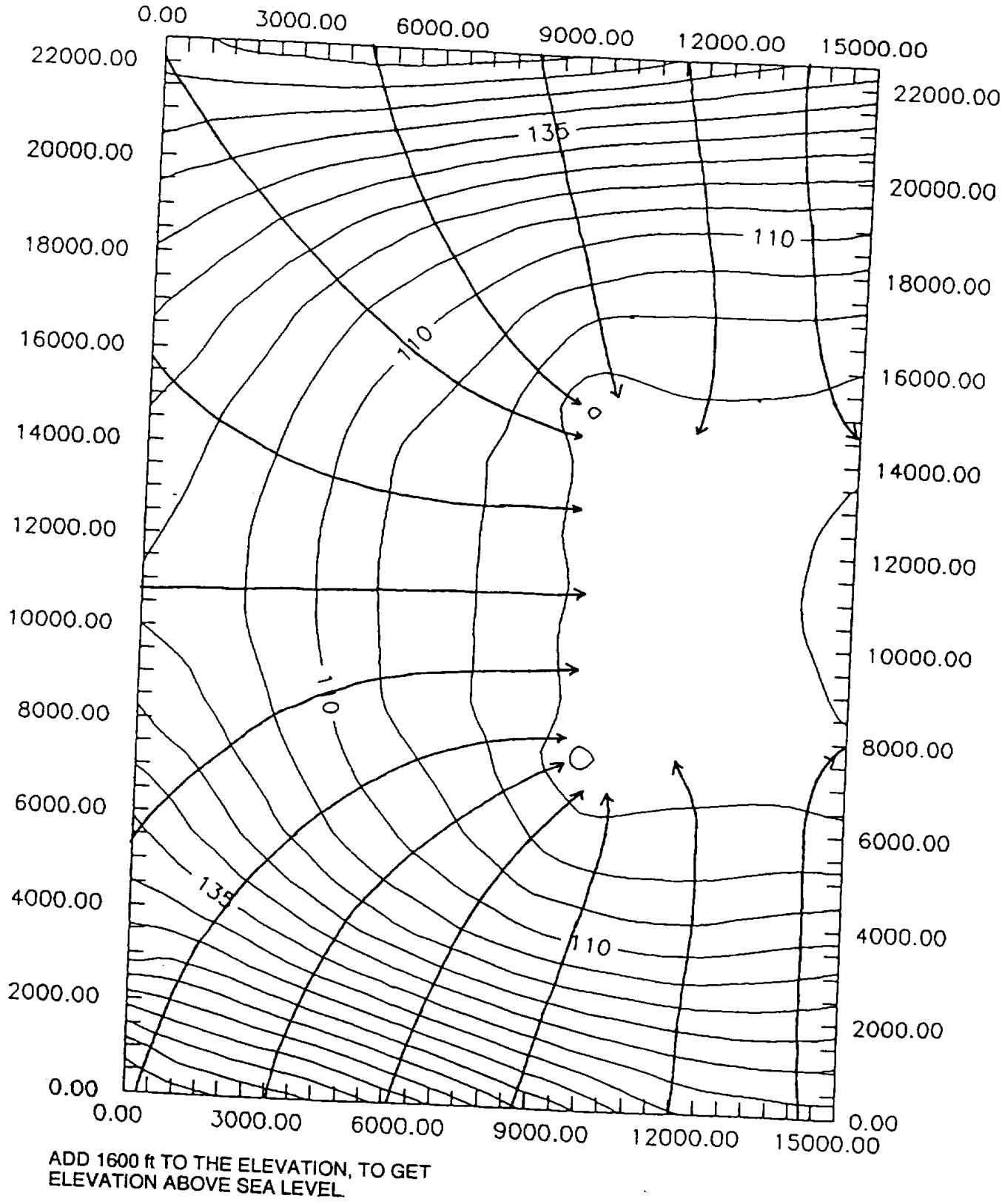

Figure 49. Contour map of piezometric surface with stream lines of brine flow with two brine aquifers.

Change in Recharge Rate

Richter and Kreitler (1986) studied the geochemistry of salt springs and shallow subsurface brines in the Rolling Plains of Texas. Based on the ratio of ions in the brine, they concluded that the source of the brine in the Dove Creek area was a combination halite-dissolution brine from the local recharge area and deep-basin brine.

In the recharge area to the west of Dove Creek salt flat, a shallow fresh water layer overlies the brine. The water table is generally less than 100 ft below the ground surface. Because of the low permeability of the sediments, the water table follows the steep gradients of the ground surface. Below the fresh water zone, the water becomes salty and within a vertical distance of several feet changes to a chloride type brine with dissolved solids more than 200,000 mg/l. The interface transects lithologic units and is not related to stratigraphy or structure. The shape of the interface is related to the thickness of the overlying fresh water.

Baker, Hughes and Yost (1964) studied aerial photographs of the Dove Creek area and were unable to detect any sink holes in the

recharge zone. The halite beds above the brine interface apparently have been dissolved.

If the precipitation is increased in the recharge zone, the recharge will increase. The water table will rise and the brine interface will be lower. Fresh water will be in contact with halite beds and the dissolution of halite will increase. The piezometric head of the brine will increase in the recharge zone and the flow of brine from the recharge zone to the Dove Creek discharge zone will increase. Conversely, a decrease in precipitation on the recharge zone will result in a decrease in brine discharge. The fresh water zone will not be in contact with halite beds and dissolution of halite will cease.

In this study, we were asked to consider the effects that both a 20 percent increase and 20 percent decrease in rainfall on the recharge zone would have on the brine discharge. A 20 percent increase or decrease in rainfall would not result in a 20 percent change in brine discharge for three reasons. First, only part of the brine originates from the local recharge area. Second, a 20 percent change in precipitation does not mean that there will be a 20 percent change in recharge. Deep percolation required for recharge of the aquifer occurs during the winter months when the

ground is saturated for an extended period of time. Additional rainfall during this period will contribute primarily to runoff. Third, with a higher water table, more of the groundwater will discharge through fresh water springs located in topographic low points. It is estimated that a 20 percent change in rainfall will result in approximately 5 to 10 percent change in brine discharge.

PRELIMINARY DESIGN OF RECOVERY SYSTEM

A preliminary design of the recovery system for planning purposes is presented in this chapter. Because of the lack of site-specific information on the hydraulic conductivity in the Dove Creek area and because of the expected large variation in aquifer parameter values between well sites, the number of recovery wells is not known. In this study two applications of the model are presented. One application considers the pessimistic values of the aquifer parameters and requires 20 wells for 100 percent brine reduction while the other application considers our best estimate of the aquifer parameter values and requires 8 wells for 100 percent brine reduction. While we anticipate that less than 10 recovery wells will be required to the eliminate natural salt springs, for planning purposes we will assume that 10 wells result in a 50 percent reduction of natural brine discharge in the Dove Creek area and 20 wells would provide a 90 percent reduction in the natural brine discharge in the Dove Creek area. Ten wells will be spaced on a N-S line through the Dove Creek salt flat 1500 ft apart, while 20 wells will be spaced along

the same line 750 ft apart. The wells depth along this line ranges from 65 ft ot 195 ft with an average depth of 115 ft. The wells are to be completed in the dolomite member of the Dog Creek formation located about 50 ft below the Dove Creek salt flat. No wells will be completed in the Childress dolomite member of the Grayburg formation.

The pumping levels in the wells should be monitored and controlled with a real time remote, automated data acquisition system (see Appendix A for cost estimate of data acquisition system). In order to have adquate space for the brine level sensor and pump, eight inch diameter wells and well screens are recommended. The wells should include a 20-ft length of well screen, gravel packed in a 20-inch diameter hole. The well casing should be PVC pipe and well screen fabricated of a sodium chloride corrosion-resistant material. Selection of the well screen slot size and gravel pack gradation will not be made in this preliminary design.

The pump capacity and motor size will vary from well to well depending on aquifer characteristics. For planning purposes, A Gundfos(225S-150) six stage, stainless steel pump with a 15HP, 460 volt motor is recommended. The casing should

be cut off below the ground surface and pitless connector should be used. Both the electrical power line and collector pipeline should be buried. A remote-controlled valve should be installed in the discharge line of each well to regulate the flow so that the pump motor does not cycle off and on frequently.

For planning purposes, the collector pipeline will consists of 10,000 ft of buried six-inch PVC and 4,000 ft of buried eight-inch PVC. The recovery well pump motors are sized to pump the water in the collector pipeline from the well to the collector station location on the knoll above the 100-yr return flood level(see Figure 50).

Table 4. Summary of Recovery Well Design

	percent brine reduction			
	40	60	80	90
No. of Wells	8	12	17	20
Average Spacing (ft)	1500	1070	880	750
Average Pumping (gpm)	55	53	52	50
Well Diameter (in)	8	8	8	8
Average Depth	115	115	115	115

SUMMARY AND CONCLUSIONS

Salient features of the model

The computer program presented here, is a three-dimensional, finite element model to simulate ground water flow under steady state conditions. The model was developed to design and evaluate the brine recovery well system in the Dove Creek area. The salient features of the model are as follows.

1. The model can handle anisotropic and heterogeneous media.
2. The features of the geological formation, such as variable slopes in x,y, and z directions can be directly incorporated in the model.
3. The automatic mesh generation algorithm incorporated in the model, redefines the position of the nodes, each iteration, until a steady state solution is obtained.
4. The usage of the pointer matrix, makes the model efficient, by reducing memory requirement.
5. The combination of the iterative Gauss-Seidel method, and the pointer matrix saves computation time, by eliminating the computation of zeros in the sparse matrix.

6. The infiltration index used in the model, enables it to consider seasonal variations of the infiltration.

Limitations of the model

The model developed, is tested for several data sets for which analytical solutions were available in literature. Eventhough the model performed satisfactorily for those simple problems, the following limitations are applicable for the model.

1. While evaluating the numerical integrals, problems may develop, if the ratio of the horizontal and vertical sizes of the element exceeds 100. Hence the user must assign the finite element proper dimensions, so that the above mentioned ratio does not exceed the limit, initially or during the solution process.

2. The model is found to be sensitive to the magnitude of convergence limit, for stopping Gauss-Seidel iterative method. Depending on the accuracy requirements and computer time available, the user must assign proper values for the convergence limit.

3. The resulting system of equations is solved, using iterative Gauss-Seidel method. Hence all the limitations applicable for Gauss-Seidel method are also applicable to the model. Other iterative methods such as Jacobi, Conjugate Gradient etc., can also be incorporated in the model.

4. Eventhough the model is based on finite element method, the problem domain should be approximated as a rectangular domain. The formation is considered to be consisting of number of parallelopiped elements. This is done to facilitate the computations of mean permeabilities of elements.

Model Usage

The model presented herein, was tested for various kinds of data including some field problems. The computer model is generally run on VAX platform. The CPU time requirement depends upon two factors, i.e., the size of the problem and magnitude of convergence limit. Large field problems, such as Dove Creek application are run on CRAY Y-MP. A closer initial guess of solution in general reduces the, CPU time requirement. For a problem with approximately 40000 nodes, and

Gauss-Seidel convergence of 0.001, the CPU time requirement on CRAY Y-MP, is around 2950 seconds. A problem with a magnitude of 1000 nodes and convergence of 0.001 requires around 18 seconds of CPU on CRAY Y-MP. These requirements may vary slightly, depending upon the nature of the problem. This model is primarily developed to design a recovery well system or to study the response of the water table elevation with respect to discharging conditions. Hence the user must carefully convert his problem domain into finite element grid, subject to the limitations mentioned above. Availability of computing resources, is an important factor while defining the problem domain. The smaller the elements, the larger the requirement of CPU time. In addition to above mentioned factors, for some kinds of data the Gauss-Seidel method used in the subroutine GS may not converge. This especially happens when the considered problem is large(more than 25000 nodes). Truncation and round-off errors make the resultant co-efficient matrix non-symmetrical. For the convergence of the solution by Gauss-Seidel method, the coefficient matrix should be symmetric positive definite. In such cases, those errors can be eliminated by adopting double precision at the expense of

computer time. To eliminate to round-off or truncation errors, the resultant coefficient matrix can be converted to symmetric matrix by assigning elements (i,j) and (j,i), an average of the magnitudes. Various alternatives were studied to substitute the iterative Gauss-Seidel method in those cases, where the Gauss-Seidel method fails. Eventhough number of efficient methods were available in literature, most of them requires a square co-efficient matrix. This imposes limitations on the size of the problem because of the memory requirement. A software package called NSPCG(non-symmetric pre conditioned conjugate gradient method), a basic matrix solver available in public domain netlib, can be utilized while dealing with large scale field problems. Depending upon the sparsity and nature of the matrix, different forms of storage and method of solution can be defined.

Conclusions

1. The water quality in the Brazos River is seriously degraded by natural salt pollution in Upper Brazos River. The primary source of the salt pollution is brine springs and seeps in the Salt Fork Brazos River watershed. The water quality in the Brazos River improves downstream because of dilution with fresh water from tributaries. Water quality in the middle reach of the Brazos River is poor with chloride concentration ranging from 300 to 1000 mg/l. Water from the three main stream reservoirs is unsuitable for municipal water supply without costly treatment.

2. Controlling the natural salt springs and seeps in the Dove Creek area will reduce the chloride concentration in the Brazos River nearly by 50 percent. Approximately 1000 tons per day of chloride is being discharged into the Upper Brazos River from natural salt springs and seeps. Brine at a representation chloride concentration of 100,000 mg/l and flow rate of 2 cfs for the Dove Creek area discharge 540 tons per day. Approximately half the chloride load in the Upper Brazos River is from the Dove Creek salt springs and seeps.

3. There are two brine aquifers in the Dove Creek area that contribute the natural salt pollution of the Brazos River. The brine springs and seeps have been studied by Blank(1955 to 1956), Mason and Johnson & Associates(1955), McMillion(1958), Baker, Hughes and Yost(1965), Keys and MacCary(1973) and Stevens(1974). Stevens(1974) mapped the brine aquifers that contribute to the natural salt pollution. The upper aquifer is the dolomite layer in the Childress formation while the lower aquifer is a dolomite layer in the Dog Creek formation.

4. A variable density model is not required to evaluate the recovery wells system. Over most of the area, a shallow fresh water layer overlies the brine. Below the freshwater, the water becomes salty and within a vertical distance of several feet, changes to a chloride type brine with dissolved solids more than 200,000 mg/l. The brine-fresh water interface is a thin transition zone between the fresh water above and brine below. In general, the interface transects lithographic units and is not related to stratigraphy or structure.

5. The brine that is discharged as natural springs and seeps in the Dove Creek area is from two sources, (1)local recharge and (2)deep-basin. Based on the ratio of ions in the brine,

Ritcher and Kreither(1986) concluded that the brine was a combination of halite dissolution brine from the local recharge and deep-basin brine. The halite beds above the brine interface in the local recharge area have apparently been dissolved.

6. Permeability measurements of the brine aquifer taken several miles away from the discharge zone are not representative values for the design of the recovery system. Flow net analysis of the brine aquifer indicates that the permeability of the aquifer increases near the discharge zone. Observations near the discharge zone indicate that the aquifer is very permeable over a relatively large area.

7. A shallow-well, brine recovery system located in the discharge zone of the brine aquifer will eliminate the natural salt springs and seeps in the Dove Creek area. Based on our best estimate of aquifer paramaters, a relatively inexpensive, shallow recovery system with less than 10 wells will be required. The recovery wells will be 8 inches in diameter, screened only in the lower aquifer, gravel packed with an average depth of 115 ft. Preliminary design indicate the wells will be spaced along a N-S line through the Dove Creek salt

flat. A brine recovery rate of approximately 2 cfs is required to lower the piezometric surface and eliminate the natural brine springs and seeps in Dove Creek area.

8. The amount of brine necessary to be pumped from the recovery system to control the natural brine springs and seeps in the Dove Creek area is expected to change very little from year to year. It was estimated that a 20 percent change in precipitation will result only a small change in brine discharge. An increase in precipitation in the recharge area will result in an increase in the elevation of the fresh water table, a decrease in the elevation of the fresh-brine interface, and an increase in discharge from fresh water springs.

REFERENCES

Aral, M. M. 1990. Ground Water Modeling in Multilayer Aquifers. Lewis, Chelsea, Michigan. 114 pp.

Babu, D. K., and G. F. Pinder. 1984. A finite element-finite difference alternating direction algorithm for three-dimensional groundwater transport, in Proceeding of the Fifth International Conference on Finite Elements in Water Resources, pp. 165-174, Springer-Verlag, New York.

Baker, R. C., L. S. Hughes, and I. D. Yost. 1964. Natural Sources of Salinity in the Brazos River, Texas. U.S. Geological Survey Water-Supply Paper 1669-CC, pp. CC1-CC81.

Bear, J. 1972. Dynamics of Fluids in Porous Media. Dover, New York, 764 pp.

Bear, J., and A. Verruijt. 1990. Modeling Groundwater flow and pollution. D. Reidel Publishing Company, Dordrecht, Holland, 414 pp.

Becker, E., G. F. Carey, and J. T. Oden. 1981. Finite Elements An Introduction. Prentice-Hall, New Jersey, 258 pp.

Carnahan, B., H. A. Luther, and J. O. Wilkes. 1969. Applied Numerical Methods. John Wiley, New York. 604 pp.

Cedergren, H. 1967. Seepage, Drainage, and Flow Nets. John Wiley & Sons, New York. 489 pp.

Cheung, Y. K., and L. Skjolingstad. 1974. Two-and three-dimensional ground water seepage by finite elements, Finite Element Method in Engineering. The University of New South Wales.

Darcy, A. 1856. Les Fontaines Publiques de la Ville de Dijon. Dalmont, Paris.

Dhatt, G., and G. Touzot. 1984. The Finite Element Method Displayed. John Wiley & Sons, New York. 509 pp.

France, P. W. 1974. Finite element analysis of three-dimensional ground-water flow problems. Journal of Hydrology, v. 21, pp. 381-398.

Freeze, R. A. 1971. Three-dimensional, transient, saturated-unsaturated flow in a groundwater basin. Water Resour. Res., v. 7, no. 2, pp. 347-366.

Frind, E. O., and M. J. Verge. 1978. Three-dimensional modeling of groundwater flow systems. Water Resour. Res., v. 14, no. 5, pp. 844-856.

Gambolati, G., G. Pini, and T. Tucciarelli. 1986. A 3-D finite element conjugate gradient model of subsurface flow with automatic mesh generation. Adv. Water Resour., v. 9, pp. 34-41.

Gupta, S. K., and K. K. Tangi. 1976. A three-dimensional Galerkin finite element solution of flow through multiaquifers in Sutter Basin, California. Water Resour. Res., v. 12, no. 2, pp. 155-162.

Gupta, S. K., C. R. Cole, and G. F. Pinder. 1984. A finite-element three-dimensional groundwater (FE3DGW) model for a multiaquifer system. Water Res. Res., v. 20, no. 5, pp. 553-563.

Huang, Y. H., and S. J. Wu. 1974. Analysis of unsteady flow toward artesian wells by three-dimensional finite elements. Res. Rep. 75, Water Resour. Inst., Univ. of Ky., Lexington.

Huang, Y. H., and S. J. Wu. 1975. Simulation of confined aquifers by three-dimensional finite elements, in Advances in computer methods for partial differential equations. R. Vichnevetsky (editor).

Huyakorn, P. S., B. G. Jones, and P. F. Andersen. 1986. Finite element algorithms for simulating three-dimensional groundwater flow and solute transport in multilayer systems. Water Resour. Res., v. 20, no. 3, pp. 361-374.

INTERCOMP Resource Development and Engineering. 1976. Development of model for calculating disposal in deep saline aquifers, Parts I and II, USGS/WRI-76-61. PB-256903. National Technical Information Service, Washington, D. C.

Istok, J. 1989. Groundwater Modeling by the Finite Element Method. American Geophysical Union, Water Resources Monograph 13, Washington, D.C., 495 pp.

Keys, W. S. and L. M. MaCary. 1973. Location and Characterization of the Interface Between Brine and Fresh Water from Geophysical Logs of Boreholes in the Upper Brazos River Basin, Texas. U.S. Geological Survey Professional Paper 809-B, pp. B1-B23.

Liggett, J. A., and P. L. F. Lui. 1983. The boundary integral equation method for porous media flow. George Allen and Unwin, London. 255 pp.

Mason and Johnson & Associates. 1955. Dove Creek Salt Study, Stonewall County, Texas: Dallas, 17 pp.

McDonald, M. G., and A. W. Harbaugh. 1984. A modular three dimensional finite difference groundwater flow model. U.S. Geol. Surv., 528 pp.

McMillion, L. G. 1958. Groundwater Geology in the Vicinity of Dove and Croton Creeks, Stonewall, Kent, Dickens, and King Counties, Texas, with special reference to salt water seepage: Texas Board of Water Engineers Bulletin 5801, 53 pp.

Narasimham, T. N., and P. A. Witherspoon. 1976. An integrated finite difference method for analyzing fluid flow in porous media. Water Resour. res., v. 12, no. 1, pp. 57-64.

Nawalany, M. 1986. Numerical model for the transport velocity representation of groundwater flow. VI International conference on finite elements in water resources, Lisboa, Portugal.

Posson, D. R., G. A. Hearne, J. V. Tracy, and P. F. Frenzel. 1980. Computer program for simulating geohydrologic systems in three dimensions. U.S. Geol. Surv., Open File Rep. 80-241 (modified version), Reston, Va.

Reeves, M., D. S. Ward, N. D. Johns, and R. M. Cranwell. 1986. Theory and implementation for SWIFT II, The Sandia Waste-Isolation Flow and Transport Model for Fractured Media. NUREG/CR-3328 and SAND83-1159, Sandia National Laboratories, Albuquerque, New Mexico.

Richter, B. C. and C. W. Kreitler. 1986. Geochemistry of Salt-Spring and Shallow Subsurface Brines in the Rolling Plains of Texas and Southwestern Oklahoma. Bureau of Economic Geology, Report of Investigations No. 155, Austin, TX.

Stevens, P. R. 1974. Geohydrology of the Upper Brazos River Basin between Lubbock and Possum Kingdom Reservoir, Texas with Special Reference to Discharge of Brine from Springs and Seep, U.S. Geological Survey, unpublished report.

Stevens, P. R. and W. F. Hardt. 1965. Preliminary Report on the Investigation of Salt Springs and Seeps in a portion of the Permian Basin of Texas: U.S. Geological Survey Open File Report, 19 pp.

Taylor, C., and P. S. Huyakorn. 1978. Three-dimensional groundwater flow with convective dispersion, in Finite Elements in Fluids, vol. 3, edited by R. H. Gallagher, John Wiley, New York, pp. 311-321.

Trescott, P. C. 1976. Documentation of finite-difference model for simulation of three-dimensional groundwater flow. U.S. Geol. Surv. Open File Rep., 75-438, 32 pp.

U.S. Army Corp of Engineers, Fort Worth District. 1983. Brazos Natural Salt Pollution Control, Brazos River Basin, Texas. Design Memorandum No. 1, General Phase I - Plan Formulation.

U.S. Army Corps of Engineers, Fort Worth District. 1973. Natural Salt Pollution Control Study, Brazos River Basin, Texas. v. 1-4, 1147 pp.

U.S. Army Corps of Engineers, Tulsa District. 1985. Red River Chloride Control Project.

U.S. Bureau of Reclamation. 1985. Technical Report on Lake Meredith Salinity Control Project, Canadian River, Texas-New Mexico.

Van Der Heijde, P., Y. Bachmat, J. Bredehoeft, B. Andrews, D. Holtz, and S. Sebastian. 1985. Groundwater Management: The Use of Numerical Models. American Geophysical Union, Water Resources Monograph, Washington, D. C.

APPENDIX

A

Real Time Remote

Automated Data Acquisition System

for

Monitoring Water Levels and Control of Pumps

for the Brine Recovery Wells

SYNERGETICS INTERNATIONAL

February 3, 1993

Mr. Wesley P. James
Civil Engineering Department
Texas A & M University
College Station, TX 77843-3136

Dear Mr. James:

I'm glad you called with questions. I had been meaning to call you. In the rush of our year end business perhaps our response to your future requirement was a bit rushed. It was our understanding that you were after area pricing for planning purposes

Attached are specification sheets for the various units to be integrated. I've included radio transceiver units, for this is over the long term the most satisfactory. Replacing wiring channeling and labor with hardware will produce a better and more troublefree operation.

Revised costs are as follows:

o Well Site (10)	
Pressure Transducer	$800.00
Data Collection Platform with radio modem and NEMA Enclosure	$1,300.00
Radio Transceiver with Antenna	$1,200.00
50 ft. of cable	$75.00
o Central Site (1)	
PC with control software	$12,500.00
Radio/DCP	$2,500.00
o Other	
* - Site survey and radio license	$1,200.00
- Training and installation supervision	$5,000.00
- Back up spares	$2,500.00
Total of Estimate	$57,450.00

* This can range from $500 to $2500 depending on site situation.

Synergetics International, Inc. 1831 Lefthand Circle Longmont, CO 80501 303-678-5200 FAX 303-678-5206

The above is a general estimate based on today's conditions. By the time you are ready to move forward prices and brands may change.

One other note, while construction and installation is in progress provision for grounding each of the hardware sites can be done. This can be another $100 to $200 worth of miscellaneous hardware.

Please let us know if more information is needed.

Sincerely

Robert R. Miner
Sales Manager

Encs

RM/jm

SYNERGETICS INTERNATIONAL

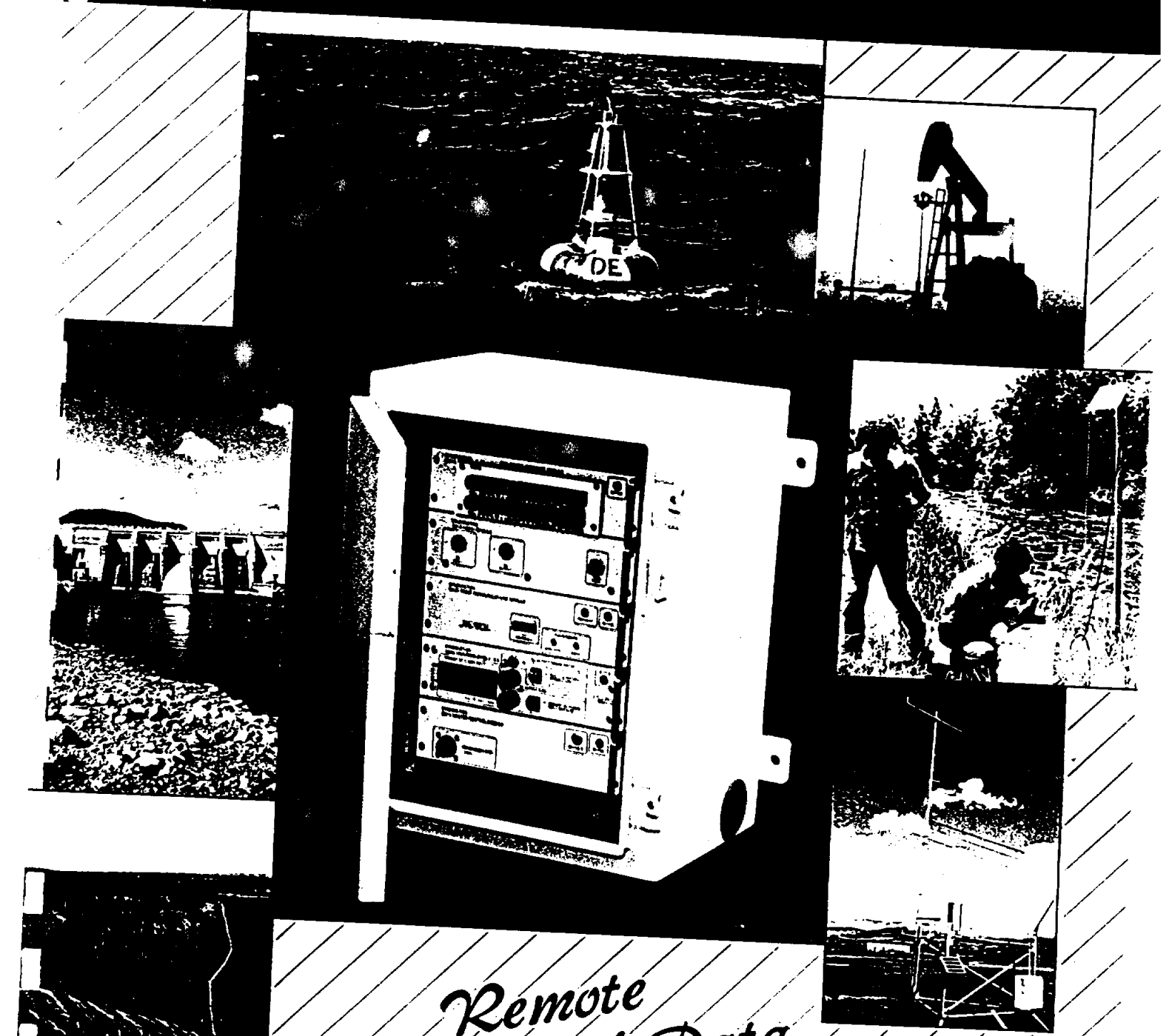

Remote Automated Data Acquisition Systems . . .

Overview

Synergetics provides complete systems for remote data acquisition and control applications. These systems allow you to automate the data collection and operation of your field instruments and sensors. You can then conveniently retrieve and analyze your field data from your office.

Typical systems include these three major components:

- A Remote Terminal Unit (RTU)
- A Communications method
- A Central Receiving Station

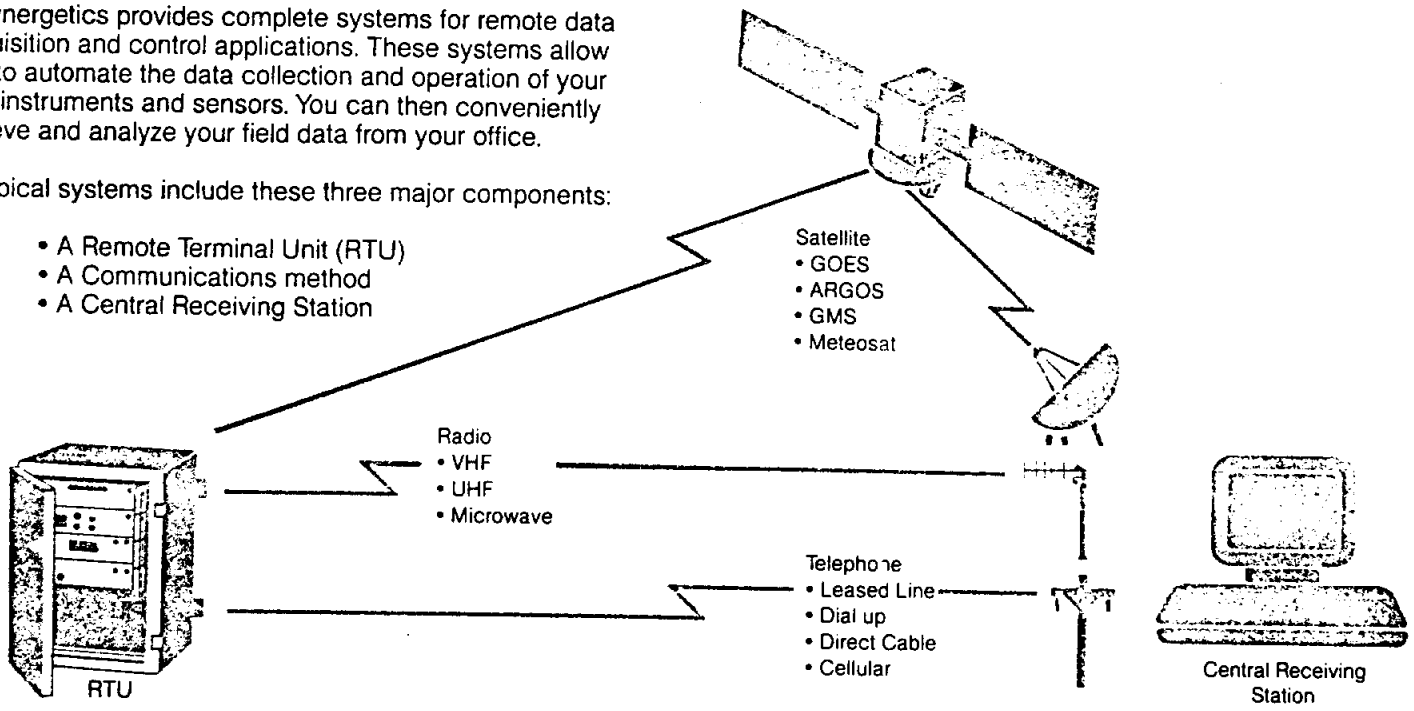

STANDARD APPLICATIONS

- Water Resource Management
- Water Quality Measurements
- Ground Water Monitoring
- Dam Safety Monitoring
- Nuclear Radiation Monitoring
- Air Quality Monitoring
- Climatic Measurements
- Seismic Monitoring
- Pipeline Monitoring
- Flood Warning Systems

INSTALLATION

Synergetics Field Service organization can provide the level of support you require, from complete installation to on-site customer training. Whatever level you select, your system will meet your specifications before we turn it over to you.

SERVICE

Synergetics offers a number of service options that can be tailored to your requirements. Services include on-site repares, field servicing, factory repair, and extended warranty programs.

SYSTEM COMPONENTS

Remote Terminal Unit

The Synergetics RTU is a complete series of control, I/O, and communications modules that can be configured to meet your specific data acquisition needs. These field proven components operate in harsh environments, with low power requirements, high reliability and rugged construction. The RTU offers a wide range of sensor input capabilities, on-site data processing and control, and scheduled transmission of formatted data.

Communications

The Synergetics communications architecture provides the link between your RTU and the Central Receiving Station. Via this component of the system, the RTU can transmit data to the Central Receiving Station over:

- Satellite
- UHF / VHF Radio / Microwave
- Telephone
- Hard-wire

Central Receiving Station

The Synergetics Central Receiving Stations control the data acquisition system from your office or local operating station. The Central Receiving Stations is comprised of a complete computer system that will collect, archive, process, analyze and display a wide variety of data.

SYNERGETICS INTERNATIONAL
1831 Lefthand Circle
Longmont, CO 80501
(303) 678-5200

FAX (303) 678-5206

SYNERGETICS INTERNATIONAL

Data Acquisition System Model 4170

The Synergetics Model 4170 is a low cost, powerful Data Acquisition System engineered for ease of use and a variety of application requirements. Standard features include 16 I/O channels, 64K bytes of CMOS RAM, and a numeric keyboard display. The 4170 has complete radio and telephone communication capabilities.

Application programming in BASIC provides easy modification of monitoring conditions and parameters.

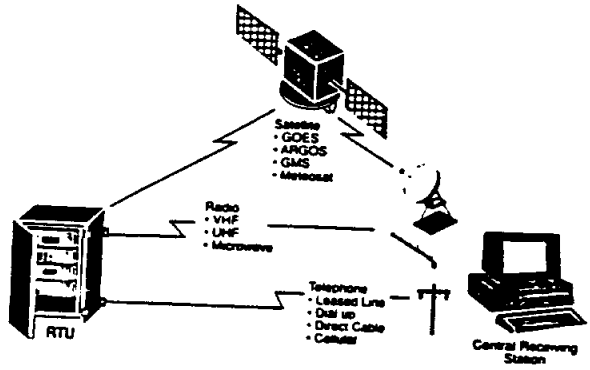

SPECIFICATIONS

LOGIC FAMILY
Low noise CMOS for noise immunity.

RAM
32K bytes CMOS static, Lithium battery back up, 24 months

EPROM
32K bytes CMOS.

MEMORY SECURITY
Write protect RAM. Triply redundant storage and voting of critical parameters. Time delay on write protect removal

WATCHDOG TIMER
Restarts unit on failure of either main or interrupt softrware.

AUTOBOOT
Unit restarts process that was active prior to power outage.

KEYBOARD
Sealed 16-key numeric.

REALTIME CLOCK/CALENDAR
Battery backed .005% accuracy; sec. min, hr, day, mo, yr.

SERIAL PORT
RS232/RS422 at 75 to 19,200 baud, software selected. Interrupt controlled 80 characters transmit and receive ring buffers.

ANALOG INPUT
4 channels, 10 bit res., 4-20 ma. pr 0-5 VDC, up to 2000 samples/sec.

DIGITAL INPUTS
8 channels, logic or dry contact

DIGITAL OUTPUTS
4 relay drivers, 100 ma. per channel, 48 VDC back EMF protected.

SOFTWARE IN EPROM
Floating pt BASIC with subroutines, indexed variables, and strings; I/O scanned and mapped to arrays; pulsecounters and event timers. Power up autoboot, critical parameter voting, clock setting, communication setting, BASIC fault trapping, CRC calculation, plotting to LCD and to printer, serial port character buffering. more.....

MODEM BOARD

INTERRFACING STANDARDS
Bell 103/212. RS232. RS422. 2-wire telephone, 4-wire radio with transmit key, CCITT compatibility optional.

DIALUP INTERFACE
Autoanswer/autodial, call progress detect, touchtone dial and detect.

MAIN TERMINAL BOARD

FIELD TERMINATIONS
I/O connections are scre type terminals so unit can be changed out without removing individual field wire.

LED INDICATORS
One for each of 8 digital inputs and 4 relay outputs.

I/O CONDITIONING
AI current sensing resistors and current/voltage selectors, DI pullup and isolation resistors, 8 amp relays for DO's fuse, power filtering and isolation diodes.

ANALOG I/O EXPANSION

ANALOG INPUT
Optically isolated 4-20 ma., 12 bit channel

POWER & ENVIRONMENT

Power 12 VAC/DC ±30%, 80 ma. to 140 ma., relays off. Temperature -40° to +88°C, except LCD 0° to 50°C. Humidity 5% to 95%, noncondensing.

ENCLOSURES
Epoxy painted steel card cages with plastic guides, in 2 slot.

SYNERGETICS INTERNATIONAL

Data Sheet

SYNERGETICS MODEL 135
REMOTE MONITORING MANAGEMENT SYSTEM

Now the collection and monitoring of sensor data and the control of all remote sites can be effectively managed from a PC-based central receiving station. Synergetics Model 135 Remote Monitoring Management System (RMMS) allows you to monitor and control a variety of field instruments and sensors. The resulting data is displayed in colorful charts, graphs, and reports that are quick and easy to read.

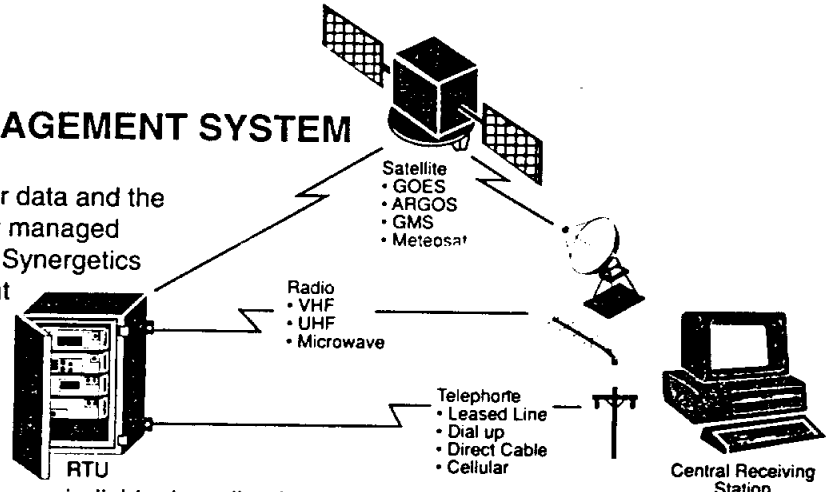

The Synergetics RMMS can be tailored to your individual application and requirements. For example: A Flood Warning System would consist of Synergetics RTUs in the field measuring rainfall, river stage and other customer specified parameters, and reporting via radio or telephone to the Central Site RMMS. The RMMS could graphically display the entire area or flood basin highlighting the RTU locations. Subsequent displays would concentrate on specific regions and graphically detail the rainfall, river level and other parameters providing on-screen warnings where appropriate. Standard RMMS features include; Trend Analysis and History Graphs that can graphically compare the river levels with precipitation amounts from different locations. The result is a quick view of the entire system combined with rapid analysis of trends to allow predictions and correspondingly appropriate action plans.

SYNERGETICS MODEL135 RMMS FEATURES:

GRAPHICAL FUNCTIONS

- User defined graphical display
- Geographic mapping of sensor points
- Alarm notification,
- Control of remote sensor sites
- Trend analysis,
- Historical data summaries.

CUSTOM REPORTS

- Numerical or graphical formats
- Data export capabilities to spreadsheets, databases or statistical programs for further analysis.

APPLICATIONS

- Water Resource Management
- Water Quality Measurement
- NPDES Monitoring
- Climatic Monitoring
- Irrigation Management

COMMUNICATION

- Telephone - standard switched network or cellular
- Radio telemetry
- Remote alarm notification

SYSTEM COMPONENTS

Synergetics can provide a complete system or individual field instruments and sensors. The system includes a central site computer, communications hardware, remote terminal units and sensors.

HARDWARE REQUIREMENTS

- IBM or compatible computer
- Math Coprocessor
- 40 MB to 300 MB Hard Disk
- 80386 or 80486 CPU
- VGA Color Monitor
- Minimum 4 MB RAM

SYNERGETICS MODEL 135

A variety of remote monitoring tasks and applications can be accomplished by installing a system composed of RTUs, sensors, communication and a Model 135 monitoring station. From remote monitoring to alarm notification and control of valves, gates or other functions can automatically be handled by the Synergetics RMMS. The following discusses the features and functionality of Synergetics Model 135 RMMS.

FEATURES	FUNCTION
• Customized Graphical Display	The Synergetics Model 135 RMMS will provide site-specific or application-specific charts, graphs and reports for instant recognition. The Synergetics Model 135 RMMS gives you outstanding display capability with graphic animation, multiple dynamic color changes, dynamic messages and on-screen trend windows.
• On-Line Monitoring	The run-time system provides on-line data acquisition for color graphic display, trending and reporting functions. Data entry fields allow you to control set point changes, on-off status changes and manual override.
• On-Line Graphic Display	Synergetics Model 135 RMMS Historical Analysis allows you to select from a library of acquisition, mathematical, logic and calculation functions. These are displayed on the screen with colorful charts, graphs and reports that can be easily read.
• Local and Remote Alarm	The system allows for alarm logging to the screen, printer or both, with or without an audible alarm. The alarm information can also be transmitted to a remote location or pager. Alarm messages are displayed in a different color until acknowledged.
• Remote SCADA applications	The Synergetics Model 135 RMMS controls the opening and closing of mechanical devices such as gates or valves. It compares existing conditions to gate or valve positions. When the positions do not match the set point, the RMMS sends a signal that triggers the appropriate adjustment necessary to maintain the desired position.

SYNERGETICS MODEL 135 RMMS GIVES YOU MAXIMUM CONTROL OVER YOUR MONITORING RESPONSIBILITIES

Is your application process control, industrial automation or remote SCADA? In any of these applications Synergetics Model 135 RMMS provides the ability to react quickly, accurately and efficiently. Synergetics provides the tools and expertise to create a monitoring management system that specifically addresses ways for you to increase your efficiency, and reduce costs.

Synergetics Model 135 RMMS gives you the control you need to:

- Optimize operations/reduce costly mistakes or delays
- React immediately/ save time and cost of operation
- Increase capabilities/ eliminate unnecessary labor costs

Please call for your free RMMS Demonstration Disk.
To order the Model135 Remote Monitoring Management System or
to combine it with other 3400 Series Modules for turnkey systems contact:

SYNERGETICS INTERNATIONAL
1831 Lefthand Circle • Longmont, Colorado 80501 U.S.A.
(303) 678-5200 FAX (303) 678-5206

PC Specification for Central Site

- A 80386 CPU or better, running at 20 MHz or faster.
- 4 Mb of RAM.
- An Intel 8087 math coprocessor, or equivalent.
- A 3.5-inch 1.44 Mb floppy disk drive.
- An internal hard drive that stores a minimum of 40 Mb of data.
- A high resolution VGA graphics card.
- Expansion slots in the CPU.
- MS-DOS.
- A minimum of one serial port and one parallel port.
- A Microsoft PS/2 serial mouse, or equivalent.
- A high resolution VGA color monitor.

Druck

DEPTH MEASUREMENT PRESSURE TRANSDUCER

Type PDCR 10/D

High accuracy
±0.1% BSL for ranges to 2000 ft. water

Good long term stability

Titanium construction

Totally submersible
With molded integral cable

Excellent overpressure acceptance
<4 times rated pressure

Good thermal stability
±0.3% total error band 30 to 86°F

The PDCR 10/D transducer has been specifically designed for depth measurement in small bore holes, reservoirs, the sea and many other applications. The titanium body and pressure fittings are electron beam welded, and a polyurethane sheathed cable is molded to the body to complete the waterproof rugged assembly.

The pressure ranges are normally vented gauge for depths less than 300 feet and sealed gauge for greater depths.

Operating pressure ranges
Standard pressure ranges are expressed in psi, gauge or sealed gauge as follows. (Approximate equivalents are also shown for feet of ground water.)

1 psi (2.5 ft. water), 2.5 psi (5.5 ft. water), 5 psi (11 ft. water) 10 psi (22 ft. water), 15 psi (33 ft. water), 22 psi (50 ft. water) 30 psi (67 ft. water), 50 psi (112 ft. water), 75 psi (168 ft. water) 100 psi (225 ft. water), 150 psi (337 ft. water), 220 psi (500 ft. water) 300 psi (675 ft. water), 500 psi (1125 ft. water), 900 psi (2025 ft. water) 1000 psi (2250 ft. water), 2000 psi (4500 ft. water)
Sealed gauge not available for ranges up to 150 psi.

Other pressure units can be specified, e.g. meters, water.

Overpressure
The rated pressure can be exceeded by the following multiples causing negligible calibration change:
10 x for 1 and 2.5 psi ranges
6 x for 5 psi range
4 x for 10 psi to 2000 psi ranges.

Pressure media
Fluids compatible with quartz and titanium.

Transduction principle
Integrated silicon strain gauge bridge.

Excitation voltage
10V d.c. regulated @ 15mA max. Polarity is important.
For other supply voltages or a.c. operation, please specify.

Output voltage
17mV for 1 psi range
25mV for 2.5 psi range
50mV for 5 psi range
100mV for 10 psi range and above.
Outputs quoted are for standard linearity and overload. Higher outputs are possible giving proportional improvement in temperature stability.

Amplified output available on request.

Output impedance
1000 ohms nominal.

Load impedance
Greater than 100K ohms for quoted performance.
For lower load impedances, please specify.

Resolution
Infinite.

Combined non-linearity and hysteresis
±0.1% BSL for 1 psi to 900 psi ranges.
±0.2% BSL for 1000 and 2000 psi ranges.
±0.06% BSL available for ranges to 300 psi on request, and the output will be 75mV for 10 psi range and above.

Zero offset
±3mV standard

Span setting
±10mV standard. Units of the same range are better than ±3mV from each other.
More accurate settings of zero and span are available for applications where interchangeability is important.

Operating temperature range
−5° to +175°F (−20° to +80°C)

Temperature effects
±0.3% total error band 30° to 86°F (−2° to +30°C).
For special applications it is possible to give improved temperature compensation over a wider temperature range.

Mechanical shock
1000g for 1ms in each of three mutually perpendicular axes will not affect calibration.

Weight
1.75 oz. nominal

Electrical Connection/Cable
3 ft. cable supplied as standard. This is molded to transducer body with polyurethane to provide watertight connection. Continuous lengths up to 1500 ft. can be supplied although it is recommended to use two-wire transmitter type PTX 160/D for lengths beyond 500 ft.
Cable specification:
6 conductor (24AWG) shielded
Polyurethane outer jacket - 0.315 ins. dia.
Kevlar strength member #29/1500 Denier
Nylon vent tube
Weight in air, 45 lbs. per 1000 ft.
Weight in water, 10 lbs. per 1000 ft.
Breaking strength, 200 pounds

Pressure connection
Illustrated front end delrin cone fitted as standard.
This incorporates a hydraulic damper to protect the device from high pressure pulses caused by underwater impact.

Conducting pressure media
When used with a conducting pressure media the +Ve supply should be at the same or a −Ve potential with respect to the pressure media, i.e. where media is at ground, the +Ve supply should be grounded, or alternatively the transducer should be floated with respect to the pressure media.

Intrinsic safety (optional) — PDCR 10/D/IS
This transducer can be certified for use with barrier systems to EEX ia gas group IIC with a T4 rating at an ambient temperature of 80°C to BS5501 part 7 and Cenelec EN5020.

Options available
For 4-20mA operation - see PTX 160/D or PTX 110/D.
For 0-5 volt output - see PDCR 130/D
For general purpose applications, differential and absolute pressures - see PDCR 10 and other data sheets.

Ordering information
Please state the following:
(1) Type number
(2) Pressure range
(3) Gauge or sealed gauge
(4) Temperature range
(5) Cable length
(6) Pressure media
For non-standard requirements please specify in detail.
Continuing development sometimes necessitates specification changes without notice.

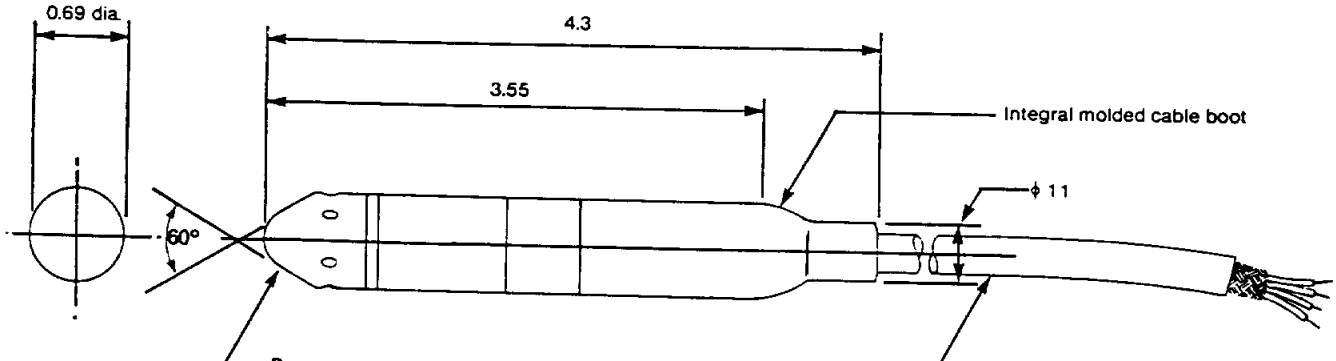

Pressure connections (optional)
1/4" NPT flat end.
7/16" UNF as MS 33656-4 (1/4 A.N)
Others available on request.

Electrical connection
4 Core shielded cable

Red	Supply positive
White	Supply negative
Yellow	Output positive
Blue	Output negative
Shield	N/C to transducer body

Any other cores not connected.

Installation
Dimensions: inches

Druck Incorporated
Miry Brook Road
Danbury, CT 06810
Telephone (203) 792 8981
Telex: 643118

Representative

HydroNet Series H-300

WaterLog Pressure Transducer

For Water Level Monitoring

River monitoring application

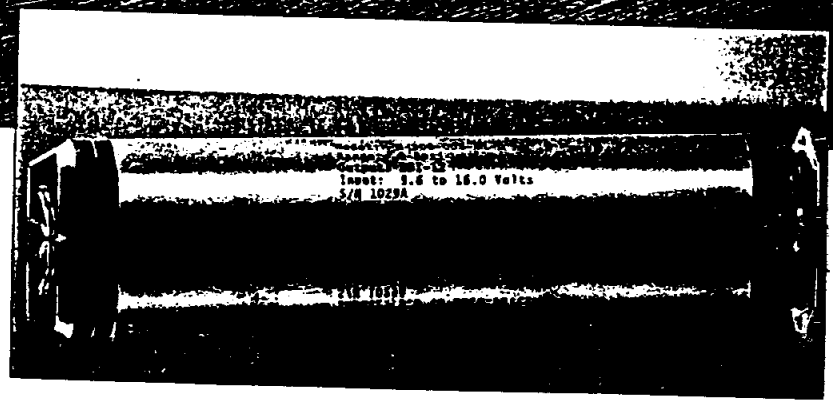

H-300 WaterLog pressure transducer >>

Key Features

- Simple to install, use, and maintain (no on-site calibration required)
- Performs extremely accurate measurements:
  - linear deviation is less than 0.02%
  - resolution is 1 part in 5,000
  - measures water pressure accurately over wide temperature ranges
  - automatically compensates for offset
  - pressure measurements can be transmitted over long cable lengths with no error
- Output Options: Frequency, SDI-12, and RS-232C

HydroNet

Family of Data Loggers and Sensors

For Measuring Environmental Conditions, from Design Analysis

Accuracy
Maximum percent of error in measuring pressure (zero to full scale) is less than or equal to 0.02% over temperature range referenced to a straight line stretched from zero psi to max. pressure

Resolution
(Smallest pressure change detectable in output signal)
1 part in 5,000

Linearity
Less than 0.02% deviation from a straight line referenced to end points

Pressure Hysteresis
Less than 0.01%

Response Times
Frequency: 2 second update
SDI-12: 30 second measurement sequence
RS-232C: 16 second measurement sequence

Long-term Stability
Less than ± 0.25% drift in accuracy per year

Environmental Restrictions
Operating Range: 0 to 50 degrees C (non-freezing)
Compensated Range: 0 to 50 degrees C
Storage: -10 to 75 degrees C

Media Compatibility
Liquids and gases compatible with glass, ceramic, silicon, RTV, and nickel

Pressure Ports (2)
With 120 mesh stainless screens, field replaceable

Power Supply
Voltage: 9.6 to 16.0 volts DC
Supply Current:
- sleep mode: 1 milliamperes max.
- active (measuring): 50 milliamperes max.

Frequency Output
Frequency Range: 100 Hz - 5100 Hz
Duty Cycle: 50%
Output Voltage Levels:
- minimum high level: 3.5 volt
- maximum low level: 0.8 volt
- maximum cable length: 1000 feet (conductor size must be equal to 22 AWG or larger)

SDI-12 Output
Baud Rate: 1200
Protocol: SDI-12, 8-bit, even parity
Output Voltage Levels:
- minimum high level: 3.5 volt
- maximum low level: 0.8 volt
- maximum cable length: 1000 ft.

RS-232C Output
Baud Rate: 1200
Protocol: RS-232C, 8-bit, even parity

Mechanical Data
Material: stainless steel barrel with PVC end caps and polyethylene vent tubing
Weight: 1.83 pounds
Size: 1.25 inches diameter x 7.0 inches long
Pressure Overload: less than 2 times the rated pressure

Cables
Sensor Cable (WaterLog to junction box): shielded, polyethylene-encased, vented, three-wire cable; 10 foot standard length (longer lengths are available if required)

Hook-up Cable (junction box to data recorder): shielded, three-wire cable; 10 foot standard length (longer lengths are available if required)

Warranty
WaterLog is warranted for six months from date of delivery.

Submersible Pressure Transmitter
MODEL PS9000

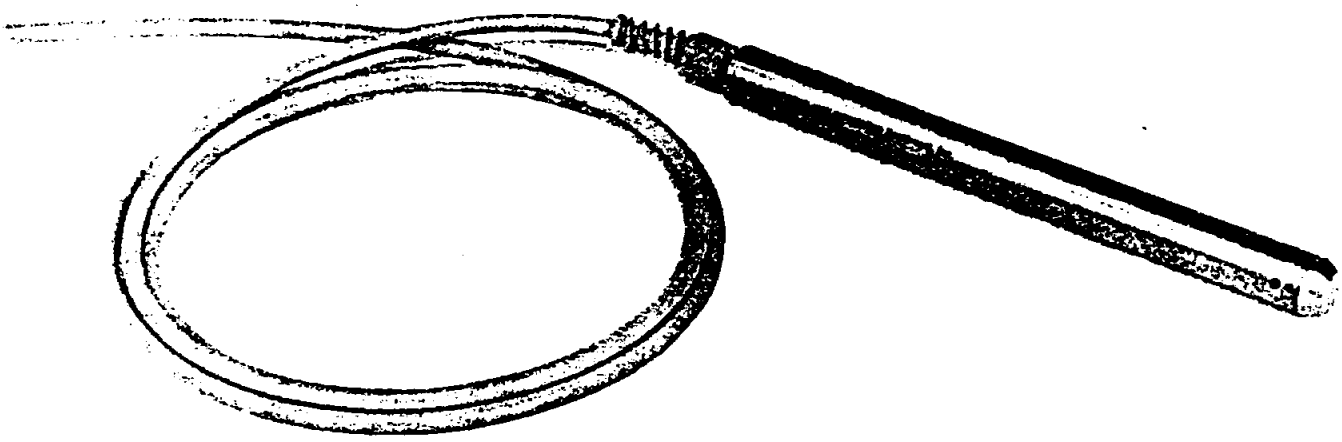

PS9000 Submersible Pressure Transmitters are designed to provide high-accuracy level measurement in all types of liquid environments. The PS9000 is a 4-20mA output device which features the latest in silicon micro-machined piezoresistive, strain gauge technology. As an industry standard, 4-20mA output is compatible with a wide variety of measurement and data logging equipment. Other advantages of 4-20mA devices include exceptional noise rejection, high signal strength, and long distance transmission. All PS9000 transmitters can be easily serviced and recalibrated at the factory.

MODEL PS9000
4-20 mA Output

Submersible Pressure Transmitter

Mechanical Specifications

Transmitter

Length:	9.125"	*Diaphragm:*	316 stainless steel
O.D.:	0.840"	*Desiccant Pack:*	Available
Body Material:	304 stainless steel	*Terminating Connector:*	Available
Wire Seal Material:	Viton/Buna-N		

Cable

Cable Jacket:	Polyurethane	*O.D.:*	maximum 0.28"
Conductor Type:	2-conductor, vented	*Break Strength:*	138 lbs.
Vent Tube:	Nylon	*Maximum Length:*	2000 ft.

Electrical Specifications

Transmitter

Linearity/Repeatability/Hysteresis:*

maximum	± 0.25% FSO
typical	± 0.1% FSO

Maximum Zero Offset (20°C): ± 0.5% FSO

Sensitivity Accuracy (20°C):

maximum	± 0.25% FSO
typical	± 0.125% FSO

Max. Power Supply Sensitivity: 0.3% FSO

Maximum Temperature Error: ± 2.0% FSO

Thermal Hysteresis:
the output will typically return to within ± 0.25% FSO of its initial reading subsequent to one full cycle over the compensated temperature range.

Transmitter Voltage: 9-24 VDC

Compensated Temp. Range: 0-50°C

Operating Temp. Range: -5°C to +70°C

**best fit straight line*

Ordering Information

Standard Ranges (PSIG):
5, 15, 30, & 50

Standard Cable (ft.):
25', 50', 75', 100', 150', & 200'

Storage Reel:
200' Capacity

Standard Desiccant Chamber:
Standard Capacity

Standard Connectors:
Mil-Spec 6 Pin

Other Transducers available:
V output, passive and active mV output

MODEL PS9000
4-20 mA Output

Submersible Pressure Transmitter

ORDERING INFORMATION

HOW TO ORDER:

1. Choose the necessary pressure range for your transducer.
2. Choose a standard or custom cable harness for your transducer. (If choosing a custom length - specify length).
3. Choose a desiccant pack.
4. Select additional options or accessories as needed.

To place an order or for further questions on these items, please call us at **(800) 776-9355.** We are happy to help!

Pressure Transmitters

Range	Part Number
5 PSI	3C205
15 PSI	3C215
30 PSI	3C230
50 PSI	3C235
100 PSI	3C240

Cable Harnesses

Length	Part Number
25'	3C150
50'	3C155
75'	3C160
100'	3C165
150'	3C170
200'	3C175
Custom Length (ft)	3C149

Desiccant Packs

Style	Part Number
Standard Capacity	6E455
High Capacity	6E457

Options

Item	Part Number
M6 Connector	6E400
M3 Connector	6E415
1/4" NPT Adapter Kit	6E410

Accessories

Item	Part Number
Standard Desiccant Refill	6E460
High Capacity Desiccant Refill	6E470
Vent Tube Protector	6E465
Cable Adapter M3M x M6F	6E516
Cable Strain Relief Kit	6E517
Reel - 200' Capacity	6E520
Reel - 500' Capacity	6E525
Reel - 1500' Capacity	6E530
Extension Cable - 200' with Reel	6E515

MOTOROLA

Official Radio Communications Sponsor for the 1984 Olympic Games

"HANDIE-TALKIE" RF LINKS

136-174 MHz, 5 Watt
403-430, 440-512 MHz, 4 or 1 Watt

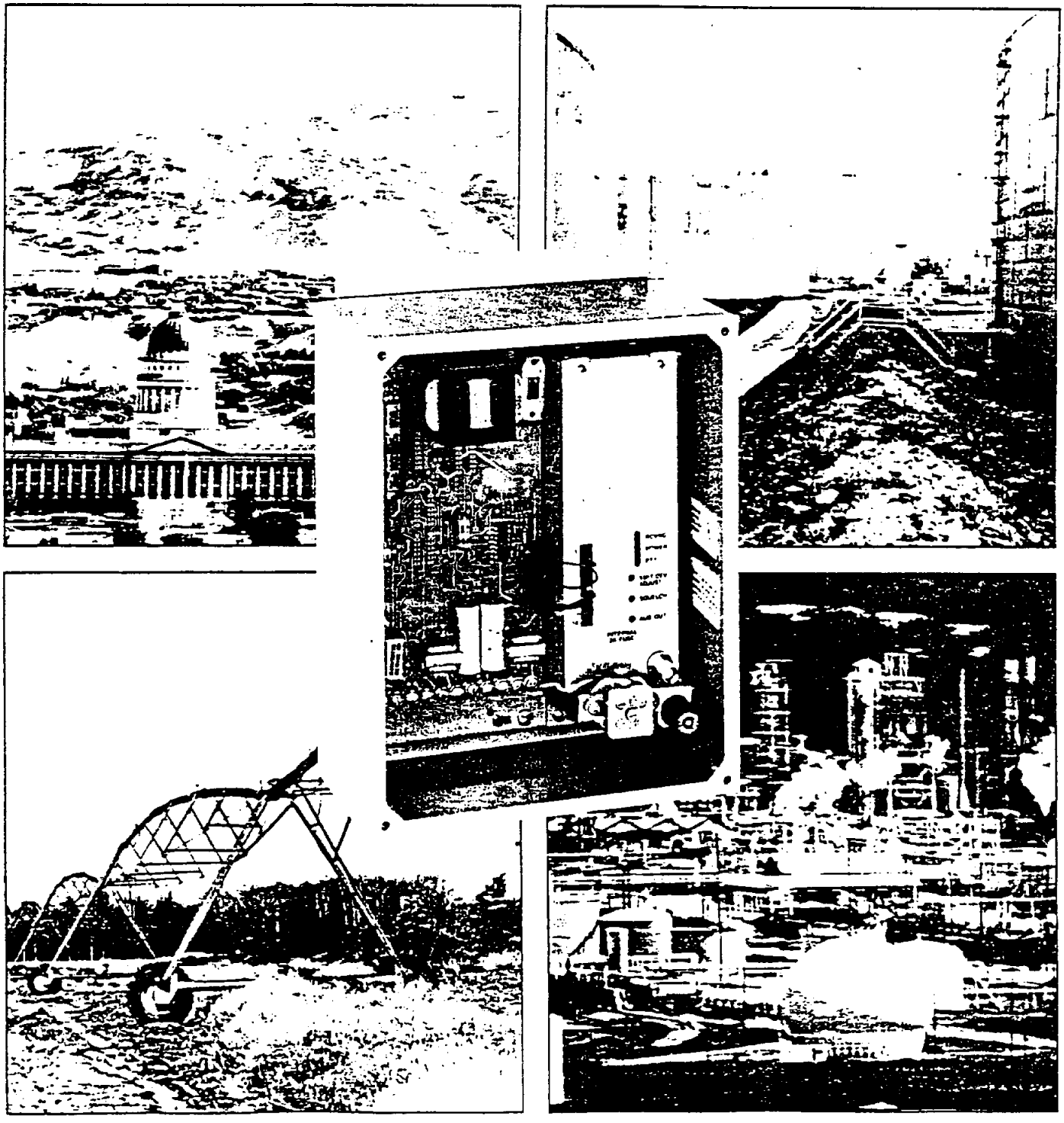

"HANDIE-TALKIE" RF LINKS

Introducing a new series of HANDIE-TALKIE RF Links which are exclusively designed as a practical substitute for certain variations of wire line applications. A choice of model configurations, all incorporating established and proven Motorola quality HANDIE-TALKIE transceivers, assure flexibility of design and top performance.

If your system requires wire-line but —

- It isn't available
- Too costly to install
- Restricted by construction codes
- Limited because of inaccessible terrain

Or, you are using wire-line but —

- The operations are unreliable
- Maintenance is too costly
- Lease rate too expensive
- System is not flexible

Then you need to consider the real advantages of an RF audio path using Motorola's low power, highly reliable and extremely flexible HANDIE-TALKIE RF Links. Whether your need is to control a base station, retrieve data, transmit an alarm, provide two-way conversation, or status control – your system design approach should include a basic or package model Motorola HANDIE-TALKIE RF Link. Motorola's experience and technological expertise provide a professional approach to optimizing system control and interface using RF as an alternative to wire-line.

"WALKIE-TALKIE" RF LINK CONFIGURATIONS

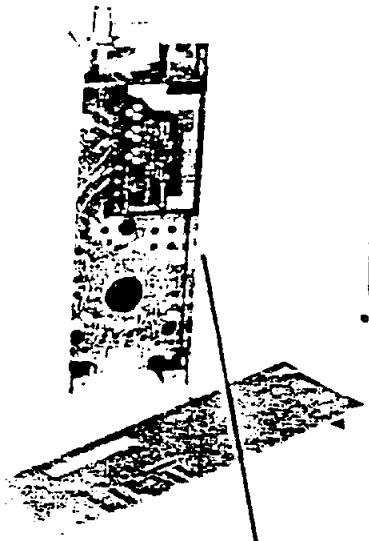

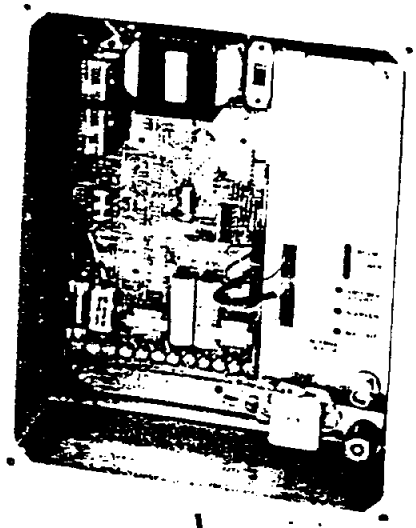

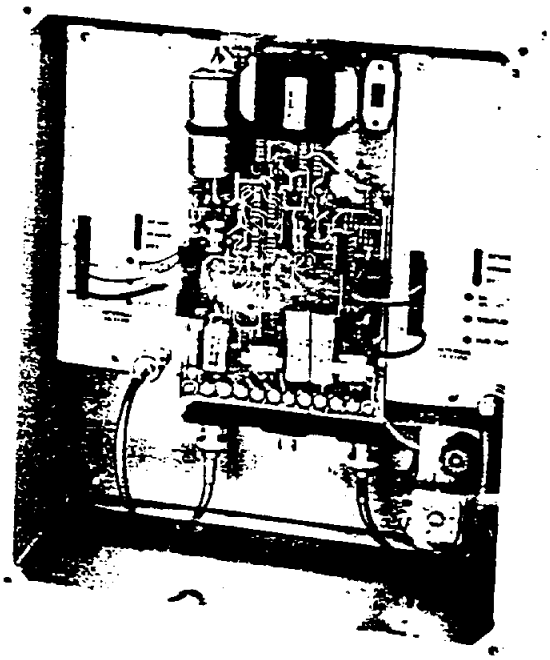

BASIC MODEL

VHF or UHF Transceiver* Module
- 12 VDC negative ground
- Interface board
- 14 Pin Molex connector
  - 12 VDC
  - receive and transmit audio
  - transmit audio modulation (adj)
  - push to talk
  - carrier indication
  - receive audio output
  - spare pins
- LED's (3)
  - Power on
  - Transmitter keyed
  - Receiving carrier
- Mounted in metal housing

*(If Transmit or Receive only is desired, one crystal may be deleted)

PACKAGE MODELS

SIMPLEX MODEL

BASIC MODEL PLUS

Function Board
Includes:
- 110/220 VAC power supply
- 13.8 V regulator*
- 4 wire audio
- 600 ohm equalization adj.
- 10 connector terminal strip
- Interconnects plug-in

*Regulator will float charge a standby battery.

Weather Resistant
Steel Housing. (NEMA #12)

Full Duplex Model (UHF)
Includes:
- Transmit transceiver module
- Receive transceiver module
- Built-in duplexer (5 MHz separation)
- All RF connectors BNC
- Module interconnects are plug-in

Features	Description	Benefits
Choice of Models	Select a basic transceiver model, a simplex package model, or a full duplex model.	Allows you to select the unit offering the features that most closely meet your needs.
Compact Size	Basic model transceiver – 7"Lx2.5"Wx1.4"D Package model 10"Lx8"Wx4"D Duplex model 12"Lx10"Wx5"D.	Allows greater ease and freedom of installation.
Choice of R.F. Power	5 watts in VHF and 1 or 4 watts in UHF.	Select the power level that best meets your needs. The 1 watt allows use of the UHF 12.5 KHZ offsets.
Low Current Drain	Transmitter 5 watt 1000 MA 4 watt 1050 MA 1 watt 450 MA Receiver Receive 43MA Standby 12MA (squelch).	Solar power and 12VDC operation are more practical.
Continuous Duty	1 watt UHF model is designed continuous duty operation.	Allows continuous flow of data transmission.
Full Duplex Operation	A 1 watt, UHF full duplex model is offered.	Simultaneous transmission and receipt of data. Also, when used in dispatch systems provides full control of the station.
Adaptability	Basic model includes a 14 pin MOLEX connector. Package model has a 10 connector terminal strip.	Provides easy, effective integration of system flexibility.
Modular Assemblies	Transceiver and function board assembly cables are plug-in.	Maintenance checks are fast and easy. Should the module require in-shop service it can be quickly removed.
L.E.D. Indicators	Three L.E.D.'s are used to indicate power on, transmitter on and receive audio.	Provides a fast, sure visual indication of operational status.
Modem Compatible	600 ohm connector allows modem interface. P.T.T. to be provided by user.	Quick and easy to install.
4 Wire Audio	A standard feature in the 1 watt full duplex model.	Eliminates cross talk and allows fast, easy installation.

Features	Description	Benefits
Coded Squelch	"Private-Line" coded squelch models are available.	Coded squelch systems reduce co-channel interference and operational fatigue.
Dust & Drip Tight Industrial Housing	Package models include a 14 gauge steel housing. European standard IEC 529, IP65 and NEMA type 12.	Provides adequate environmental protection for most installations.
Battery Charger	Package models include a power supply that will float charge a 12 volt battery.	Optional 12 volt stand-by power is practical.
Primary Power	Allows 110/220 VAC (50/60 Hz) or 12 VDC operation.	Units can be operated from a variety of power sources including solar panels. Also, power supply will float charge 12 volt battery.
Emergency Power Reverting	Automatically allows switching to a standby 12 VDC power source when 110/220 power outage occurs.	This feature increases system reliability by keeping the link on the air during AC power failures.

RF LINK TRANSCEIVER MODULES

Performance Specifications

General	VHF	UHF
Model Series:	K33LCF	K24LCF, K34LCF
Frequency:	136-174 MHz	403-430 MHz, 440-512 MHz
Power Supply:	110/220 V AC (50/60 Hz), 12 V DC (Negative Ground)	
Dimensions (H x W x D)/ Weight (ounces) Basic Model	7.00" x 2.50" x 1.44" (10.25 oz.)	
Simplex Package Model with Housing	10" x 8" x 4" (10 lbs. 8 oz.)	
Duplex Package Model with Housing	12" x 10" x 5" (approx. 18 lbs.)	

Performance Specifications

TRANSMITTER	VHF	UHF
RF Output:	5W	4W, 1W*
Current Drain on Transmit (13.6 VDC)	1000 mA	1050 mA 450 mA
Key-Up Time to Full Output:	10 MS Typical	
Frequency Stability:	± .0005%	± .0005%
− 30°C to 60°C		
− 0°C to 50°C (+ 25°C Ref.)		± .00025%
Modulation:	15F2, 16F3, 16F9 ± 5 KHz Max. Deviation for 100% Modulation @ 1000 Hz	
Spurious & Harmonic Frequencies:	More than 50dB below carrier	
Audio Response: (Package Models)	Better than 3002 Grade Line End to End	
(Basic Models)	± 1, − 3dB from 6dB/octave Preemphasis Characteristic from 300 − 3KHz	
Audio Sensitivity for 3.5 MHz Deviation: Basic Model	Adjustable 1 VRMS to .1 VRMS	
Package Model	0 dBM to − 20 dBM @ 1000 Hz	
Audio Distortion:	Less than 5% @ 1000 Hz 3KHz deviation	
PL Modulation:	± 1 KHz Max. ± 500 Hz Min.	

*All UHF 1 Watt models are continuous duty.

RECEIVER	VHF	UHF
Channel Spacing:	30KHz	25 KHz
Current Drain (Basic Model): 13.6 VDC	Receive 1 VRMS Output 1 KHz, 600 ohm Load 43mA, Standby (Squelched): 12mA	
Usable Band Width:	± 5KHz	
Audio Output: Basic Model	70 mV to 700 mV	
Package Model	− 20 to 0 dBM (600 ohm)	
Frequency Stability: − 30°C to + 60°C (+ 25°C Ref.)	.0010%	.0007%
Sensitivity: 20 dB Quieting	.35 mV Max.	.5 mV Max.
12 dB SINAD	.25 mv Max.	.35 mV Max.
Selectivity:	More than 75dB @ ± 30KHz (EIA SINAD)	More than 70dB @ ± 25KHz (EIA SINAD)
Intermodulation:	More than 65dB at the adjacent channel	
Spurious and Image Frequency Rejection:	More than 55dB below carrier (136-140 MHz) More than 65dB below carrier (140-174 MHz)	More than 60dB below carrier
Squelch Opening Time:— Carrier Squelch	40 MS	
PRIVATE-LINE (PL)	120 MS	
Receiving Quieting Time*:	10 MS Typ.	
Maximum Data Rate	1200 Baud	
RF Input	BNC Connector (50 ohms)	
Data Connection	Terminal Strip	
Power Connection	Terminal Strip	

*Time between application of an RF signal and the unsquelched receiver audio output quieting.

NATIONAL MOTOROLA Communications SERVICE

Support Services
Wherever Motorola sells, our product is backed by service. In the U.S., we have 900 authorized or company-owned centers. In addition, our products are serviced throughout the world by a wide network of company or authorized independent distributor service organizations.

Motorola, Inc. is an Equal Employment Opportunity/ Affirmative Action Employer.

MOTOROLA
1301 East Algonquin Rd., Schaumburg, Illinois 60196
(312) 307-1000

Specifications subject to change without notice.
®, MOTOROLA, HANDIE-TALKIE and PRIVATE-LINE are trademarks of Motorola, Inc. (8409) C.G.
MOLEX is a registered trademark of Molex Incorporated.

Printed in U.S.A.

MOTOROLA Radius Division

RNet™ SERIES TELEMETRY RADIO

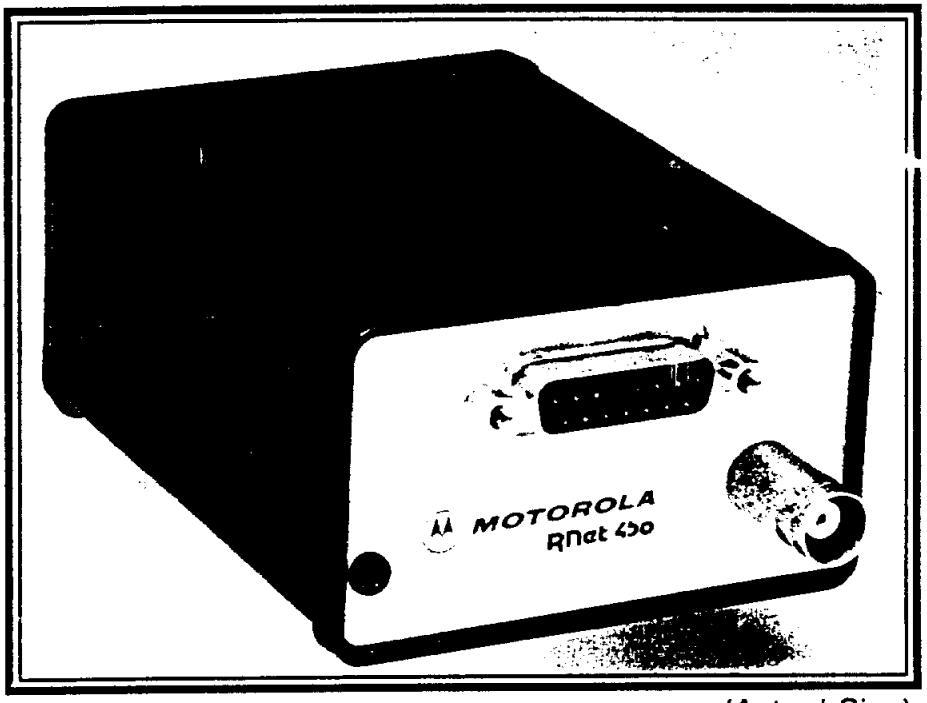

(Actual Size)

- Competitively Priced
- Small, Compact Size
- Low Current Drain
- VHF or UHF Frequencies
- VHF-2 or 5 Watts, UHF-2 or 4 Watts
- Voice or Data Capable
- Built-in Time-Out-Timer
- Two Channel Capability
- 3 Year Parts and Labor Warranty
- MADE IN U.S.A.

GENERAL	RNet™ 450 UHF TELEMETRY SPECIFICATIONS	RNet™ 150 VHF TELEMETRY SPECIFICATIONS
Frequency	403-416MHz, 416-430MHz and 450-470MHz	136-150.8MHz, 150.8-162MHz and 162-174MHz
Channels	1 or 2 - switchable via DB-15 front panel connector	1 or 2 - switchable via DB-15 front panel connector
Channel Spacing	25kHz	25kHz / 30kHz
Operating Temperature	-30°C to +60°C	-30°C to +60°C
Supply Voltage (Internally Regulated)	10-17 VDC (2watt) / 14-20 VDC (4watt)**	10-17 VDC (2watt) / 14-20 VDC (5watt)**
Supply Voltage(Inter. Reg. Bypassed)	6-9 VDC (2watt) / 9-13.5 VDC (4watt)	6-9 VDC (2watt) / 9-13.5 VDC (5watt)
Maximum Tx Separation	8MHz on two channel models	3MHz on two channel models
Maximum Rx Separation	3MHz on two channel models	1MHz on two channel models
Nominal Dimensions	L 3.30", W 1.52", H 2.70"	L 3.30", W 1.52", H 2.70"
Approximate Weight	10.2 ounces	10.2 ounces
RF Connector	Front panel mounted BNC 50 ohms	Front panel mounted BNC 50 ohms
Interface Connector	Front panel mounted DB-15 pin	Front panel mounted DB-15 pin
Standby Current Drain	16mA	20mA
RECEIVER		
Sensitivity	12dB SINAD < 0.45µV	12dB SINAD < 0.25µV
Frequency Stability	±10PPM	±10PPM
Selectivity	60dB	60dB
Intermodulation	60dB	60dB
Spurious Rejection	55dB	55dB
Image Rejection	50dB	55dB
Modulation Acceptance	±7.5kHz	±7.5kHz
FM Hum & Noise	40dB	40dB
Audio Output : AC Level	0-600mV Pk-Pk adjustable at pin 8 into 2k ohms load	0-600mV Pk-Pk adjustable at pin 8 into 2k ohms load
	0 -1VRMS adjustable on de-emphasized pin	0 -1VRMS adjustable on de-emphasized pin
Audio DC Level	2.5 VDC (Pins 8 & 12)	2.5 VDC (Pins 8 & 12)
Audio Output Impedence	51ohms	51 ohms
Audio Response	6dB de-emphasis or flat (switchable)	6dB de-emphasis or flat (switchable)
Audio Distortion	Less than 10%	Less than 10%
Carrier Detect Attack Time	Less than 10msec	Less than 10msec
Current Drain	20mA	24mA
TRANSMITTER		
RF Power Out	2 Watt or 4 Watt	2 Watt or 5 Watt
Conducted Spurs	-49dBc (2 Watt) & -52dBc (4 Watt)	-49dBc (2 Watt) & -53dBc (5 Watt)
Frequency Stability	±5 PPM	±5 PPM
FM Hum & Noise	40dB	40dB
Audio Input: Deviation Level	±5kHz adjustable flat or pre-emphasized	±5kHz adjustable flat or pre-emphasized
Audio Input Level	40mVRMS for 3kHz deviation	40mVRMS for 3kHz deviation
Audio DC Level	0VDC Data In input pin	0VDC Data In input pin
	5VDC Mic Audio input pin	5VDC Mic Audio input pin
Audio Input Impedence	2k ohms Audio In (Pin 4) / 10k ohms Data In (Pin 7)	2k ohms Audio In (Pin 4) / 10k ohms Data In (Pin 7)
Audio Response	6dB pre-emphasis or flat (switchable)	6dB pre-emphasis or flat (switchable)
Audio Distortion	Less than 5%	Less than 5%
Attack Time	Less than 10msec	Less than 10msec
Typical Current Drain	865mA @ 2 Watt	870mA @ 2 Watt
	1120mA @ 4 Watt	1275mA @ 5 Watt
Maximum Current Drain	1050mA @ 2 Watt	1150mA @ 2 Watt
	1350mA @ 4 Watt	1450mA @ 5 Watt

Specifications subject to change without notice.

**For 4 or 5 watt models power will be degraded if voltage is less than 14 vdc.

MOTOROLA

RNet™ SERIES TELEMETRY RADIO

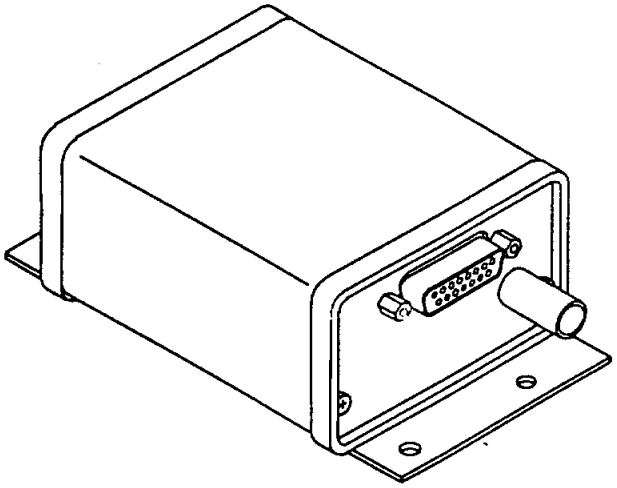

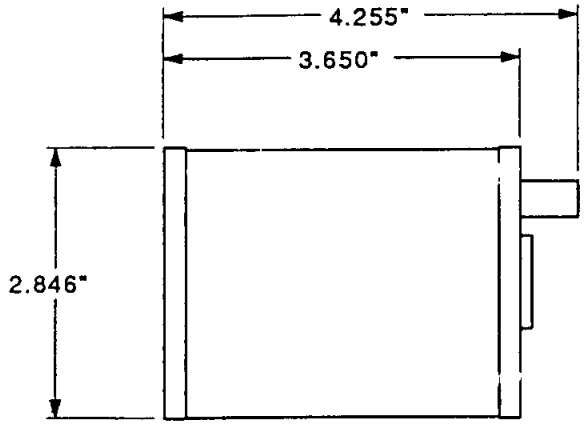

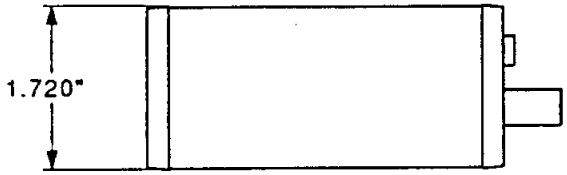

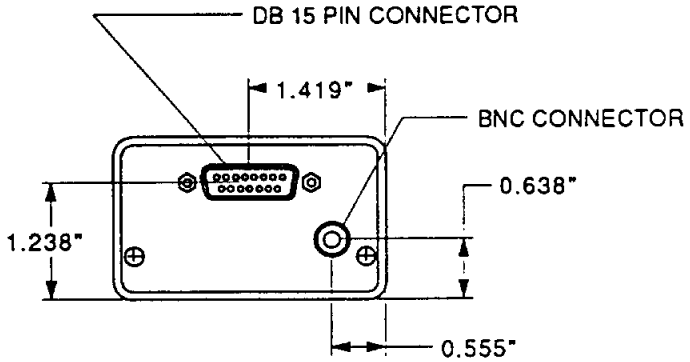

MOUNTING PLATE

DIMENSIONS: .XX = +/ - .020
.XXX= +/- .010

MATERIAL: .060 THICK ALUMINUM (3033)

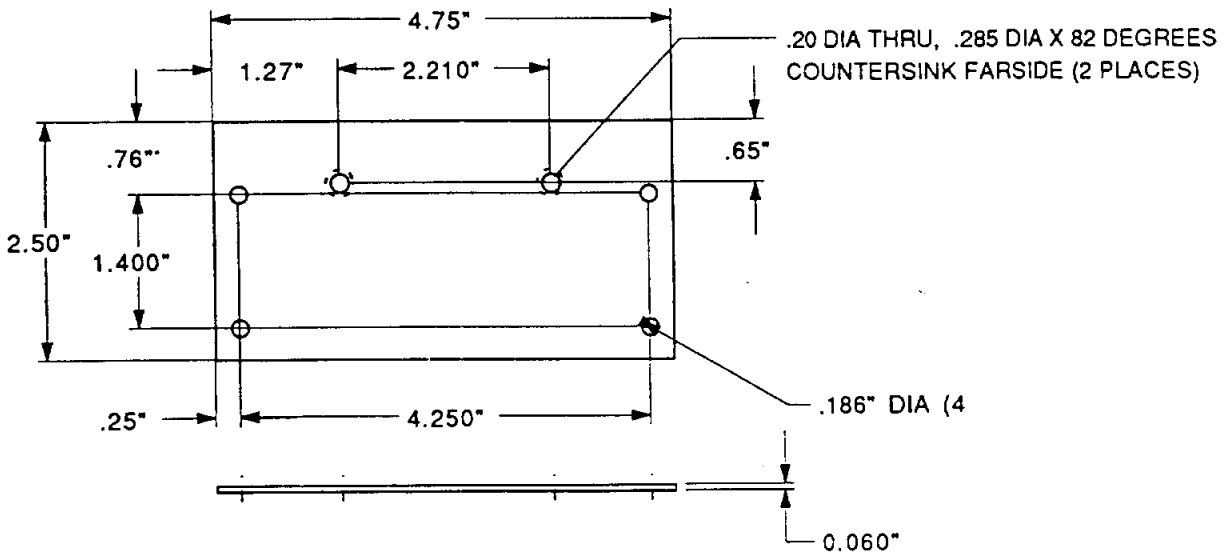

MOTOROLA Radius Division

RNet™ SERIES TELEMETRY RADIO

RF INTERFACE

The RF Interface is a BNC connector with 50 ohm nominal impedance.

DATA/VOICE INTERFACE

The data/voice interface is a standard DB-15 connector.

DB-15 CONNECTOR PIN-OUTS

PIN NUMBER	FUNCTION
1	Not Used
2	Not Used
3	Not Used
4	Mic Audio Input (6dB pre-emphasis)
5	Channel Select
6	B+ Input
7	Data Input (flat response)
8	Data Output (flat response)
9	Not Used
10	Not Used
11	Squelch Disable
12	Audio Output (6dB de-emphasis)
13	Carrier Detect
14	PTT
15	Ground

DIP Switch programmable features:

PTT enable-logic high or low
Carrier detect output-active high or low
Data output-flat or 6dB de-emphasized
Data input-flat or 6dB pre-emphasized
60 second time-out-timer -- enabled or disabled

For further information contact:

MOTOROLA

Manufactured by the Radius Division
in Mt. Pleasant, Iowa, U.S.A.

1-800-624-8999 Ext.105

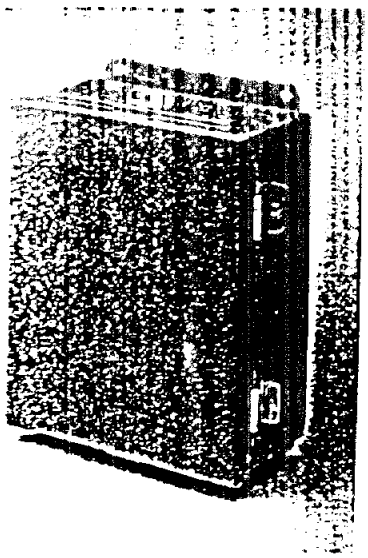

- Heavy gauge construction
- Optional keyplate
- Stainless steel hinge pin
- Oil-resistant gasket and adhesive
- Knockouts provided for mounting optional panels and terminal kits in size 6.00 x 4.00 (152 x 102) and larger
- Specify side to be hinged when ordering custom boxes
- For optional CSA approved grounding see page 435

Application

Designed for use in areas which may be regularly hosed down or are otherwise very wet. Suitable for use in dairies, breweries, and similar installations. Also suitable for outdoor use.

Construction

- 16 gauge or 14 gauge steel
- Seams continuously welded and ground smooth, no holes or knockouts
- Stainless steel clamps on three sides of cover assure watertight seal

Finish

ANSI 61 gray polyester powder coating inside and out over phosphatized surfaces. Optional panels are white enamel. An additional protective finish may be necessary if the enclosure is located in a corrosive outdoor setting. Hoffman can supply custom finishes based on environmental requirements. Consult factory for details.

Industry Standards

NEMA/EEMAC Type 4, Type 12, and Type 13
UL 50 Type 4
JIC standard EGP-1-1967
CSA Enclosure 4 (Specify CSA label when ordering)
IEC 529, IP66

Accessories

Need More Information?

Modifying Your Enclosure?

We can modify or customize this enclosure to your specs. See page 446 for more information.

Standard Sizes

"CHNF" NEMA 4 Continuous Hinge Clamp Cover Boxes

Box Catalog Number	Gauge	Box Size AxBxC	*Panel Catalog Number	Panel Size DxE	Mounting GxH	Overall LxW	F		K	N	T	V	Y
A-404CHNF	16	4.00x4.00x3.00 (102x102x76)	No Panel	No Panel	4.75x2.00 (121x51)	5.50x4.94 (140x125)	—	2.56 (65)	1.38 (35)	1.38 (35)	3.00 (76)	—	—
A-604CHNF	16	6.00x4.00x3.00 (152x102x76)	A-6P4	4.88x2.88 (124x73)	6.75x2.00 (171x51)	7.50x4.94 (191x125)	2.50 (64)	2.56 (65)	1.38 (35)	2.38 (60)	3.00 (76)	0.31 (8)	0.56 (14)
A-806CHNF	14	8.00x6.00x3.50 (203x152x89)	A-8P6	6.75x4.88 (171x124)	8.75x4.00 (222x102)	9.50x6.94 (241x176)	3.00 (76)	3.06 (78)	2.38 (60)	3.38 (86)	5.00 (127)	0.25 (6)	0.62 (16)
A-606CHNF	16	6.00x6.00x4.00 (152x152x102)	A-6P6	4.88x4.88 (124x124)	6.75x4.00 (171x102)	7.50x6.94 (191x176)	3.50 (89)	3.56 (90)	2.38 (60)	2.38 (60)	5.00 (127)	0.31 (8)	0.56 (14)
A-1008CHNF	14	10.00x8.00x4.00 (254x203x102)	A-10P8	8.75x6.88 (222x175)	10.75x6.00 (273x152)	11.50x8.94 (292x227)	3.50 (89)	3.56 (90)	3.38 (86)	1.00 (25)	7.00 (178)	0.25 (6)	0.62 (16)
A-1210CHNF	14	12.00x10.00x5.00 (305x254x127)	A-12P10	10.75x8.88 (273x225)	12.75x8.00 (324x203)	13.50x10.94 (343x278)	4.50 (114)	4.56 (116)	2.00 (51)	3.00 (76)	9.00 (229)	0.25 (6)	0.62 (16)
A-10086CHNF	14	10.00x8.00x6.00 (254x203x152)	A-10P8	8.75x6.88 (222x175)	10.75x6.00 (273x152)	11.50x8.94 (292x227)	5.50 (140)	5.56 (141)	3.38 (86)	1.00 (25)	7.00 (178)	0.25 (6)	0.62 (16)
A-1212CHNF	14	12.00x12.00x6.00 (305x305x152)	A-12P12	10.75x10.88 (273x276)	12.75x10.00 (324x254)	13.50x12.94 (343x329)	5.50 (140)	5.56 (141)	2.50 (64)	2.50 (64)	11.00 (279)	0.25 (6)	0.62 (16)
A-1412CHNF	14	14.00x12.00x6.00 (356x305x152)	A-14P12	12.75x10.88 (324x276)	14.75x10.00 (375x254)	15.50x12.94 (394x329)	5.50 (140)	5.56 (141)	2.00 (51)	3.00 (76)	11.00 (279)	0.25 (6)	0.62 (16)
A-1614CHNF	14	16.00x14.00x6.00 (406x356x152)	A-16P14	14.75x12.88 (375x327)	16.75x12.00 (425x305)	17.50x14.94 (445x379)	5.50 (140)	5.56 (141)	3.50 (89)	1.00 (25)	13.00 (330)	0.25 (6)	0.62 (16)

Millimeter dimensions ( ) are for reference only; do not convert metric dimensions to inch.
* Panels must be ordered separately. Optional stainless steel and aluminum panels are also available for most sizes. See Accessories.

900 Ehlen Drive
Anoka, MN 55303

APPENDIX B

PRELIMINARY COST ESTIMATE

COST ESTIMATE

FOR

BRAZOS CHLORIDE STUDY, SECTION 22
BRINE RECOVERY SYSTEM
Upper Brazos River Basin, Texas

Prepared by: U. S. Army Engineer District, Forth Worth

Submitted By:

Corky P. Cobern, P.E.
Chief, Cost Engineering Branch

Lanora Wright, Study Manager
Planning Division

Estimate Preparation Date: 17 May 1993

Effective Pricing Date: 17 May 1993

COST ESTIMATE FOR
BRINE RECOVERY SYSTEM

Brazos Chloride Study, Sect. 22
Upper Brazos River Basin, Texas

Designed By:
Estimated By: CESWF-ED-C

Prepared By: GAC

Date: 05/17/93

This cost estimate for the proposed Brine Recovery System is based on the following assumptions:

1) The system consists of ten (10) Recovery Wells with an average depth of 115 feet, one (1) Injection Well at a depth of 5,280 feet, an Automated Data Acquisition System, and a Collector Station.

2) Unit costs for the recovery wells and injection well are for complete installation (including costs for drilling\casing wells and development of well heads).

3) A lump sum cost was included in the estimate to provide for installation of new transmission lines, line poles, transformers, etc. Electrical costs in this estimate are for installation of hardware alone and does not include annual electric service.

NOTE: Electrical service is available through a local Electric Cooperative servicing the area where the system will be set up. Power demand of the entire system was determined by calculating the power requirements of ten (10) Gundos (225S-15D) 15 Hp, 460 Volt motors for the recovery wells, a motor for the injection well, the Automated Data Acquisition System, and the Collector Station. Electric usage for this project assumes running the system continously for 24 hours per day, 365 days per year.

4) The Real Estate cost is for securing a permanent easement for operation and maintenance of the Brine Recovery System.

5) A 30% contingency is included in the estimate and is considered appropriate for this stage of the project.

No Backup Reports...

* * * END TABLE OF CONTENTS * * *

		QUANTY	UOM	CONTRACT	Contngny	TOTAL COST	UNIT
1	Project						
1.01	Recovery Wells, Complete	1150.00	LF	129,369	38,811	168,180	146.24
1.02	Injection Well, Complete	5280.00	LF	806,066	241,820	1,047,886	198.46
1.03	Collector Station	400.00	SF	27,909	8,373	36,282	90.71
1.04	6" Dia. PVC Pipeline	10000	LF	106,738	32,021	138,759	13.88
1.05	8" Dia. PVC Pipeline	4000.00	LF	53,974	16,192	70,166	17.54
1.06	Automated Data Acquisition Sys.			79,769	23,931	103,699	
1.07	Electrical Service			168,328	50,498	218,826	
1.08	Real Estate			25,000	7,500	32,500	
	Project			1,397,153	419,146	1,816,299	
	COST ESTIMATE FOR			1,397,153	419,146	1,816,299	

** PROJECT INDIRECT SUMMARY - LEVEL 2 **

		QUANTY	UOM	DIRECT	OVERHEAD	H.O.Oh.	Profit	BOND	Esc	TOTAL COST	UNIT
1	Project										
1.01	Recovery Wells, Complete	1150.00	LF	93,173	13,976	5,357	11,251	1,238	4,375	129,369	112.50
1.02	Injection Well, Complete	5280.00	LF	580,536	87,080	33,381	70,100	7,711	27,258	806,066	152.66
1.03	Collector Station	400.00	SF	20,101	3,015	1,156	2,427	267	944	27,909	69.77
1.04	6" Dia. PVC Pipeline	10000	LF	76,874	11,531	4,420	9,282	1,021	3,609	106,738	10.67
1.05	8" Dia. PVC Pipeline	4000.00	LF	38,872	5,831	2,235	4,694	516	1,825	53,974	13.49
1.06	Automated Data Acquisition Sys.			57,450	8,618	3,303	6,937	763	2,697	79,769	
1.07	Electrical Service			121,231	18,185	6,971	14,639	1,610	5,692	168,328	
1.08	Real Estate			25,000	0	0	0	0	0	25,000	
	Project			1,013,237	148,235	56,824	119,330	13126	46,401	1,397,153	
	COST ESTIMATE FOR			1,013,237	148,235	56,824	119,330	13126	46,401	1,397,153	
	Contingency									419,146	
	TOTAL INCL OWNER COSTS									1,816,299	

1.01. Recovery Wells, Complete	QUANTITY UOM	MnHr	Labor	Equip	Matrl	TOTAL COST	UNIT COST
1. Project							
1.01. Recovery Wells, Complete							
USR AA <02550 0001 > Recovery Wells, Complete		0.00	0.00	0.00	81.02	81.02	
Unit price per linear foot for 10 wells at an average depth of 115 feet (per well).	1150.00 LF	0	0	0	93,173	93,173	81.02
Recovery Wells, Complete	1150.00 LF	0	0	0	93,173	93,173	81.02

1.02. Injection Well, Complete		QUANTITY	UOM	MnHr	Labor	Equip	Matrl	TOTAL COST	UNIT COST
1.02. Injection Well, Complete									
USR AA <02550 0001 >	Injection Well, Complete			0.00	0.00	0.00	109.95	109.95	
	Unit price per linear foot for 1 well at an approximate depth of 5,280 feet.	5280.00	LF	0	0	0	580,536	580,536	109.95
	Injection Well, Complete	5280.08	LF	0	0	0	580,536	580,536	109.95

1.03. Collector Station		QUANTITY	UOM	MnHr	Labor	Equip	Matrl	TOTAL COST	UNIT COST
1.03. Collector Station									
USR AA <04000 0001 >	Collector Station - Building			0.10	0.92	0.09	49.24	50.25	
	Masonry-type building, complete. Includes slab on grade, roof construction, CMU walls, 2 windows, 1 door, and components to provide electrical power to the building.	400.00	SF	41	368	36	19,696	20,101	50.25
	Collector Station	400.00	SF	41	368	36	19,696	20,101	50.25

1.04. 6" Dia. PVC Pipeline

	QUANTITY	UOM	MnHr	Labor	Equip	Matrl	TOTAL COST	UNIT COST
1.04. 6" Dia. PVC Pipeline								
MIL AA <15064 5121 > 6" pipe, pvc sch40			0.22	3.34	0.08	2.04	5.46	
	10000.00	LF	2151	33,365	786	20,400	54,552	5.46
L MIL AA <02221 1913 > Trenching			0.02	0.39	0.61	0.00	1.00	
	2777.78	CY	57	1,084	1,681	0	2,765	1.00
MIL AA <02221 8001 > Bedding			0.03	0.53	0.46	13.60	14.59	
	833.00	CY	26	439	382	11,329	12,150	14.59
L MIL AA <02221 5004 > Backfill Trench			0.01	0.21	0.47	0.00	0.68	
	2236.00	CY	22	469	1,057	0	1,526	0.68
L MIL AA <02221 7002 > Compact Fill			0.12	0.91	0.09	0.00	1.00	
	2236.00	CY	269	2,026	210	0	2,236	1.00
L MIL AA <02221 6001 > Waste material			0.01	0.19	0.44	0.00	0.63	
	5750.68	SY	53	1,120	2,526	0	3,645	0.63
6" Dia. PVC Pipeline	10000.00	LF	2579	38,503	6,642	31,729	76,874	7.69

1.05. 8" Dia. PVC Pipeline	QUANTITY UOM	MnHr	Labor	Equip	Matrl	TOTAL COST	UNIT COST
1.05. 8" Dia. PVC Pipeline							
MIL AA <15064 5122 > 8" pipe, pvc sch40		0.26	3.98	0.09	3.23	7.30	
	4000.00 LF	1026	15,913	375	12,920	29,208	7.30
L MIL AA <02221 1913 > Trenching		0.02	0.39	0.61	0.00	1.00	
	1111.11 CY	23	434	672	0	1,106	1.00
MIL AA <02221 8001 > Bedding		0.03	0.53	0.46	13.60	14.59	
	333.33 CY	11	176	153	4,533	4,862	14.59
L MIL AA <02221 5004 > Backfill Trench		0.02	0.46	1.04	0.00	1.50	
	894.00 CY	20	412	930	0	1,342	1.50
L MIL AA <02221 7002 > Compact Fill		0.12	0.91	0.09	0.00	1.00	
	894.00 CY	107	810	84	0	894	1.00
L MIL AA <02221 6001 > Waste material		0.01	0.19	0.44	0.00	0.63	
	2304.00 SY	21	449	1,012	0	1,460	0.63
8" Dia. PVC Pipeline	4000.00 LF	1208	18,193	3,226	17,453	38,872	9.72

1.06. Automated Data Acquisition Sys.	QUANTITY UOM	MnHr	Labor	Equip	Matrl	TOTAL COST	UNIT COST
1.06. Automated Data Acquisition Sys.							
USR AA <16900 0001 > Automated Data Acquisition Sys.		0.00	0.00	0.00	57450	57450.00	
	1.00 LS	0	0	0	57,450	57,450	57450.00
Automated Data Acquisition Sys.		0	0	0	57,450	57,450	

1.07. Electrical Service

		QUANTITY	UOM	MnHr	Labor	Equip	Matrl	TOTAL COST	UNIT COST
1.07. Electrical Service									
USR EL <16301 0001 >	Installation: New transmission lines, line poles, transformers, etc.	1.00	LS	0.00 0	0.00 0	0.00 0	121231 121,231	121231.00 121,231	121231.00
	Electrical Service			0	0	0	121,231	121,231	

1.08. Real Estate

		QUANTITY	UOM	MnHr	Labor	Equip	Matrl	TOTAL COST	UNIT COST
1.08. Real Estate									
USR	<01000 1000 > Permanent Easements			0.00	0.00	0.00	500.00	500.00	
		50.00	AC	0	0	0	25,000	25,000	500.00
	Real Estate			0	0	0	25,000	25,000	
	Project			3827	57,064	9,904	946,268	1,013,237	
	COST ESTIMATE FOR			3827	57,064	9,904	946,268	1,013,237	